AN ABSTRACT OF THE DISSERTATION OF

Taiowa A. Montgomery for the degree of Doctor of Philosophy in Molecular and Cellular Biology presented on August 26, 2008.

Title: Small RNA Pathways in Plants

Abstract approved:

_____

James C. Carrington

miRNA-guided cleavage initiates entry of primary transcripts into the trans-acting siRNA (tasiRNA) biogenesis pathway involving RNA-DEPENDENT RNA POLYMERASE6 (RDR6), DICER-LIKE 4 (DCL4), and SUPPRESSOR OF GENE SILENCING3 (SGS3). *Arabidopsis thaliana TAS1* and *TAS2* families yield tasiRNA that form through miR173-guided initiation cleavage on the 5' side of the siRNA-generating regions. The *TAS3* family yields tasiRNA that form through miR390-guided initiation cleavage on the 3' side of the siRNA-generating regions. miR390 also functions in a non-cleavage mode on the 5' side of the siRNA-generating regions. *TAS1* and *TAS2* tasiRNA target several transcripts encoding pentatricopeptide repeat (PPR) proteins and proteins of unknown function. *TAS3* tasiRNA regulate mRNAs encoding several AUXIN RESPONSE FACTORs.

The *TAS1c* and *TAS3a* loci were modified to produce synthetic (syn) tasiRNA to target an endogenous transcript encoding PHYTOENE DESATURASE (PDS). *TAS1c*- and *TAS3a*-based syn-tasiRNA were used to test the unique requirement for miR173 and miR390 in routing *TAS1c* and *TAS3a* transcripts, respectively, through the RDR6/SGS3/DCL4-dependent tasiRNA pathway. miR173 was unique in its ability to initiate *TAS1c*-based syn-tasiRNA formation. Surprisingly, targeting by miR173 was sufficient to route non-*TAS* transcripts into the tasiRNA pathway as well. AGO1 is shown to associate with miR173, and to be required for *TAS1* and *TAS2* tasiRNA formation, indicating that the miR173-AGO1 complex functions in a distinct mode from other miRNA-AGO1 complexes.

TAS3, but not *TAS1* and *TAS2,* tasiRNA are shown to require ARGONAUTE7 (AGO7) and to regulate the juvenile-to-adult phase transition through suppression of *ARF3* mRNA. miR390-AGO7 complexes are shown to function in either cleavage or non-cleavage modes at two target sites in *TAS3a* transcripts. The AGO7 cleavage, but not the non-cleavage, function could be provided by AGO1, but only when AGO1 was guided to a modified target site through an alternate miRNA. AGO7 was highly selective for interaction with miR390, and miR390 in turn was excluded from association with AGO1 due entirely to an incompatible 5' adenosine. Analysis of AGO1, AGO2 and AGO7 revealed a potent 5' nucleotide discrimination function for some, although not all, ARGONAUTEs. miR390 and AGO7, therefore, evolved as a highly specific miRNA guide/effector protein pair to function at two distinct tasiRNA biogenesis steps.

Small RNA Pathways in Plants

by

Taiowa A. Montgomery

A DISSERTATION

submitted to

Oregon State University

in partial fulfillment of

the requirements for the

degree of

Doctor of Philosophy

Presented August 26, 2008

Commencement June 2009

Doctor of Philosophy dissertation of Taiowa A. Montgomery presented on August 26, 2008.

APPROVED:

_____

Major Professor, representing Molecular and Cellular Biology

_____

Director of the Molecular and Cellular Biology Program

_____

Dean of the Graduate School

I understand that my dissertation will become part of the permanent collection of Oregon State University libraries. My signature below authorizes release of my dissertation to any reader upon request.

_____

Taiowa A. Montgomery, Author

ACKNOWLEDGEMENTS

The author expresses sincere appreciation to everyone who provided advice and support during this dissertation. A special thanks to Jim Carrington, who taught me how to think like a scientist, Kristin Kasschau for her guidance, Carrington lab members, both past and present, and the CGRB faculty and staff. Thanks also to family and friends, above all my beautiful wife Brooke.

CONTRIBUTION OF AUTHORS

Chapter 1: Taiowa Montgomery and James Carrington wrote the introduction.

Chapter 2: Taiowa Montgomery, Noah Fahlgren, Miya Howell, and James Carrington conceived and designed the experiments and wrote the paper. Sarah Dvorak and Amanda Alexander provided technical assistance, and Edwards Allen helped conceive experiments and develop constructs.

Chapter 3: Taiowa Montgomery and James Carrington conceived and designed the experiments and wrote the paper. Miya Howell, Joshua Cuperus, Dawei Li, Jesse Hansen, Amanda Alexander, Elisabeth Chapman, and Noah Fahlgren provided technical assistance. Edwards Allen helped conceive and design the synthetic tasiRNA constructs.

Chapter 4: Taiowa Montgomery and James Carrington conceived and designed the experiments and wrote the paper. Seong Jeon Yoo, Noah Fahlgren, Sunny Gilbert, Miya Howell, Amanda Alexander, Goretti Nguyen, and Christopher Sullivan provided technical assistance. Edwards Allen helped conceive and design the synthetic tasiRNA constructs.

Chapter 5: Taiowa Montgomery wrote the discussion.

TABLE OF CONTENTS

LIST OF FIGURES

LIST OF FIGURES (Continued)

LIST OF TABLES

CHAPTER 1

General Introduction

Taiowa A. Montgomery and James C. Carrington

Published in part in

Proceedings of the National Academy of Sciences

500 Fifth Street, NW, NAS 340

Washington, DC 20001

Issue 105 pages 8489-8490.

mRNA maturation and quality control in eukaryotes is a tightly regulated, multistep process that starts on nascent transcripts. A 7-methyl guanosine (^{7}MeG) cap structure is added to the 5' end of pre-mRNA as it emerges from the exit channel of RNA Polymerase II. The multifunctional nuclear cap-binding complex (CBC), consisting of two protein subunits (CBP80 and CBP20), assembles at the pre-mRNA cap early during transcript formation and helps recruit the splicesome machinery to the cap-proximal intron (Aguilera, 2005; Lewis and Izaurralde, 1997a). Termination of transcription involves cleavage and polyadenylation at the 3' end, and the mature mRNA is retained in the nucleus or exported to the cytoplasm. In either case, the mRNA undergoes a pioneer round of translation and surveillance by the nonsense mediated mRNA decay (NMD) pathway to eliminate defective or misspliced transcripts. Although the CBC localizes primarily to the nucleus, it remains associated with mRNAs during export to the cytoplasm and during the pioneer round of translation and mRNA surveillance. Following the first round of translation, the CBC is replaced by the eukaryotic initiation complex eIF4F and the mRNA steady state translation initiation complex is formed (Maquat, 2004). But not all RNA Pol II transcripts are pre-destined for translation. Primary transcripts for microRNA (pri-miRNA) are retained in the nucleus where they are processed into ~21-22 nt miRNA that generally function as posttranscriptional regulators of mRNA expression. While it has been known that pri-miRNA transcripts form by RNA Pol II transcription, the extent to which pri-miRNA and pre-mRNA transcripts share common processing components is far from settled. Recently,

Laubinger et al (Laubinger et al., 2008) identified an important relationship between mRNA maturation and miRNA primary transcript processing in plants.

The CBC was initially identified in human cells through its role in splicing and has since been shown to be important for multiple mRNA functions (Aguilera, 2005; Izaurralde et al., 1994). The plant homolog of the large subunit of the CBC, CBP80, was first isolated in a genetic screen for *Arabidopsis thaliana* mutants with hypersensitivity to the plant hormone abscisic acid ABA and, thus, was designated *ABA HYPERSENSITIVE1* (*ABH1*). ABH1/CBP80 was shown to interact with an *Arabidopsis* homolog of the smaller subunit of the CBC, CBP20, and to form a complex that binds the ^{7}MeG cap of mRNA, confirming that the CBC shares biochemical functions in plants, humans and yeast (Hugouvieux et al., 2001). Although ABH1/CBP80 and CBP20 are not essential for plant viability under controlled or luxurious growth conditions, plants lacking or deficient in these factors display pleiotropic abnormalities, including jagged-edge leaf morphology defects and increased drought tolerance (Bezerra et al., 2004; Hugouvieux et al., 2001; Papp et al., 2004).

Laubinger et al. (Laubinger et al., 2008) recognized, as did others (Bezerra et al., 2004; Gregory et al., 2008), that the serrated leaf phenotype of *abh1/CBP80* and *cbp20* mutant plants was reminiscent of a phenotype observed nearly forty years earlier in the mutant *serrate* (Redei, 1964). Convergence of this specific leaf phenotype could mean that the affected genes function in the same biochemical or developmental pathway. Whereas *abh1/CBP80* and *cbp20* mutants have relatively mild phenotypes, hypomorphic *serrate* alleles have a variety of severe developmental defects relating to developmental

timing, phylotaxy, meristem function, and patterning in leaves and flowers (Clarke et al., 1999; Grigg et al., 2005; Prigge and Wagner, 2001). *serrate* null mutants are embryonic-lethal (Lobbes et al., 2006), and similar to *abh1/CBP80* mutants, *serrate* mutants are hypersensitive to ABA (Bezerra et al., 2004). *SERRATE* encodes a zinc-finger protein (Prigge and Wagner, 2001). Although *SERRATE* had not been implicated in mRNA metabolism, it had been shown to be a critical component of the pri-miRNA processing machinery and to interact and colocalize with other miRNA biogenesis factors (Fang and Spector, 2007; Fujioka et al., 2007; Lobbes et al., 2006; Yang et al., 2006). Until now, the link between *SERRATE* and the CBC remained elusive.

SERRATE is one of several factors involved in miRNA processing. Similar to other RNA Pol II products, pri-miRNA transcripts contain a ^{7}MeG cap structure at the 5' terminus and a 3' poly(A) tail, but they are distinguished from mRNA by lacking a functional coding sequence and possessing a self-complementary foldback region. In addition to SERRATE, miRNA processing in plants requires DICER-LIKE1 (DCL1), an RNase III-type enzyme, and HYPONASTIC LEAVES1 (HYL1), a double-stranded RNA-binding protein. Hypomorphic mutations in any of the critical components of the miRNA processing machinery cause severe developmental defects. Similar to *SERRATE*, null alleles of *DCL1* are embryonic lethal. Null alleles of *HYL1* are viable, possibly due to redundancy with closely related factors. Following processing, the mature miRNA is loaded as a guide RNA into a complex containing an ARGONAUTE (AGO) protein, the effector component. The AGO-miRNA complex functions to suppress transcripts by

either irreversible cleavage or translational repression (Figure 1.1) (Chapman and Carrington, 2007).

Laubinger et al (Laubinger et al., 2008) described an elegant series of experiments using whole genome tiling array technology, as well as traditional RNA blot and PCR assays, to examine the roles of the CBC and SERRATE in both mRNA splicing and miRNA processing. The authors first tested whether or not the CBC was required for normal accumulation of miRNA using RNA blot assays. Strikingly, several of the miRNA tested by blot assays were reduced in *abh1/CBP80* and *cbp20* mutants, relative to wild-type plants, indicating a previously unknown role for the CBC in the miRNA pathway.

The reduction in miRNA levels observed in *abh1/CBP80* and *cbp20* mutants could be due to reduced accumulation of the pri-miRNA, defective processing of pri-miRNA transcripts into mature miRNA, or destabilization of the mature miRNA. To distinguish between these possibilities, the authors analyzed pri-miRNA transcript levels at great depth in *abh1/CBP80, cbp20,* and *serrate* mutants. Over one hundred and sixty pri-miRNA transcripts were analyzed using a tiling array platform containing 3.2 million probe pairs tiled across most of the non-repetitive component of the *Arabidopsis* genome. A subset of the pri-miRNAs analyzed had significantly elevated levels in *abh1/CBP80, cbp20,* and *serrate* mutants relative to wild-type plants. Although *serrate* mutants had the broadest effect on pri-miRNA processing, there was considerable overlap in the pri-miRNA affected in *serrate*, *abh1/CBP80,* and *cbp20* mutants. This indicates a novel role for the CBC in pri-miRNA processing and provides a comprehensive analysis of

SERRATE dependent miRNA loci. Another recent study, using a similar tiling array based approach, also identified a role for ABH1/CBP80 in pri-miRNA processing (Gregory et al., 2008).

Although the CBC was previously shown to be an important factor in recruiting splicing machinery to pre-mRNA in yeast (Lewis and Izaurralde, 1997b), there was only suggestive evidence that it was involved in splicing in *Arabidopsis* as well (Kuhn et al., 2007). Armed with whole genome tiling array data, Laubinger et al. (Laubinger et al., 2008) set out to exhaustively analyze the role of the CBC, as well as the role of SERRATE, in splicing across the *Arabidopsis* genome. The authors identified a significant number of introns that had elevated hybridization signals in the *abh1/CBP80* and *cbp20* mutants, indicating intron retention resulting from decreased splicing efficiency. Surprisingly, *serrate* mutants also had elevated hybridization signals for a partially overlapping, though somewhat smaller, set of introns. In each of the CBC mutants and *serrate*, typically only a single intron from a gene was affected, most commonly the 5' cap proximal intron, consistent with the role of the CBC in yeast (Aguilera, 2005; Lewis and Izaurralde, 1997b). Importantly, the authors did not observe any difference in intron retention in *dcl1* and *hyl1* mutants relative to wild-type plants, indicating that the splicing defect observed in *serrate* mutants was not an indirect consequence of disruption of the miRNA pathway. These finding indicate a novel role for SERRATE in mRNA splicing that is independent of its role in pri-miRNA transcript processing, as well as independent roles for the CBC in pri-miRNA processing and mRNA splicing.

From this and previous studies, a picture emerges of SERRATE as a mediator between the CBC and both the splicing commitment complex and the pri-miRNA processing machinery. One possibility is that SERRATE functions as a physical link between the CBC and distinct RNA processing machineries for pre-mRNA splicing and pri-miRNA processing (Figure 1.1). SERRATE was previously shown to interact with HYL1 and DCL1 in specialized nuclear dicing bodies (Fang and Spector, 2007; Fujioka et al., 2007). It will be important to learn if SERRATE interacts with components of the CBC and splicing commitment complex as well. Unlike SERRATE, the CBC is not essential for survival, indicating that SERRATE might interact with other factors bound to the 5' cap, such as the eIF4F complex, to mediate loading of splicing and pri-miRNA processing machinery. Does a similar mediator function in mRNA and miRNA metabolism in other eukaryotes? There are several potential homologs of *SERRATE* in non-plant species, including the mammalian gene *ASR2*, as well as genes in *Drosophila*, *C. elegans*, and *S. pombe* (Prigge and Wagner, 2001). The CBC, which is conserved across eukaryotes, may function in pri-miRNA processing in other eukaryotes as well. In support of this idea, a mutant for one component of the cap-binding complex was identified in a screen for RNAi-deficient mutants in *C. elegans* (Parry et al., 2007). Finally, given its role in splicing and dicing, one wonders if there may be additional roles yet to be discovered for *SERRATE* in RNA metabolism.

tasiRNA are a distinct class of small RNA. In plants, primary transcripts are processed by miRNA-guided cleavage at initiation sites. One of the products is stabilized, possibly by SUPPRESSOR OF GENE SILENCING3 (SGS3), and converted to dsRNA

by RNA-DEPENDENT RNA POLYMERASE6 (RDR6) (Allen et al., 2005; Peragine et al., 2004; Vazquez et al., 2004b; Yoshikawa et al., 2005). The resulting double-stranded RNA is processed sequentially by DICER-LIKE4 (DCL4) into 21 nt siRNA duplexes in register with the miRNA-guided cleavage site (Gasciolli et al., 2005; Xie et al., 2005b; Yoshikawa et al., 2005).

Arabidopsis thaliana has eight characterized tasiRNA-generating (*TAS*) loci belonging to four families. *TAS1* and *TAS2* tasiRNA target multiple different mRNAs, including several encoding pentatricopeptide repeat (PPR) proteins (Allen et al., 2005; Axtell et al., 2006; Chen et al., 2007; Howell et al., 2007; Peragine et al., 2004; Vazquez et al., 2004b). *TAS4* tasiRNA target mRNA encoding several MYB transcription factors (Rajagopalan et al., 2006). *TAS3* tasiRNA target *AUXIN RESPONSE FACTORs* (*ARF3* and *ARF4*) (Allen et al., 2005). In addition to its role in development via the tasiRNA pathway, the RDR6/SGS3/DCL4 silencing pathway contributes to antiviral defense and posttranscriptional transgene silencing (Beclin et al., 2002; Dalmay et al., 2000; Deleris et al., 2006; Mourrain et al., 2000; Muangsan et al., 2004).

The *TAS3* family is highly conserved in land plants, whereas *TAS1*, *TAS2* and *TAS4* families are restricted to Arabidopsis or close relatives (Allen et al., 2005; Axtell et al., 2006; Axtell et al., 2007; Rajagopalan et al., 2006; Talmor-Neiman et al., 2006; Vazquez et al., 2004b). Unlike *TAS3* transcripts, *TAS1*, *TAS2*, and *TAS4* transcripts each have only a single known miRNA target site. miR173 functions to initiate tasiRNA biogenesis from *TAS1* and *TAS2* loci, whereas miR828 serves to initiate *TAS4* tasiRNA formation. These three families also differ from *TAS3* in that the tasiRNA-generating regions in *TAS1*,

TAS2 and *TAS4* transcripts originate from the RNA fragment on the 3' side of the cleavage site (Allen et al., 2005; Rajagopalan et al., 2006; Yoshikawa et al., 2005). Thus, the mechanism of *TAS1*, *TAS2*, and *TAS4* tasiRNA formation may suggest a distinct route into the RDR6/SGS3/DCL4 silencing pathway.

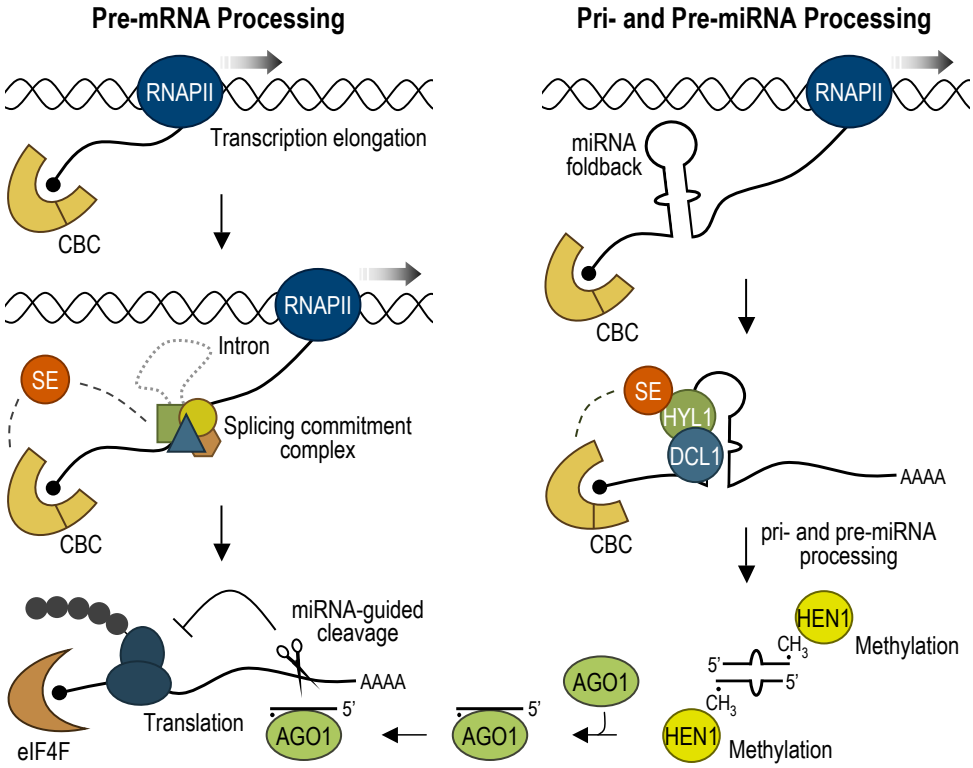

Figure 1.1. Pre-mRNA and pri-miRNA processing in plants. The cap-binding complex (CBC) consists of two subunits, CBP20 and CBP80. The eIF4F complex consists of eIF4E, eIF4A and eIF4G. The AGO-miRNA complex suppresses target mRNA by cleavage or through translational repression. SE, SERRATE.

CHAPTER 2

Regulation of *AUXIN RESPONSE FACTOR3* by *TAS3* trans-acting siRNA Controls Developmental Timing and Patterning in *Arabidopsis thaliana*

Noah Fahlgren,* Taiowa A. Montgomery,* Miya D. Howell,* Edwards Allen,

Sarah K. Dvorak, Amanda L. Alexander, and James C. Carrington

*These authors contributed equally to this work

Current Biology, Cell Press

600 Technology Square, 5th floor

Cambridge, Massachusetts 02139

Volume 16 pages 133-146.

ABSTRACT

MicroRNAs (miRNAs) and trans-acting siRNAs (ta-siRNAs) in plants form through distinct pathways, although they function as negative regulators of mRNA targets by similar mechanisms (Allen et al., 2005; Gasciolli et al., 2005; Peragine et al., 2004; Vazquez et al., 2004b; Xie et al., 2005b; Yoshikawa et al., 2005). Three ta-siRNA gene families (*TAS1, TAS2, TAS3*) are known in *Arabidopsis thaliana*. Biogenesis of *TAS3* ta-siRNAs, which target mRNAs encoding several AUXIN RESPONSE FACTORs (including ARF3/ETTIN and ARF4 (Allen et al., 2005; Williams et al., 2005)) involves miR390-guided processing of primary transcripts, conversion of a precursor to dsRNA through RNA-DEPENDENT RNA POLYMERASE6 (RDR6) activity, and sequential DICER-LIKE4 (DCL4)-mediated cleavage events. We show that the juvenile-to-adult phase transition is normally suppressed by *TAS3* ta-siRNAs, in an ARGONAUTE7-dependent manner, through negative regulation of *ARF3* mRNA. Expression of a non-targeted *ARF3* mutant (*ARF3mut*) in a wild-type background reproduced the phase change phenotypes detected in *rdr6-15* and *dcl4-2* mutants, which lose all ta-siRNAs. Expression of either *ARF3* or *ARF3mut* in *rdr6-15* plants, in which both endogenous and transgenic copies of *ARF3* were de-repressed, resulted in further acceleration of phase change and severe morphological and patterning defects of leaves and floral organs. In light of the functions of *ARF3* and *ARF4* in organ asymmetry, these data reveal multiple roles for *TAS3* ta-siRNA-mediated regulation of *ARF* genes in developmental timing and patterning.

RESULTS/DISCUSSION

ZIP (AGO7) is Required for the Accumulation of *TAS3* ta-siRNAs

Loss of function mutations affecting ta-siRNA biogenesis factors lead to accelerated juvenile-to-adult phase change in *Arabidopsis*. Characteristics associated with the adult stage, such as downward curled leaves, abaxial trichomes and elongated leaves, appear sooner in *rdr6-15* and *dcl4-2* mutants compared to wild-type (Col-0) plants (Hunter et al., 2003; Peragine et al., 2004; Willmann and Poethig, 2005; Xie et al., 2005b). Similar phenotypes are associated with *zip-1*, which has a defect in AGO7 (Hunter et al., 2003) (Figure 2.1A). To test the hypothesis that *ZIP* has a specific role in ta-siRNA function, RNA blot assays for *TAS1*, *TAS2*, and *TAS3* ta-siRNAs were done using triplicate samples from wild-type Col-0, *zip-1* and *rdr6-15* plants. In addition, four miRNAs (miR171, miR173, miR390, miR391) were analyzed. *ZIP* was not required for any of the miRNAs tested, although there were quantitative effects for each (Figure 2.1C). Similarly, *ZIP* was not required for *TAS1* (ta-siR255) or *TAS2* (ta-siR1511) ta-siRNAs (Figure 2.1C). In contrast, *TAS3*-derived ta-siRNAs (Figure 2.1B) required *ZIP*, as these were lost in the *zip-1* mutant (Figure 2.1C). The unique requirement of *TAS3* ta-siRNAs for *ZIP* differed from the dependence of all ta-siRNAs on *RDR6* (Figure 2.1C).

Assuming AGO7 is similar to AGO1 (Vaucheret et al., 2004) and AGO4 (Zilberman et al., 2003; Zilberman et al., 2004), small RNAs that function in association with AGO7 are generally predicted to be destabilized and accumulate to low or non-detectable levels in *zip-1* mutant plants. Given that *TAS3* ta-siRNAs are lost in *zip-1* plants, we predict that AGO7 functions with *TAS3*-derived ta-siRNAs. It is also possible that AGO7

functions with miR390 during *TAS3* transcript processing, although the elevated level of miR390 in *zip-1* plants (Figure 2.1C) argues against this idea. As a *TAS1* ta-siRNA was shown to associate with AGO1 (Baumberger and Baulcombe, 2005), we conclude that distinct ta-siRNAs are functionally associated with different AGO proteins in effector complexes.

Non-Targeted *ARF3mut* Triggers Accelerated Phase Change

Given that general ta-siRNA defective mutants (*rdr6-15* and *dcl4-2*) and *zip-1* exhibit accelerated vegetative phase change phenotypes(Gasciolli et al., 2005; Hunter et al., 2003; Peragine et al., 2004; Xie et al., 2005b), and that *ZIP*-dependent *TAS3* ta-siRNAs are known to target *ARF3* and *ARF4* (Allen et al., 2005), we hypothesized that the phase change phenotypes are due to deficiencies in regulation of *ARFs* by *TAS3* ta-siRNAs. Based on genetic analyses, *ARF3* and *ARF4* likely have overlapping functions in leaf and floral organ patterning, and cooperate with *KANADI* genes to specify abaxial cell identity [11]. Members of the ARF family generally function by interaction with auxin response elements after dissociating from inhibitory AUX/IAA proteins in the presence of auxin (Hagen and Guilfoyle, 2002; Tiwari et al., 2003). A *TAS3* ta-siRNA-insensitive mutant of *ARF3* (*ARF3:ARF3mut*) was generated by introducing silent mutations into the 'A' and 'B' target sites (Figure 2.2A). The mutations placed each site in violation of targeting 'rules' (Allen et al., 2005; Jones-Rhoades and Bartel, 2004; Schwab et al., 2005). Both targeted *ARF3* and non-targeted *ARF3mut* were introduced with their authentic 5' and 3' regulatory sequences into wild-type Col-0 and *rdr6-15* mutant plants.

Additionally, control Col-0 and *rdr6-15* plants were transformed with the empty cloning vector.

Relative levels of *ARF3* sequences in Col-0 and *rdr6-15* plants expressing each construct were measured by quantitative RT-PCR. As shown previously, *ARF3* transcripts accumulated to higher levels in control *rdr6-15* inflorescences relative to the *ARF3* transcript levels in Col-0 inflorescences (Figure 2.2B) (Allen et al., 2005; Peragine et al., 2004; Xie et al., 2005b). *ARF3* transcript levels similar to those in rdr6-*15* plants were detected in Col-0 inflorescences expressing the targeted *ARF3* transgene, and at levels above those in *rdr6-15* in plants expressing the non-targeted *ARF3mut* transgene (Figure 2.2B). This suggests that elevated *ARF3* transcript levels detected in Col-0 plants expressing targeted *ARF3* were due to an increase in copy number, while the further increases in the non-targeted *ARF3mut* lines were due to higher copy number and derepression of the *ARF3mut* transcript. This was supported further by analysis of *rdr6-15* plants transformed with targeted *ARF3* and non-targeted *ARF3mut* transgenes, which both led to significantly higher transcript levels (Figure 2.2B). In contrast to Col-0 plants expressing the transgenes, *ARF3* transcripts in *rdr6-15* plants expressing either targeted or non-targeted transgenes accumulated to comparable levels. This was consistent with expectations, as both endogenous *ARF3* and transgene-derived *ARF3* or *ARF3mut* sequences lacked negative regulation by *TAS3* ta-siRNAs in *rdr6-15* plants. *ARF3* levels in rosette tissue from Col-0 and *rdr6-15* plants containing the *ARF3:ARF3mut transgene* were also measured. As in inflorescence tissue, *ARF3* transcripts in *rdr6-15* transgenic plants accumulated to higher levels compared to Col-0 transgenic plants (Figure 2.2B).

These data indicate that the sensitivity of *ARF3:ARF3mut* transgene mRNA to *TAS3* ta-siRNAs was decreased due to the mutations at the target sites.

The timing of first appearance of abaxial trichomes and of appearance of extended leaves, as well as leaf curvature properties, were analyzed in 12-32 independent transformants of Col-0 and *rdr6-15* plants expressing empty vector, *ARF3:ARF3* or *ARF3:ARF3mut* transgenes. In Col-0 plants, the non-targeted *ARF3:ARF3mut* transgene was predicted to confer dominant, accelerated phase change phenotypes resembling those of *rdr6-15* and *zip-1* plants. The first abaxial trichomes in *rdr6-15* and *zip-1* plants appeared approximately two leaf positions ahead of abaxial trichomes in Col-0 (Figures 2.3A and 2.3B). Introduction of the *TAS3*-insensitive *ARF3:ARF3mut* transgene into Col-0 reproduced the precocious abaxial trichome phenotype to a level that was statistically indistinguishable from that in *rdr6-15* plants (p-value = 0.23, permutation test) (Figure 2.3B). The *TAS3*-targeted *ARF3:ARF3* transgene in Col-0 resulted in an intermediate abaxial trichome timing phenotype that was only marginally different (p-value = 0.052) from timing in Col-0 control plants (Figure 2.3B). In contrast, appearance of abaxial trichomes in *rdr6-15* plants expressing either *ARF3:ARF3* or *ARF3:ARF3mut* transgenes was accelerated significantly more than in Col-0 transgenic plants and was statistically distinguishable (p-value < 0.002) from *rdr6-15* control plants (Figure 2.3B). These data indicate a correlation between *ARF3* expression levels resulting from derepression from *TAS3* and acceleration of abaxial trichomes.

The timing of appearance of extended or elongated leaf morphology during development was analyzed. Leaves emerging at or after position 3 in rosettes of ta-

siRNA-deficient mutants (*rdr6-15, dcl4-2, zip-1*) were elongated compared to equivalent leaves in wild-type or control plants (Figs. 2.1A, 2.3C). Col-0 plants containing the targeted *ARF3:ARF3* transgene had rosette leaves with an accelerated elongation phenotype, with leaf blade length/petiole length ratios increasing at successive positions faster than in Col-0 plants (Figure 2.3D). These plants had blade/petiole ratios that were similar to *rdr6-15* plants at each position (Figure 2.3D). The timing of elongated leaves in Col-0 plants containing non-targeted *ARF3:ARF3mut* was also accelerated, but with exaggerated ratios at each position (Figure 2.3D). In plants with only moderate developmental abnormalities, both the *ARF3:ARF3* and *ARF3:ARF3mut* transgenes in *rdr6-15* plants conferred an enhanced elongated leaf phenotype (data not shown). However, this was complicated by the high frequency of severe leaf morphology defects in *rdr6-15* plants containing targeted and non-targeted constructs (Figure 2.3C), precluding measurements from most leaves.

The proportion of plants exhibiting downward curling of margins in rosette leaves was similar in *rdr6-15* control plants and Col-0 plants expressing either *ARF3:ARF3* or *ARF3:ARF3mut* transgenes (Table 2.1). In these three sets, at least 89% of plants had downward margin curvature of at least 90˚. However, Col-0 plants containing *ARF3:ARF3mut* displayed a more severe curling phenotype, with over 41% of plants displaying at least 360˚ of curvature. In *rdr6-15* plants expressing either *ARF3:ARF3* or *ARF3:ARF3mut* transgenes, curvature when present was generally greater than 360˚, again indicating that the effects of *ARF3* and *ARF3mut* expression were stronger in the

rdr6-15 background. A high proportion (37%-50%) of these plants also had severe leaf lobing (Table 2.1), stunting and other patterning defects (see below).

These data show that characteristics typically associated with accelerated juvenile-to-adult phase change in ta-siRNA-deficient plants were reproduced (or enhanced) in Col-0 plants expressing the non-targeted *ARF3:ARF3mut* transgene and, to a limited extent, in plants expressing the targeted form. This supports the hypothesis that accelerated timing defects of ta-siRNA-deficient mutants are due primarily to derepression of *ARF* gene targets of *TAS3* ta-siRNAs. The quantitatively weaker timing defect in Col-0 expressing the targeted *ARF3:ARF3* transgene, combined with the stronger defects in *rdr6-15* plants expressing either targeted or non-targeted transgenes, further suggests that the phase change phenotype is *ARF3* dosage-dependent. As dosage progressively increases in different lines - by addition of *ARF3* copies, derepression of endogenous or transgenic copies, or copy number addition plus derepression - phase change timing is progressively accelerated. A role for *ARF3*, and potentially other *ARFs* with *TAS3* ta-siRNA target sites, in developmental timing suggests a key role for auxin signaling in the juvenile-to-adult phase transition.

Targeted and Non-targeted *ARF3* Transgenes in *rdr6-15* Cause Patterning Defects

The timing defects in *rdr6-15* plants and Col-0 plants containing the non-targeted *ARF3:ARF3mut* transgene were accompanied by additional phenotypes in reproductive organs, including reduced seed set as shown previously for *rdr6* mutants (Peragine et al., 2004). Combining the *ARF3:ARF3* or *ARF3:ARF3mut* transgenes with the *rdr6-15*

mutation, however, resulted in severe vegetative and reproductive phenotypes. In rosettes, leaves were narrow, highly twisted and curled, and irregularly shaped (Figures 2.3C and 2.3E). In the most severely affected plants, leaves were deeply lobed. Lobed leaves contained ectopic radial leaf primordia that emerged either from the margin of the petiole near the base of the leaf or from the tips of veins near the sinuses of the lobes on the abaxial surface (Figure 2.3E). The lobing and ectopic leaf primordia were reminiscent of plants that overexpress class I *KNOTTED1*-like homeobox (*KNOX*) genes (Ori et al., 2000), and of *asymmetric leaves2* (*as2*) *rdr6* double mutants, which contain abaxialized leaves (Li et al., 2005). These phenotypes were not detected in *rdr6* mutants alone, indicating that derepression and overexpression of *ARF3* triggers these effects. These data suggest that *ARF3* may positively regulate *KNOX* genes, perhaps through negative regulation of *AS1/AS2* (Byrne et al., 2000; Semiarti et al., 2001; Xu et al., 2003). This scenario specifies *TAS3* ta-siRNAs as negative regulators of abaxial cell fate through suppression of *ARF3* and, likely, *ARF4*.

Developing flowers of *rdr6-15* plants expressing either *ARF3:ARF3* or *ARF3:ARF3mut* transgenes had many severe defects. Sepals and petals were downwardly curled, narrow, twisted, and failed to enclose the inner organs (Figure 2.4A). Stamens were short with anthers lacking pollen, and gynoecia were irregular in shape, swollen, and frequently split or open at the apical end (Figure 2.4A). These flowers were sterile, although gynoecia continued to expand to resemble short, wide siliques with unfertilized ovules (Figures 2.4A and 2.4B). Valve tissue at the apical end was often folded back on itself, with little or no style tissue and irregular patches of stigmatic tissue

(Figure 2.4D). Ectopic gynoecia, ovules, filaments and disorganized growths, some with stigmatic tissue, emerged from open gynoecia (Figures 2.4C and 2.4D). The ectopic organs initiated from the placentas, filling the apices of the gynoecia and accounted for the swollen and irregular shapes. These organs continued to grow past stage 17 when wild-type flowers were developing into siliques. To determine if *ARF3* expression was associated with these ectopic organs, *rdr6-15* plants were transformed with *ARF3:ARF3-GUS* and *ARF3:ARF3mut-GUS* transgenes containing β-glucuronidase (GUS) translationally fused to *ARF3* and *ARF3mut* coding sequences. In all flowers with a severe phenotype containing either transgene, GUS activity was detected in the ovules and the ectopic growths, indicating that *ARF3* was highly expressed in the proliferating tissues of these flowers (Figure 2.4E).

Severely affected gynoecia also had split septa that were occasionally still fused at the basal end (Figure 2.4E). Mutants of *TOUSLED* (*TSL*), *LEUNIG* (*LUG*), *AINTEGUMENTA* (*ANT*), *SPATULA* (*SPT*), and *CRABS CLAW* (*CRC*) also have split septa and carpels (Alvarez and Smyth, 1999; Liu et al., 2000; Roe et al., 1997). Genetic data indicate that *ARF3* represses or restricts the expression of both *TSL* and *SPT* (Heisler et al., 2001; Roe et al., 1997), suggesting that the gynoecium phenotypes observed in *rdr6-15* plants containing *ARF3:ARF3* or *ARF3:ARF3mut* could be due to spatial of temporal repression of *TSL*, *SPT*, and possibly other flower patterning factors. Ta-siRNA-defective mutants also form carpels with a split septum that produces stigmatic tissue at the apical end (Peragine et al., 2004), although to a lesser extent than that observed in *rdr6-15* plants containing *ARF3:ARF3* or *ARF3:ARF3mut*. Loss of septum

and transmitting tract tissue may indicate abaxialization, or loss of adaxial tissues, in carpels.

It is not clear how *ARF3* activity, and regulation of *ARF3* by *TAS3* ta-siRNAs, affects both vegetative timing and polarity of lateral organs. It is possible that timing of the juvenile-to-adult transition is merely a consequence of subtle, *TAS3* ta-siRNA-mediated changes in adaxial/abaxial polarity factors to an extent that does not dramatically affect establishment of organ asymmetry. Alternatively, differential regulation of *ARF3* by *TAS3* ta-siRNAs at different times or in different domains during primordia development may result in two different outputs.

ACKNOWLEDGEMENTS

We thank Al Soeldner and Teresa Sawyer for scanning electron microscopy, Heather Sweet for excellent plant management and care, Bobby Babra for help with RNA blot assays, Kristin Kasschau for advice on microscopy, Scott Poethig for *zip-1* seed, and Detlef Weigel for helpful discussions. This work was supported by grants from National Science Foundation Grant MCB-0209836, National Institutes of Health Grant AI43288 and U.S. Department of Agriculture Grant 2005-35319-15280.

Table 2.1. Effect of *ARF3* and *ARF3mut* transgenes on leaf curvature and shape.

Genotype		n	Leaf Curvature*			
			None	Class 1	Class 2	Lobing
	Vector	17	100.0	-	-	-
Col-0	*ARF3:ARF3*	12	8.3	91.7	-	-
	ARF3:ARF3mut	29	10.3	48.3	41.4	-
	Vector	16	6.3	93.7	-	-
rdr6-15	*ARF3:ARF3*	32	-	-	62.5	37.5
	ARF3:ARF3mut	12	8.3	-	41.7	50.0

*Leaf margin curvature and lobing are shown as a percentage of plants displaying phenotype. None, 0-90˚ curvature; class 1, 90-360˚ curvature; class 2, >360˚ curvature.

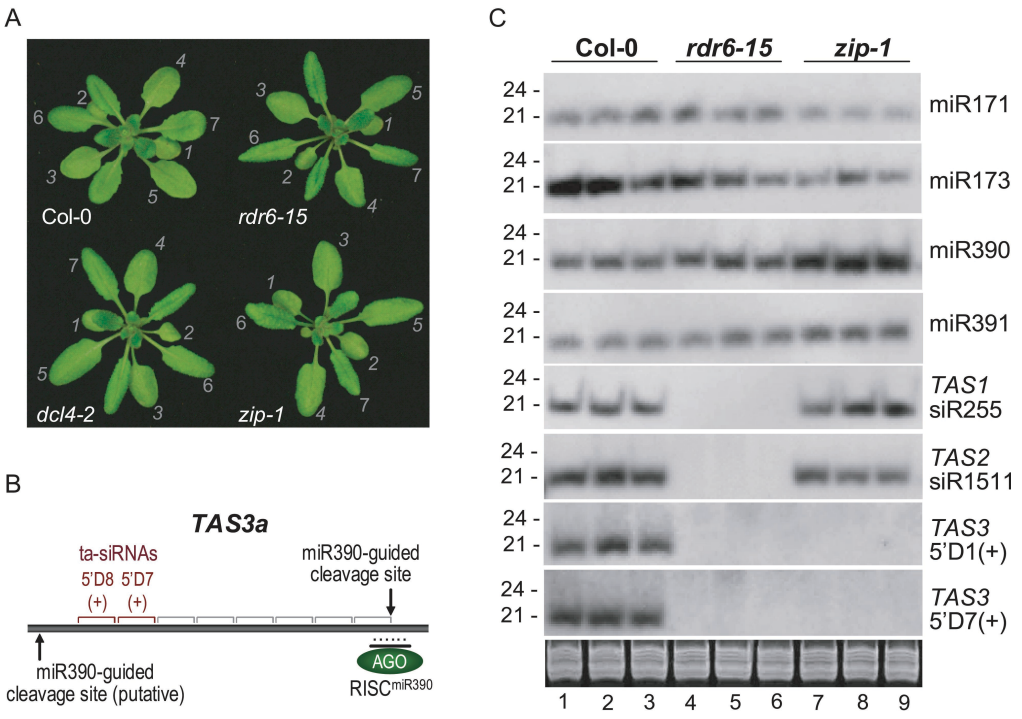

Figure 2.1. Trans-acting siRNAs and vegetative development. (A) Rosette phenotypes associated with *rdr6-15*, *dcl4-2*, and *zip-1*. Leaves 1-7 are indicated. (B) Organization of the *TAS3a* transcript. The ta-siRNAs from the 5'D7(+) and 5'D8(+) positions are indicated, as are the validated and predicted miR390-guided cleavage sites. (C) RNA blot assays for four miRNAs [miR171, miR173, miR390, and miR391] and four ta-siRNAs [*TAS1*-siR255, *TAS2*-siR1511, *TAS3*-5'D1(+), and *TAS3*-5'D7(+)]. Three independent samples for each genotype were analyzed. Ethidium bromide-stained 5S ribosomal and tRNAs are also shown as a loading control.

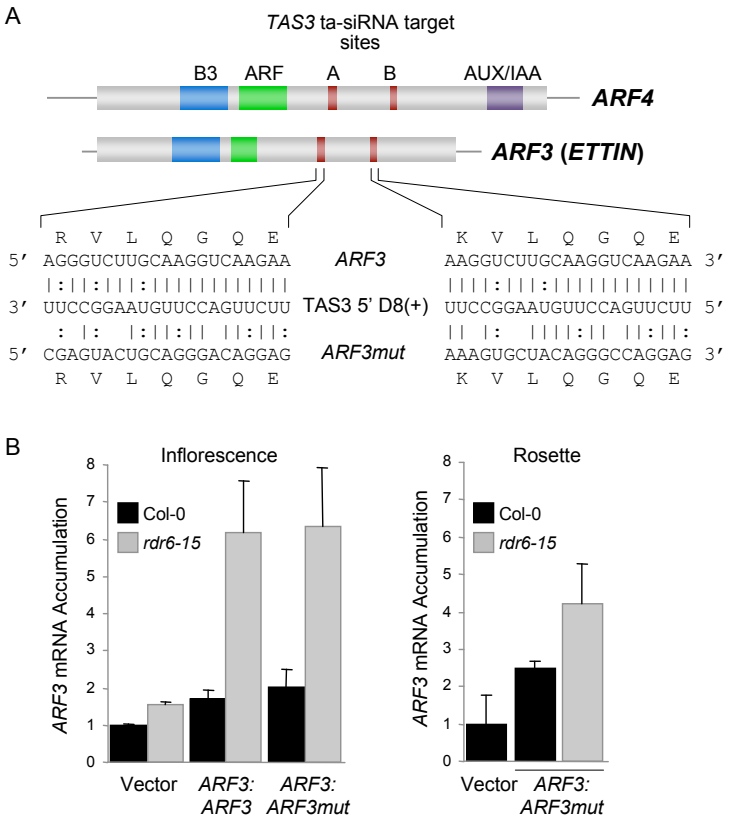

Figure 2.2. Expression of targeted and nontargeted *ARF3* transgenes. (A) Domain organization of *ARF3* and *ARF4* mRNAs. The *TAS3* ta-siRNA target sites ('A' and 'B' sites) in *ARF3*, and mutagenized sites in *ARF3mut*, are shown with base-pairing to the *TAS3*-5'D8(+) ta-siRNA. (B) Quantitative RT-PCR showing relative abundance of *ARF3* mRNA after normalization to *ACT2* mRNA (Col-0 vector-transformed level = 1.0). Left, inflorescence tissue; right, rosette tissue.

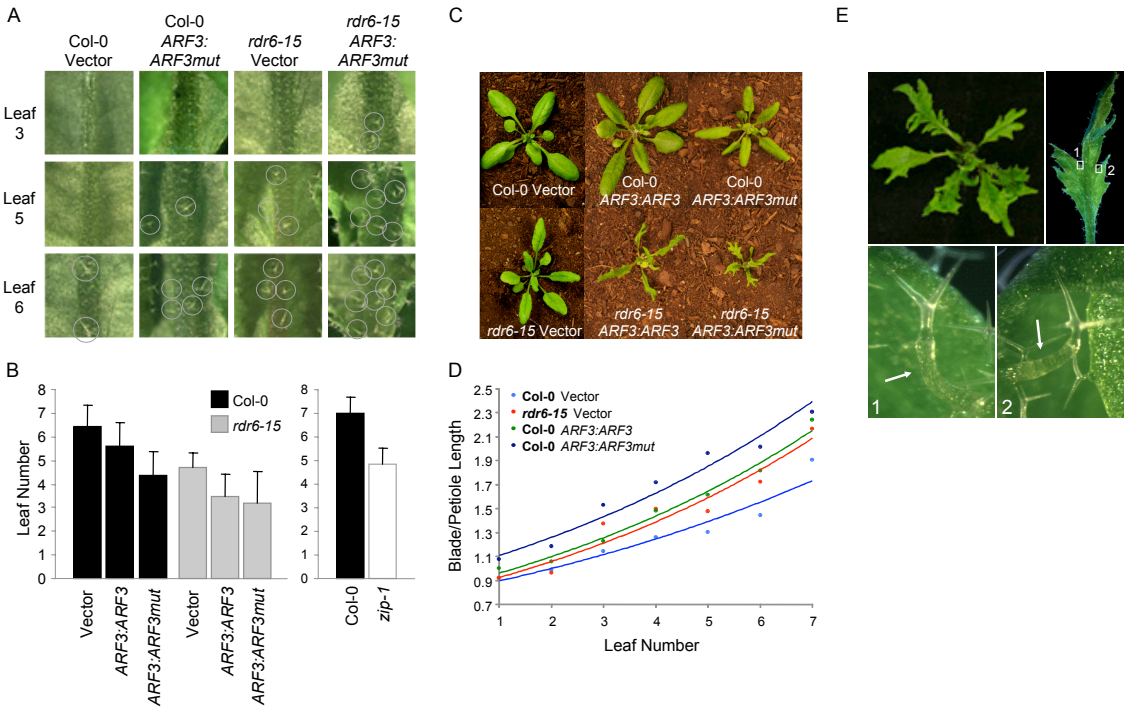

Figure 2.3. Accelerated phase change and leaf morphology phenotypes of Col-0 and *rdr6-15* plants expressing either targeted or non-targeted *ARF3* transgenes. (A) Abaxial surfaces of leaves 3, 5 and 6 in four plant lines as indicated above each column. Trichomes are circled. (B) Mean (±SD) leaf position at which abaxial trichomes were first detected. The two graphs show data for two independent experiments. (C) Rosettes of 28-day old plants. (D) Ratio of leaf blade length/petiole length in leaves 1-7. Note that data are not shown for *rdr6-15* plants containing either transgene, as severe leaf distortion and lobing precluded accurate measurements. (E) Rosette and cauline leaf of a *rdr6-15* plant containing the *ARF3:ARF3mut* transgene. The enlarged images show ectopic leaf primordia on abaxial surfaces (arrows).

Figure 2.4. Flower phenotypes of Col-0 and *rdr6-15* plants expressing *ARF3:ARF3* and *ARF3:ARF3mut* transgenes. (A) Whole flower phenotypes (stage 15). (B) Siliques or non-fertile gynoecia. (C) Apical zones of a stage 17+ flowers (Col-0 vector-transformed) or aberrant gynoecia in *rdr6-15* plants containing the *ARF3:ARF3* transgene. (D) SEM images of apical ends of gynoecia of stage 15 flowers from Col-0 vector-transformed or *rdr6-15 ARF3:ARF3mut*-transformed plants. (E) GUS activity in gynoecia of *rdr6-15* plants transformed with either empty vector (left) or *ARF3:ARF3-GUS* transgene (right). Arrows point to a split septum.

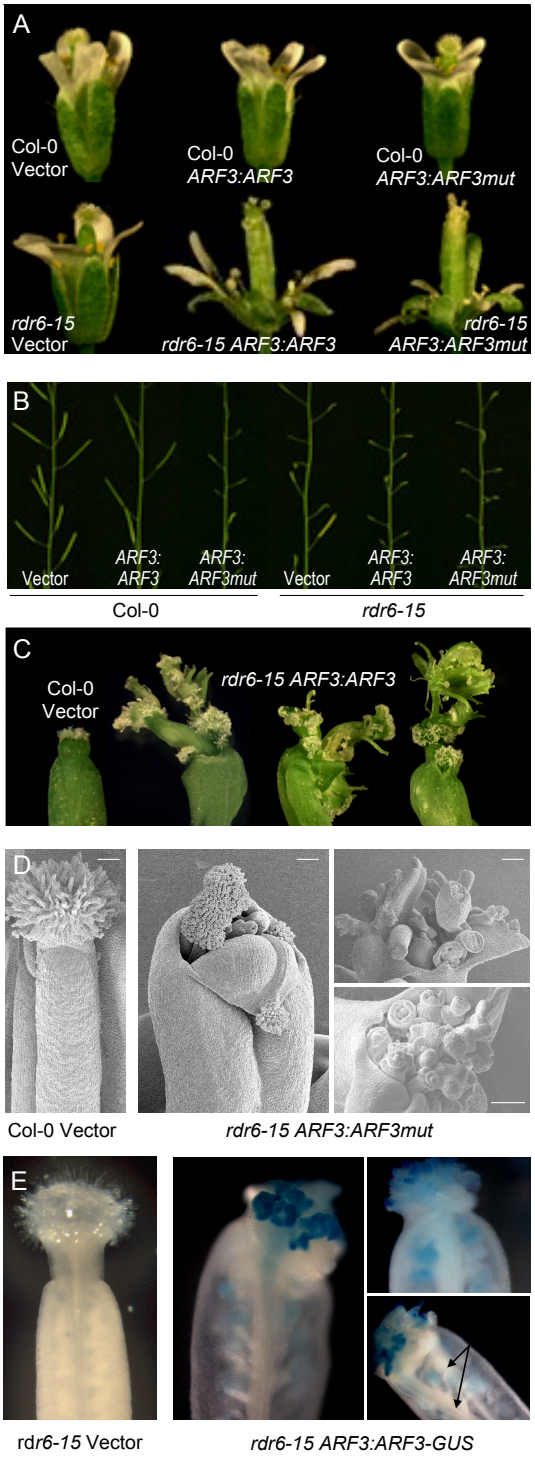

Figure 2.4. Flower phenotypes of Col-0 and *rdr6-15* plants expressing *ARF3:ARF3* and *ARF3:ARF3mut* transgenes.

SUPPLEMENTAL DATA
MATERIAL AND METHODS

Plant Materials, Transformation Protocol, and Growth Conditions

Mutant lines for *rdr6-15, dcl4-2,* and *zip-1* were previously described (Allen et al., 2004; Hunter et al., 2003; Xie et al., 2005b; Xie et al., 2004). *Arabidopsis thaliana* plants were transformed by the vacuum-infiltration method (Clough and Bent, 1998) using *A. tumefaciens* GV3101 carrying constructs for *ARF3:ARF3, ARF3:ARF3mut,* or empty vector. Seed from primary transformants were sterilized and grown on Murashige and Skoog plates under selection for hygromycin resistance. Plants were transplanted to soil after 7 days and subsequently maintained at 22˚C and 16 hr light/8 hr dark cycles in a growth chamber.

Construction of *ARF3* and *ARF3mut* Transgenes

The sequence for *ARF3* (At2g33860), including 3,024 bp and 292 bp of 5' and 3' regulatory sequences respectively, was amplified from genomic DNA by PfuUltra polymerase (Stratagene) and cloned into pENTR/D-TOPO (Invitrogen). Mutations at the TAS3 ta-siRNA target sites were added using megaprimer PCR mutagenesis (Tyagi et al., 2004). *ARF3:ARF3* and *ARF3:ARF3mut* clones were recombined from pENTR/D-TOPO to the binary vector pMDC99 (gift from U. Grossniklaus). *ARF3:ARF3-GUS* and *ARF3:ARF3mut-GUS* clones were made the same way as the non-fusion clones except that they were not cloned with the 3' regulatory sequence and they were recombined into pMDC163. All constructs were sequenced and verified to be accurately cloned.

RNA Blot Assays and Quantitative PCR

Total RNA was extracted from three independent pools of aerial tissue of 22 day-old Col-0, *rdr6-15,* and *zip-1* plants using Trizol reagent (Johansen and Carrington, 2001). For detection of small RNAs, small RNA blot assays were done using synthetic RNA oligonucleotides (Dharmacon Research, Layfayette, CO) as standards. RNA samples (20 μg) were separated by gel electrophoresis and blot hybridization were done as described in (Allen et al., 2004). DNA probes complementary to miR171, miR173, miR390, and miR391 or LNA probes (Exiqon and Sigma-Proligo) complementary to ta-siR255, ta-siR1511, *TAS3* 5'D1(+), and *TAS3* 5'D7(+) were end-labeled using γ^{32}P-ATP and Optikinase (Amersham). Blot signals were measured with an Instant Imager (Packard Bioscience, Boston, MA).

For quantitative PCR, total RNA was extracted from inflorescence or rosette tissue using the RNeasy Plant Mini kit (Qiagen) and treated with RNase-free DNaseI (Ambion). Superscript III (Invitrogen) and oligo(dT) primer were used for first-strand cDNA synthesis. Primers ACT2_F (5'-GCCATCCAAGCTGTTCTCTC-3') and ACT2_R (5'-GAACCACCGATCCAGACACT-3') and ARF3_F (5'-GAAGATGCATCTGAGAGAAG-3') and ARF3_R (5'-CTAGAGAGCAATGTCTAGCAAC-3') were used to amplify *ACTIN2* (At3g18780) and *ARF3* (At2g33860) specific sequences respectively. PCR products at three cycle times were imaged by gel electrophoresis and quantified by spot densitometry using AlphaEaseFC 4.0 (Alpha Innotech, San Leandro, CA). *ARF3* mRNA abundance was normalized to *ACT2* mRNA and then to the value of Col-0 plants with empty vector, whose value was arbitrarily fixed to 1.0.

Phenotype Analysis

Abaxial trichomes were scored by scanning all leaves of 26 day old plants. Leaf blade and petiole lengths were measured with a digital caliper (Mitutoyo, Japan) at day 27. For scanning electron microscopy, tissues were fixed overnight in 2% glutaraldehyde/2% paraformaldehyde/0.05 M PIPES (pH 7.2). Samples were dehydrated through a series of ethanol treatments (30%, 50%, 70%, 95%, and 100%) for 10 minutes at each step. The 100% ethanol treatment was repeated two more times. Dehydrated samples were put in a critical point dryer, mounted on SEM stubs, and sputter-coated using gold-palladium. Samples were viewed with an acceleration voltage of 7 kV.

Assays for GUS activity using inflorescence and leaf tissue from ARF3:ARF3-GUS plants were performed in 100 mM sodium phosphate (pH 7), 1 mM potassium ferricyanide, 1 mM potassium ferrocyanide, 16 mM EDTA, 20% methanol, and 1 mg/ml X-glucuronic acid, at 37^{o}C for 3 hours, after an initial 5 minutes vacuum infiltration of the assay solution. After staining, tissue was decolorized in two washes of 50% ethanol for 15 minutes followed by 2 washes of 95% ethanol for 30 minutes. Tissues were photographed with an Olympus SZX12 microscope (Japan) using bright-field illumination in 50% glycerol.

Statistical Analysis

A permutation test was used to compare the leaf number at which abaxial trichomes first appeared. For this test, a distribution of the difference in sample means was generated by making 10,000 random regroupings of two groups (sizes n_1 and n_2). The two-sided p-value is calculated by comparing the observed mean difference to the distribution of mean

differences from the random regroupings. This test was performed using the S+Resample plug-in for S-PLUS 6.2 (Insightful, Seattle, WA).

To compare leaf blade length to petiole length across leaves 1 through 7 the sample means were plotted on a XY scatterplot and exponential trendlines were fit to each sample using Microsoft Excel (Microsoft, Redmond, WA).

CHAPTER 3

Specificity of ARGONAUTE7-miR390 Interaction and Dual Functionality in *TAS3* Trans-Acting siRNA Formation

Taiowa A. Montgomery, Miya Howell, Josh T. Cuperus, Dawei Li, Jesse Hansen, Amanda Alexander, Elisabeth J. Chapman, Noah Fahlgren, Edwards Allen, and James C. Carrington.

Cell

600 Technology Square, 5th Floor

Cambridge, Massachusetts 02139

Volume 133 pages 128-141.

ABSTRACT

Trans-acting siRNA form through a refined RNAi mechanism in plants. miRNA-guided cleavage triggers entry of precursor transcripts into an RNA-DEPENDENT RNA POLYMERASE6 pathway, and sets the register for phased tasiRNA formation by DICER-LIKE4. miR390-ARGONAUTE7 complexes were shown to function in either cleavage or non-cleavage modes at two target sites in *TAS3a* transcripts. The AGO7 cleavage, but not the non-cleavage, function could be provided by AGO1, the dominant miRNA-associated AGO, but only when AGO1 was guided to a modified target site through an alternate miRNA. AGO7 was highly selective for interaction with miR390, and miR390 in turn was excluded from association with AGO1 due entirely to an incompatible 5' adenosine. Analysis of AGO1, AGO2 and AGO7 revealed a potent 5' nucleotide discrimination function for some, although not all, ARGONAUTEs. miR390 and AGO7, therefore, evolved as a highly specific miRNA guide/effector protein pair to function at two distinct tasiRNA biogenesis steps.

INTRODUCTION

miRNA and tasiRNA are distinct classes of small RNAs that guide silencing of target RNAs through cleavage or non-degradative repression mechanisms (Chapman and Carrington, 2007). miRNAs arise from transcripts that adopt imperfect, self-complementary foldback structures, whereas tasiRNAs arise from a refined adaptation of the RNAi pathway. *TAS* transcripts are first processed by miRNA-guided cleavage, which forms a discrete 5' or 3' end, and then transcribed by RNA-DEPENDENT RNA POLYMERASE6 (RDR6). The resulting dsRNA is processed into siRNA duplexes in end-dependent, 21 nucleotide steps by DICER-LIKE4 (DCL4) (Allen et al., 2005; Gasciolli et al., 2005; Peragine et al., 2004; Vazquez et al., 2004b; Xie et al., 2005b; Yoshikawa et al., 2005). Effector complex formation involves strand separation and selective association with an ARGONAUTE (AGO) protein.

Arabidopsis contains four characterized *TAS* gene families. *TAS1*, *TAS2,* and *TAS4* tasiRNA biogenesis initiates with miR173- (*TAS1* and *TAS2*) or miR828-guided (*TAS4*) cleavage on the 5' side of the tasiRNA-generating region, while *TAS3* tasiRNAs form by miR390-guided cleavage on the 3' side. miR390 also interacts in a non-cleavage mode with a second site near the 5' end (Axtell et al., 2006; Howell et al., 2007). Features of the *TAS3* family, including targeting by miR390, are highly conserved in land plants (Allen et al., 2005; Axtell et al., 2006; Axtell et al., 2007; Talmor-Neiman et al., 2006). *TAS3* tasiRNAs, but not those from *TAS1* or *TAS2*, are dependent on a specialized ARGONAUTE, AGO7 (also called ZIP) (Adenot et al., 2006; Fahlgren et al., 2006; Hunter et al., 2006). *TAS3* tasiRNAs target mRNAs encoding several AUXIN

RESPONSE FACTORs (ARF3 and ARF4), negative regulation of which is necessary for proper developmental timing and lateral organ development along the adaxial-abaxial axis (Adenot et al., 2006; Fahlgren et al., 2006; Garcia et al., 2006; Hunter et al., 2006).

The mechanisms for recognition and routing of transcripts through the tasiRNA or RDR6/DCL4-dependent pathway are not well understood. Axtell et al. (2006) proposed a two-hit trigger mechanism, in which transcripts with two or more small RNA target sites are preferentially routed into the RDR6/DCL4 pathway. This explains some aspects of *TAS3* tasiRNA formation and the routing of several known, multiply targeted transcripts (Axtell et al., 2006; Chen et al., 2007; Howell et al., 2007), although not necessarily *TAS1*, *TAS2*, and *TAS4* tasiRNA biogenesis. How the factors associated with miR828, miR173, and miR390 function to provide routing information remains an unresolved problem. In this paper, we show that miR390 is uniquely adapted to initiate *TAS3* tasiRNA biogenesis due to its specific association with AGO7, and that AGO7-miR390 complexes function in two distinct modes to process and route transcripts through the RDR6/DCL4 pathway. We also found an AGO function that discriminates among small RNAs on the basis of 5' nucleotide identity.

RESULTS

Design and Validation of Syn-tasiRNAs

Based on the predictable phased pattern of tasiRNA formation from the miR390-guided cleavage site, we generated *TAS3a*-based synthetic (syn) tasiRNAs to silence the Arabidopsis *PHYTOENE DESATURASE* (*PDS*) transcript. Silencing of *PDS* mRNA

results in photobleaching of green tissues (Kumagai et al., 1995). Canonical targeting rules were followed for syn-tasiRNA development, including incorporation of a 5'U and perfect complementarity between syn-tasiRNA nucleotides 2-13 (from the 5' end) and the mRNA target (Allen et al., 2005; Jones-Rhoades and Bartel, 2004; Schwab et al., 2005). Two 35S promoter-driven *TAS3a*-based constructs (*35S:TAS3aPDS-1* and *35S:TAS3aPDS-2*) with tandem syn-tasiRNAs in the 5'D7(+) and 5' D8(+) positions (Allen et al., 2005) were developed (Figure 3.1A). These positions normally yield tasiR2141 and tasiR2142, which target *ARF* transcripts.

In Col-0 (wt) plants expressing *35S:TAS3aPDS-1* and *35S:TAS3aPDS-2*, photobleaching emanated from the midrib and major veins, and was more apparent from the adaxial side (Figure 3.1B). *PDS* mRNA accumulation was suppressed by 33% in *35S:TAS3aPDS-1*-transformed plants and 50% in *35S:TAS3aPDS-2*-transformed plants, but was suppressed to a slightly greater extent in midrib tissue compared to non-midrib leaf tissue (p-value < 0.05; Figures 3.1C and 3.1D). Cotyledons displayed photobleaching that emanated from the apex along the petiole (Figure 3.1B). Mild photobleaching was also detected in flowers and siliques of *35S:TAS3aPDS-2*-transformed plants. Syn-tasiRNAs and the photobleaching phenotype were RDR6-, DCL4-, and AGO7 (ZIP)-dependent (Figures 3.1B and 3.1E; Table 3.1). *PDS* mRNA levels were not significantly different between Col-0 vector-transformed plants and *rdr6-15*, *dcl4-2*, and *zip-1* *35S:TAS3aPDS-2*-transformed plants (p-values between 0.26 – 0.86, two-sample t-tests; Figure 3.1C). These results are consistent with the genetic requirements of *TAS3*

tasiRNA, indicating that the syn-tasiRNA system faithfully reflects the endogenous pathway.

Limited Activity and Expression of AGO7

Plants expressing *35S:TAS3aPDS-1* and *35S:TAS3aPDS-2* displayed strongest photobleaching in vasculature-proximal tissue. To determine if expression patterns of known *TAS3*-specific factors explain this pattern, promoter-*GUS* fusion constructs were developed with *TAS3a*, *MIR390a*, *MIR390b*, and *AGO7* promoters. The GUS activity patterns in seedlings expressing *TAS3a:GUS*, *MIR390a:GUS*, and *MIR390b:GUS* were similar to the patterns of activity driven by the 35S promoter (*35S:GUS*). In contrast, seedlings expressing *AGO7:GUS* had activity that was detected primarily in the vasculature (Figure 3.1F). Syn-tasiRNA formation was tested in the presence or absence of ectopic AGO7 in *N. benthamiana* leaves. When transiently coexpressed with *35S:MIR390a* or *35S:MIR390b*, the *35S:TAS3aPDS-2* construct failed to yield syn-tasiRNA (Figure 3.1H; lanes 7 and 8). But when coexpressed with *35S:MIR390a* or *35S:MIR390b* and a 35S-promoter driven *AGO7* construct (*35S:HA-AGO7*; Figure 3.1G), *35S:TAS3aPDS-2* yielded relatively high levels of syn-tasiRNA (Figure 3.1H, lanes 9 and 10). The partial overlap between *AGO7* promoter activity and *TAS3a*-based syn-tasiRNA activity, and the ability of constitutively active AGO7 to overcome limitations to syn-tasiRNA formation in *N. benthamiana* leaves, suggest that AGO7 is limiting in leaves.

Distinct Roles for miR390 at the *TAS3a* 5' and 3' Target Sites

TAS3 tasiRNAs originate from sequences between two miR390 target sites. In flowering plants, but not in moss or pine, the miR390-target interaction at the 5' proximal site contains key mispairs that prevent cleavage, and conversion to a cleavable miR390 target site inactivates the *TAS3a* locus (Axtell et al., 2006). In contrast, the 3' proximal site is cleaved across plant species (Axtell et al., 2006). The unique roles of miR390 at the two target sites were analyzed with single and combination target site substitutions using *35S:TAS3aPDS-1* and 35S*:TAS3aPDS-2* in Col-0 and *zip-1* plants. The 3' site substitutions generated miR171 or miR159 sites, or a non-recognized site (Figures 3.2A and S3.1A). The 5' substitutions yielded an authentic, cleavable miR171 site, or target sites for five miRNAs that approximated the characteristics of the non-cleavable miR390/*TAS3a* 5' target interaction, including mispairs or G:U pairs at positions 9, 10 and 11 of the miRNA (Figures 3.2A and S3.2A, and Table S3.1). A construct with 5' site substitutions that destroyed targeting was also generated (Figure S3.2A). A dual target site substitution construct contained cleavable versions of miR171 target sites (Figure 3.2A).

The 3' and 5' target site substitution mutants were first tested for transcript cleavage properties using a 5' RACE assay with transgenic plant extracts. Cleavage at the canonical position of the authentically paired miR390, miR171, and miR159 3' target sites, but not at the destroyed target site (*35S:TAS3a-PDS-3'390mut*), was detected in the majority of cloned 5' RACE products (Figures 3.2A and S3.1A). At miR171 target sites, cleavage offset by three nucleotides from the canonical position was also detected, likely a result of cleavage guided by the distinct miR171b/c isoform (Figures 3.2A, S3.1A, and

S3.1B). Cleavage was not detected at the authentic 5’ miR390 target site from any construct or at the destroyed 5’ site, and was rare at predicted non-cleavable heterologous 5’ target sites (Figures 3.2A and S3.2A; data not shown). Therefore, the 5’ and 3’ substitution variants generally possessed target site cleavage properties as intended.

The miR171 and miR159 3’ target site substitution and parental constructs triggered photobleaching in 65-97% of plants (Figures 3.2A and S3.1A). Photobleaching was absent in plants with a non-cleavable 3’ target site construct (*35S:TAS3aPDS-3’390mut*; Figure S3.1A). Syn-tasiRNA levels were not significantly different in Col-0 plants with either the parental *35S:TAS3aPDS-2* or the miR171 3’ target substitution construct (*p*-value = 0.55, two-sample t-test), but importantly, photobleaching triggered by both constructs was lost in *zip-1* plants (Figure 3.2A). This indicated that substitution of the 3’ miR390 target site with a functional, alternative target site is tolerated, but does not overcome the system requirement for AGO7.

In contrast to the functional 3’ substitutions, both cleavable (*35S:TAS3aPDS-5’171cle-2* and *35S:TAS3aPDS-5’3’171cle-2*) and non-cleavable (*35S:TAS3aPDS-5’171nc-2*) miR171 target substitutions at the 5’ site eliminated photobleaching and reduced syn-tasiRNAs to background levels in Col-0 plants, regardless of the identity of the 3’ target site (Figures 3.2A and 3.2B). Each of the other heterologous 5’ target sites, and the destroyed 5’ site, resulted in low or non-detectable syn-tasiRNA levels and loss of photobleaching (Figures S3.2A and S3.2B). It is possible that loss of syn-tasiRNA was caused by misprocessing of the transcripts, such that tasiRNAs were formed upstream (5’) of the 5’ target sites. However, we failed to detect small RNAs using probes

corresponding to sequences on the 5' side of any of the modified 5' target sites (Figure S3.2B). The collective target site substitution data indicate requirements for a 5' miR390 target site [in a non-cleaved format (Axtell et al., 2006)] and a functional 3' cleavage site, though not necessarily a miR390 site.

Role of AGO7 in *TAS3a* Transcript Processing

To determine if AGO7 is required for cleavage of endogenous *TAS3a* transcripts, 5' RACE assays were done using wt and mutant plants. 5' RACE product corresponding to cleavage of *TAS3a* transcript at the 3' miR390 target site was detected in Col-0 plants (Figure 3.3A). A slightly larger 5' RACE product corresponding to cleavage 33 bases upstream of the miR390 cleavage site was also detected (Figure 3.3A, lanes 1-3). As shown previously (Allen et al., 2005), this product corresponds to cleavage guided by a secondary siRNA [*TAS3a* 5' D2(-)] derived from the *TAS3a* complementary strand. In *rdr6-15* plants, 5' RACE product corresponding to cleavage at the 3' miR390 site, but not at the secondary site, was detected (Figure 3.3A, lanes 4-6). Loss of secondary cleavage in *rdr6-15* was expected due to lack the complementary RNA strand from which the secondary siRNA originates. In *zip-1* plants, 5' RACE products corresponding to both miR390-guided and secondary cleavage events were lost (Figure 3.3A, lanes 7-9), indicating that AGO7 is necessary for initiation cleavage of endogenous *TAS3a* transcript.

To further explore the connection between AGO7 and miR390-guided cleavage, parental *35S:TAS3aPDS-2* and each single and dual miR171 target site substitution

construct (Figure 3.2A) was transiently expressed in *N. benthamiana*. When expressed alone or in combination with *35S:MIR171a* and *35S:MIR390a*, each construct failed to yield syn-tasiRNA (Figure 3.3C, lanes 3-12). But when co-expressed with *35S:MIR171a*, *35S:MIR390a,* and *35S:HA-AGO7*, both the parental construct and the single 3' miR171 target site substitution construct yielded relatively high levels of syn-tasiRNA (Figure 3.3C, lanes 13 and 14). However, none of the single or dual miR171 substitution constructs with a 5' miR171 target site yielded syn-tasiRNA, even when coexpressed with *35S:HA-AGO7* (Figure 3.3C, lanes 15-17). Cleavage was detected at each of the 3' and cleavable 5' miR171 target sites in the presence and absence of HA-AGO7 (Figure 3.3D, lanes 3, 5, 6, 8, 10, and 11), indicating that another AGO protein (likely AGO1, see below) functions in association with miR171. Ectopic miR171 was not required for cleavage at miR171 target sites due to relatively high levels of endogenous miR171 (Figure 3.3D, lanes 3, 5, and 6). In contrast to miR171 target sites, processing at the authentic 3' miR390 target site was dependent on co-expression with *35S:HA-AGO7*, irrespective of the corresponding 5' target site (Figure 3.3D, lanes 7, 9, and 10 vs. lanes 12, 14, and 15). The requirements for AGO7 and miR390 in cleavage and syn-tasiRNA formation are summarized in Figure 3.3E. The requirement of AGO7 for cleavage specifically at the 3' miR390 target site, but not at miR171 target sites, suggests that AGO7 functions as a miR390-specific slicer.

AGO7 Associates Specifically with miR390

To determine if AGO7 associates specifically with miR390, an HA-tagged AGO7 construct (*AGO7:HA-AGO7*) containing authentic 5' and 3' regulatory sequences was introduced into Col-0 and *zip-1* plants and analyzed for small RNA association in co-immunoprecipitation (co-IP) assays. *zip-1* plants exhibit a number of developmental abnormalities, including defects in leaf development, vegetative timing and seed set. The *AGO7:HA-AGO7* construct complemented the *zip-1* developmental defects and restored *TAS3* tasiRNA (Figure 3.4A). Pre-IP (input) and anti-HA IP fraction from extracts of *zip-1* vector- and *AGO7:HA-AGO7*-transformed plants were analyzed for AGO7, miR171 and miR390. HA-AGO7 was detected only in the input and IP fractions from *zip-1* plants with *AGO7:HA-AGO7*. miR171 and miR390 were detected in the input fraction of both *zip-1* vector- and *AGO7:HA-AGO7*-transformed plants, but only miR390 co-immunoprecipitated with HA-AGO7 (Figure 3.4B). Neither miR171 nor miR390 were detected in the IP fraction from *zip-1* vector-transformed plants (Figure 3.4B, lane 2).

The AGO7-associated small RNAs were probed more exhaustively by sequencing amplified small RNA populations from HA-AGO7 input and IP fractions (Figure 3.4B, flow chart). Small RNA of the 24 nt size class were most abundant in the input fraction, whereas 21 nt small RNAs were most abundant in the IP fraction (Figure S3.3A). Read numbers for previously defined Arabidopsis miRNA and tasiRNA families were recorded from the input (10,226) and IP (14,226) fractions (Table S3.2). Absolute read counts as a reflection of AGO7-associated small RNAs in the IP fraction, however, are not directly interpretable due to the effects of contamination with AGO7-non-associated small RNA. For example, reads of a highly enriched, but low-abundance, miRNA could be dwarfed

by reads from a normally abundant miRNA that contaminates the IP fraction. Therefore, small RNA association with AGO7 was assessed by calculating enrichment in the IP fraction relative to the input fraction. Overall representation of individual family reads/total miRNA+tasiRNA reads in IP and input fractions was determined for each family, and enrichment or depletion in the IP fraction was calculated using the IP representation/input representation ratio. Only miRNA or tasiRNA families that were represented in both input and IP fractions, and by at least five reads in either fraction, were included in the analysis. miR390 and miR391, which comprise one miRNA family, were treated independently here because of their specific relevance to the *TAS3* pathway.

The majority of miRNA families were underrepresented in the IP fraction (Figure 3.4B). Similarly, each of three tasiRNA families were underrepresented. In contrast, miR390 was enriched ~28-fold in the IP fraction. miR390 was the only miRNA enriched more than 3.1 fold (Figure 3.4B), suggesting that AGO7 has a unique affinity for miR390. Interestingly, miR391 was underrepresented in the IP fraction. Also, several miRNA families were neither enriched nor depleted in the IP fraction. While this could conceivably reflect a weak or unstable association with AGO7, the high endogenous levels for most of these families suggests it is more likely due to non-specific contamination.

The apparent preference of AGO7 for miR390 in Arabidopsis plants could be explained by a unique overlap in expression domains of *AGO7* and *MIR390* genes. To eliminate confounding spatial and temporal effects, competition-IP assays were done using the transient expression system. In three of four assays, *35S:HA-AGO7* or empty

vector was coexpressed with *35S:TAS3aPDS-2, 35S:MIR390a*, and one or two additional 35S promoter-driven *MIRNA* constructs (for miR171, miR159, miR167, and miR319). In a fourth assay, *35S:HA-AGO7* or empty vector was coexpressed with *35S:MIR390a*, *35S:TAS3aPDS-2, 35S:MIR173a,* and a 35S-driven *TAS1c*-based synthetic tasiRNA construct (*35S:TAS1cPDS-2*). miR390 co-immunoprecipitated with HA-AGO7 in each of the competition assays (Figure 3.4C, lane 4; only one experiment). In contrast, none of the other miRNAs or syn-tasiRNAs tested co-immunoprecipitated with HA-AGO7 (Figure 3.4C, lane 4), strongly supporting the hypothesis that AGO7 associates specifically with miR390.

miR390 Selectivity for AGO7

The association of AGO7 with miR390 led to the question of whether or not miR390 is excluded from the other Arabidopsis AGO proteins that associate with miRNAs. HA-AGO1 and HA-AGO2 were compared to HA-AGO7 for their association with miR390, miR171 and miR173 in competition-IP assays. AGO1 is known to associate with most miRNAs, *TAS1* tasiRNA, and some viral siRNA (Baumberger and Baulcombe, 2005; Qi et al., 2005; Qi et al., 2006; Zhang et al., 2006). Little is known about AGO2 functionality, but it was chosen because of close relatedness to AGO7 within the 10-member AGO family in Arabidopsis (Tolia and Joshua-Tor, 2007). *35S:HA-AGO1, 35S:HA-AGO2, 35S:HA-AGO7* or empty vector was co-expressed with *35S:MIR171a* alone or a mixture of *35S:MIR173a* and *35S:MIR390a*. Consistent with previous experiments, only miR390 co-immunoprecipitated with AGO7 (Figure 3.4D, lanes 5 and

6). Conversely, miR171 and miR173, but not miR390, co-immunoprecipitated with AGO1 (Figure 3.4D, lanes 3 and 4), indicating reciprocal specificity between AGO7 and AGO1 for the miRNAs tested. miR390 co-immunoprecipitated with AGO2, but at a relatively low level, while miR171 and miR173 did not (Figure 3.4D, lanes 7 and 8). Using transgenic Col-0 plants expressing HA-AGO2 from authentic regulatory signals (*AGO2:HA-AGO2*), small RNAs associated with AGO2 were sequenced, and enrichment/depletion ratios were calculated. Small RNAs in the HA-AGO2 IP fraction were primarily 21 nt in length (Figure S3.3B). Most miRNAs and tasiRNAs were depleted in the HA-AGO2 IP fraction, but with a few notable exceptions. Six miRNAs were moderately or slightly enriched (Figure 3.4E; Table S3.3). Although the miR390 ratio was neutral, it ranked seventh among miRNA families. Interestingly, six of the top seven ranking miRNAs, including miR390, contain 5'A residues, which contrasts with the vast majority of miRNAs, including miR171 and miR173, which contain 5'U. Additionally, the 5'A-containing subset of tasiRNAs from three families were specifically enriched by HA-AGO2 IP, whereas non-5'A-containing tasiRNAs were depleted. These results hint at a prospective 5' rule for specificity of AGO1 and AGO2, in which they interact preferentially with 21 nt small RNAs containing 5'U or 5'A, respectively. AGO7 specificity for miR390, however, may have more complex requirements than can be explained by a simple 5' feature.

Specificity in AGO7-miR390 Complex Formation and 5' Nucleotide Discrimination

To test directly the miR390 5'nucleotide requirement, as well as the roles of additional features of the *MIR390a* foldback, in AGO7 loading specificity, mutant and chimeric miR390- and miR171-expressing constructs were analyzed (Figure 3.5A). As described above, these experiments were done in the context of AGO1, AGO2 and AGO7 proteins to understand both the AGO7-miR390-specific features and the broader principles of AGO-miRNA complex formation.

We first hypothesized that the strong association of miR390 with AGO7 is dictated by the miR390 5'A. We also hypothesized that miR171 associates with AGO1 due to a 5'U. Parental *35S:MIR171a* and *35S:MIR390a* were mutated to convert the 5' nucleotides of miR171 and miR390 to A and U (forming *35S:MIR171a-5'A* and *35S:MIR390a-5'U*), respectively, and miRNA association with HA-tagged AGO1, AGO2 and AGO7 was assessed in co-IP assays (Figure 3.5A). HA-AGO1 specifically co-immunoprecipitated with each 5'U-containing miRNA (miR171 and miR390-5'U), but not with 5'A-containing miRNAs (miR390 and miR171-5'A) (Figure 3.5B). In the reciprocal pattern, HA-AGO2 specifically co-immunoprecipitated with 5'A-containing miRNAs (miR390 and miR171-5'A), but not with either miRNA containing a 5'U (miR171 and miR390-5'U) (Figure 3.5B). These data reveal the 5' nucleotide as a simple specificity determinant for inclusion/exclusion from AGO1 (5'U) and AGO2 (5'A) complexes. However, loading of AGO1 with miR390-5'U, or AGO2 with miR390, in the absence of AGO7 was insufficient to trigger syn-tasiRNA formation in co-expression assays with *35S:TAS3aPDS-2* (Figure 3.5C, lanes 7 and 10).

In sharp contrast, HA-AGO7 co-immunoprecipitated with miR390 containing either a 5'A or 5'U, and failed to associate with either miR171 or miR171-5'A (Figure 3.5B). Co-expression of either *35S:MIR390a-5'U* or *35S:MIR390a* with *35S:HA-AGO7* and *35S:TAS3aPDS-2* triggered syn-tasiRNA formation, although syn-tasiRNA levels were lower in the assay containing *35S:MIR390a-5'U* (Figure 3.5C, lanes 8 and 9). AGO7, therefore, neither loads miR390 on the basis of a 5'A nor excludes miR171 due to a 5'U, and the 5' identity has only modest effects on functionality of miR390-AGO7 complexes during tasiRNA biogenesis.

Finally, to determine if the *MIR390a* foldback contains unique sequence or structural features for loading miR390 into AGO7, chimeric *MIR171a* and *MIR390a* constructs were tested in co-IP assays with HA-AGO1 and HA-AGO7. In the first series, two miR171 duplex forms, one with an authentic miR171 duplex-mispair structure (C:C and C:U mispairs, *35S:MIR390a-171sub2*) and the other with a miR390-like duplex mispair structure (single G:A mispair, *35S:MIR390a-171sub1*), were introduced into the *MIR390a* precursor in place of the miR390 duplex (Figure 3.5A). miR171 expressed from these chimeric constructs accumulated to higher levels than when derived from the authentic *MIR171a* context, but co-immunoprecipitated specifically with HA-AGO1 regardless of the precursor context (Figure 3.5D, lanes 7-12). None of the chimeric miR171-generating precursors yielded miR171 with the capacity to co-IP with HA-AGO7 (Figure 3.5D, lanes 13-18), indicating that neither the *MIR390a* precursor stem-loop backbone, nor the positions of mispairs within the *MIR390a* miRNA-miRNA* duplex, are sufficient to direct association with AGO7. In the second series, two miR390a

duplex forms, one with an authentic miR390 duplex-mispair structure (G:A mispair, *35S:MIR171a-390sub2*) and the other with a miR171-like duplex mispair structure (C:C and C:U mispairs, *35S:MIR171a-390sub1*), were introduced into the *MIR171a* precursor in place of the miR171 duplex (Figure 3.5A). miR390 was only weakly expressed from the chimeric *MIR171a*-based constructs, although miR390 levels from both constructs were above the low endogenous miR390 levels (2.8-4.1 fold; Figure 3.5E, lanes 9, 13 and 15). miR390 derived from the authentic miR390 precursor, as well as from both of the chimeric *MIR171a*-based constructs, co-immunoprecipitated with HA-AGO7 (Figure 3.5E, lanes 11-16), but not with HA-AGO1 (data not shown). These results indicate that selective association of AGO7 with miR390 cannot be explained by a 5' nucleotide rule or a foldback-related structure, but rather point to a specific non-5' nucleotide feature of the miR390 sequence itself.

DISCUSSION

Using the syn-tasiRNA system, we identified mechanistic features by which two miR390 target sites function specifically with AGO7 to route *TAS3* transcripts through the RDR6/DCL4 pathway. Cleavage at the 3' target site of *TAS3a*-derived transcripts forms the 3' end at which RDR6 initiates transcription, synthesizing a dsRNA substrate for subsequent processing by DCL4. Cleavage at the miR390 target site requires AGO7, irrespective of targeting at the 5' site, suggesting that AGO7 functions as a miR390-guided slicer. The requirement for AGO7 slicer function is bypassed when the 3' miR390 target site is substituted for heterologous miRNA target sites, indicating that AGO7 is

dispensable at this site if another AGO is delivered via an alternate miRNA guide. The obvious prediction from this result, that AGO7 is uniquely associated with miR390, was confirmed in multiple co-IP assays. Therefore, the functionality of AGO7 at the 3' target site is dictated entirely by its miR390-guided slicer activity.

The *TAS3a* 5' miR390-target site duplex contains requisite mispairs that interfere with cleavage (Axtell et al., 2006). However, this site is clearly active, and in contrast to the 3' target site, the 5' site is far less tolerant of target site substitutions. The dependence on a 5' miR390 target site may reflect several possible requirements. There may be a requirement for a miR390 guide and/or miR390 target sequence per se, although the unique contribution of the nucleotide sequences themselves is not obvious. Furthermore, AGO1-miR390-5'U complexes failed to trigger tasiRNA formation, suggesting that there is a unique requirement for an AGO7-containing complex at the 5' target site. The preference for a 5' miR390 site, therefore, is likely due to a requirement for interaction of an AGO7-miR390 complex with the precursor transcript. Given that the 5' site functions in a non-cleavage mode, the AGO7-miR390 complex is proposed to operate through a "stable" interaction.

How might stable association with an AGO7-miR390 complex facilitate routing of *TAS3a* transcripts through the RDR6/DCL4 pathway? One simple model states that AGO7 stabilizes the processed *TAS3* transcript and provides greater opportunity for interaction with RDR6 (Figure 3.6A). Alternatively, AGO7 may actively recruit RDR6 through direct interaction or through associated factors, such as SGS3 (Figure 3.6A). In Arabidopsis, AGO4 interacts with NRPD1b, a subunit of PolIVb (Li et al., 2006) (El-

Shami et al., 2007), so there is precedence for AGO proteins interacting with a polymerase-like protein. A 3' end formed by small RNA-directed cleavage or by other cleavage mechanisms may be a preferred end for RDR6 activity, possibly due to loss of the poly(A) tail and associated factors. As another possibility, stable association of AGO7 might physically direct transcripts into an RDR6/DCL4-containing processing center (Figure 3.6A). Although an RDR6/DCL4 processing center has not been identified, RNA processing centers with roles in silencing, such as P-bodies (Liu et al., 2005), have been identified.

Most miRNA target transcripts are not routed through the RDR6/DCL4 pathway (Axtell et al., 2006; Howell et al., 2007; Lu et al., 2006; Ronemus et al., 2006), and this may relate to rapid dissociation of the AGO-containing complex after cleavage interaction at single sites. Among the relatively few targets that feed into the RDR6/DCL4 pathway are several transcripts encoding pentatricopeptide repeat (PPR) proteins (Axtell et al., 2006; Chen et al., 2007; Howell et al., 2007; Lu et al., 2006). Notably, these are targeted for cleavage by miR161 isoforms and *TAS1/TAS2*-derived tasiRNAs, but are also predicted to be targeted by miR400 (Howell et al., 2007; Peragine et al., 2004; Sunkar and Zhu, 2004). miR400 fails to direct cleavage (Howell et al., 2007), and may associate stably with *PPR* target transcripts. Thus, the combination of small RNA-directed cleavage and non-cleaving AGO-containing complexes on a transcript may provide key signals or structures to efficiently recruit RDR6.

Why is AGO1, which will associate with functional miR390-5'U, unable to substitute for AGO7 at the 5' target site? Perhaps AGO1 fails to recognize or associate stably with

more highly mispaired target sites, whereas AGO7 may be more accommodating of miRNA-target mispairs. Alternatively, AGO1 may lack an AGO7-like ability to efficiently recruit RDR6 to target transcripts. The known role of AGO1 in RDR6-dependent transgene silencing (Fagard et al., 2000) argues against this idea, although AGO1 may only be necessary for activity (not biogenesis) of secondary siRNA. This idea is weakened further by the fact that *TAS1* and *TAS2* tasiRNA formation requires RDR6 but not AGO7. It will be important to learn if other miRNAs involved in tasiRNA initiation cleavage, such as miR173 and miR828, have unique AGO associations that facilitate routing through the RDR6 pathway.

How did the specialized interaction between AGO7 and miR390 in *TAS3* tasiRNA formation arise? Given the antiquity of the *TAS3* pathway, it is likely that AGO7 has been finely tuned through hundreds-of-millions of years of evolution to recognize miR390 and exclude other miRNAs. We suggest that AGO7 has subfunctionalized at both the biochemical and expression levels, the result being only a few miRNA target transcripts ushered into the RDR6/DCL4 pathway by AGO7. Similarly, miR390 adopted a 5'A feature that excludes association with AGO1. This 5' nucleotide exclusion mechanism should limit miR390 activity outside of the AGO7 expression domain. Given the widespread activity of AGO1 as an effector protein for many posttranscriptional silencing pathways, and the apparent broad expression domain of *MIR390a* and *MIR390b*, the 5' nucleotide exclusion mechanism should focus miR390 activity to cells that co-express AGO7. We recognize that, despite the unique affinity of AGO7 for miR390, and the exclusion of miR390 from AGO1, miR390 also associates weakly with AGO2, as well as

with AGO4 (Qi et al., 2006). The functional significance of either AGO2 or AGO4 interaction is not understood. Association of miR390 with AGO2 is clearly driven by the 5'A, but the basis for association with AGO4, which interacts primarily with 24 nt siRNA (Qi et al., 2006), is not known. The phenotype of AGO4 mutants does not overlap the phenotype of *TAS3* tasiRNA-deficient mutants (Zilberman et al., 2003). Additionally, AGO7-, *TAS3*-, and RDR6-deficient mutants have similar developmental defects (Adenot et al., 2006; Hunter et al., 2003; Peragine et al., 2004), indicating that neither AGO2 nor AGO4 functions redundantly with AGO7.

Although we could not identify a role for the miRNA 5' nucleotide as an AGO7 specificity determinant, the 5' nucleotide was clearly defined as an inclusion/exclusion specificity determinant for both AGO1 and AGO2. AGO1 prefers a 5'U and excludes a 5'A, whereas AGO2 possesses the reciprocal preference for 5'A and exclusion of 5'U. Thus, the selective pressure for a 5'U in the majority of plant miRNAs, which as a class function broadly through AGO1, is now understood. Given the widespread presence of 5'U in animal miRNA, as well as 5'U or other 5' nucleotide preferences in other small RNA classes (Ruby et al., 2006), similar AGO selectivity determinants very likely explain at least some observed 5' nucleotide biases more widely. Structural studies show that AGO-siRNA 5' end interactions are important for recognition, stability and fidelity of an active effector complex (Ma et al., 2005; Rivas et al., 2005). Indeed, the 5' terminal base interacts directly through base-stacking interactions with residues in a highly conserved 5' nucleotide binding pocket (Ma et al., 2005; Parker et al., 2005). In *Archaeglobus fulgidus* Piwi protein, mutation of a tyrosine residue within the 5'

nucleotide binding pocket known to interact with the 5' base results in decreased siRNA binding affinity (Ma et al., 2005). Thus, it is possible that variation within this pocket accounts for differing 5' nucleotide specificities among AGO1, AGO2, and AGO7.

Analysis of the chimeric foldbacks indicated that neither the *MIR390a* stem-loop context nor the miR390/miR390* basepair and mispair features account for the affinity of AGO7 for miR390 (Figure 3.6B). However, small RNA duplex structure does specify loading for Ago1 and Ago2 in Drosophila. miRNAs with central mispairs in the miRNA/miRNA* duplex are preferentially loaded into Ago1, whereas perfectly paired siRNA duplexes are preferentially loaded into Ago2 (Forstemann et al., 2007; Tomari et al., 2007). A similar sorting mechanism exists in *C. elegans* (Steiner et al., 2007). Thus, AGO specificity can be directed by specific 5' nucleotide identities as well as base-pair structure of precursors. The finding that miR390-AGO7 association depends on additional features suggests there are more specificity determinants to discover.

Finally, the apparent restricted domain of AGO7 promoter activity in Arabidopsis plants, and the ability of ectopic AGO7 to overcome limitations to syn-tasiRNA formation in *N. benthamiana* leaves, suggest that AGO7 may limit activity of the *TAS3* tasiRNA pathway. Interestingly, the syn-tasiRNA-induced photobleaching phenotype appears to emanate from tissue with AGO7 promoter activity. Expansion of the phenotype away from vascular cells may reflect cell-nonautonomy of syn-tasiRNAs. Given that DCL4 products likely function as mobile silencing signals (Dunoyer et al., 2005), *TAS3a*-derived tasiRNAs might function in a cell-nonautonomous manner during plant growth and development.

EXPERIMENTAL PROCEDURES

Transgenes

Transgene sequences were PCR-amplified from genomic DNA or cDNA (Supplemental Experimental Procedures). Syn-tasiRNA sequences, miRNA target site substitutions, and miR171 and miR390 substitutions were introduced by site-overlap extension PCR (Ho et al., 1989). The resulting products were cloned in pENTR (Invitrogen), followed by recombination into the plant transformation vector pMDC32, pMDC163 (a GUS fusion vector), or pMDC99 (Curtis and Grossniklaus, 2003).

Plant Materials

rdr6-15, dcl4-2, and *zip-1* alleles were previously described (Allen et al., 2004; Hunter et al., 2003; Xie et al., 2005b). Arabidopsis plants were transformed using *Agrobacterium tumefaciens* GV3101 (Clough and Bent, 1998). Transgenic plants were grown on MS medium containing hygromycin (50 ug/ml) for 7 days, transferred to soil, and maintained in a standard greenhouse with 16 hr light/8 hr dark supplemental light cycle.

RNA Blots, Quantitative PCR and 5'RACE Assays

RNA blot assays were done as described (Allen et al., 2005). Except where noted, triplicate samples from pools of independent primary transformants were analyzed. Quantitative RT-PCR was done using the same RNA preparations used for RNA blots. *PDS* mRNA levels were normalized against *ACTIN2* mRNA levels. miRNA-guided

cleavage was tested using RNA ligase-mediated 5' RACE (Llave et al., 2002b) (Supplemental Experimental Procedures).

Transient Expression Assays

Agrobacterium-mediated transient assays in *N. benthamiana* leaves were done as described (Llave et al., 2002b). Within each experiment, concentrations of *Agrobacterium* containing each construct were equalized by adjusting the concentration of *Agrobacterium* culture containing empty vector. RNA was analyzed 48 hours post-infiltration.

GUS Assays

Plants were infiltrated with 100 mM sodium phosphate (pH 7), 1 mM potassium ferricyanide, 1 mM potassium ferrocyanide, 16 mM EDTA, 20% methanol, and 1 mg/ml X-glucuronic acid, followed by incubation at 37^{o}C for 3 or 6 hours. Tissue was cleared in ethanol and photographed with an Olympus SZX12 microscope.

Immunoprecipitation

Immunoprecipitation and subsequent RNA isolation were done using HA antibody (clone 12CA5, Roche) (Chapman et al., 2004). For immunoprecipitation from Arabidopsis tissue, flower stages 1-12 was used.

Small RNA Sequencing

Flower tissue (stages 1-12) from *zip-1 AGO7:HA-AGO7*- or Col-0 *AGO2:HA-AGO2*-transformed plants was ground in lysis buffer (Chapman et al., 2004). Cell debris was removed by centrifugation for 10 min at 12,000 g and the supernatant was partitioned into input and IP fractions. RNA was isolated immediately from the input fraction by phenol/chloroform extraction, followed by ethanol precipitation. HA-AGO7 and HA-AGO2 were immunoprecipitated using HA antibody and Protein A agarose beads. After removal of an aliquot, beads were treated with proteinase K. RNA was isolated from the supernatant, and amplicons for sequencing were prepared as described (Kasschau et al., 2007) with the exception of the adaptor sequences and the use of Phusion High Fidelity DNA Polymerase (Finnzymes). Sequencing-by-synthesis was done using an Illumina 1G Genome Analyzer.

Statistical Analysis

Statistical analyses were done using S-PLUS (Insightful) and Excel (Microsoft). For multiple comparisons, Bonferroni adjustments were applied to *p*-value significance level cutoffs.

ACKNOWLEDEMENTS

We thank Bobby Babra, Desiree Boltz, and Amy Shatswell for technical assistance, Chris Sullivan, Scott Givan and Zach Miller for computational assistance, Kristin Kasschau and Mark Dasenko for assistance with sequencing, and Jim Roberts for stimulating discussions. This work was supported by grants from NSF (MCB-0618433), NIH

(AI43288), USDA-NRI (2006-35301-17420), NSFC (30325001), and Monsanto Corporation.

Table 3.1. Effects of *TAS3a*-based syn-tasiRNA on wild-type and mutant plants.

		Syn-tasiRNA[a]		Relative Photobleaching[b]		
Genotype	n	PDSd7[c]	PDSd8[d]	None	Weak	Moderate
Col-0						
Vector	90	-	-	100.0	0	0
35S:TAS3aPDS-1	81	+	+	3.5	96.5	0
35S:TAS3aPDS-2	12	+	+	8.3	16.7	75.0
rdr6-15						
35S:TAS3aPDS-1	85	-	-	100.0	0	0
35S:TAS3aPDS-2	36	-	-	100.0	0	0
dcl4-2						
35S:TAS3aPDS-1	5	-	-	100.0	0	0
35S:TAS3aPDS-2	36	-	-	100.0	0	0
zip-1						
35S:TAS3aPDS-1	12	-	-	100.0	0	0
35S:TAS3aPDS-2	36	-	-	100.0	0	0

[a] Syn-tasiRNA are scored as either present (+) or absent (-) as determined by RNA blot assays.

[b] Photobleaching is shown as a percentage of plants in each category.

[c] The PDSd7 [position 5'D7(+)] syn-tasiRNA differs between each of the syn-tasiRNA constructs.

[d] The PDSd7 [position 5'D8(+)] syn-tasiRNA is the same in each of the syn-tasiRNA constructs.

Figure 3.1. Functionality and genetic requirements of *TAS3a*-based syn-tasiRNA. (A) Organization of syn-tasiRNA constructs. The miR390-guided cleavage site is indicated by the arrow. The tasiRNA region is indicated by brackets. (B) Phenotypes of Col-0 and mutant plants containing empty vector, *35S:TAS3aPDS-1*, and *35S:TAS3aPDS-2* (Ad = adaxial, Ab = abaxial). (C) Mean relative level +/- SE of *PDS* mRNA in rosette tissue (Col-0 vector = 1.0). (D) Mean relative level +/- SE of *PDS* mRNA in leaf midrib and lamina tissue (Col-0 vector = 1.0). (E) Mean relative level +/- SE of syn-tasiRNA (Col-0 *35S:TAS3aPDS-2* = 1.0). Inset shows small RNA blot data. (F) GUS activity in seedlings of Col-0 plants transformed with the indicated constructs. (G) Organization of *HA-AGO7*. (H) Mean relative levels +/- SE of syn-tasiRNA with blot images for miR390 and syn-tasiRNA from one replicate (*35S:MIR390a* + *35S:TAS3aPDS-2* + *35S:HA-AGO7* = 1.0) from a transient assay in *N. benthamiana*.

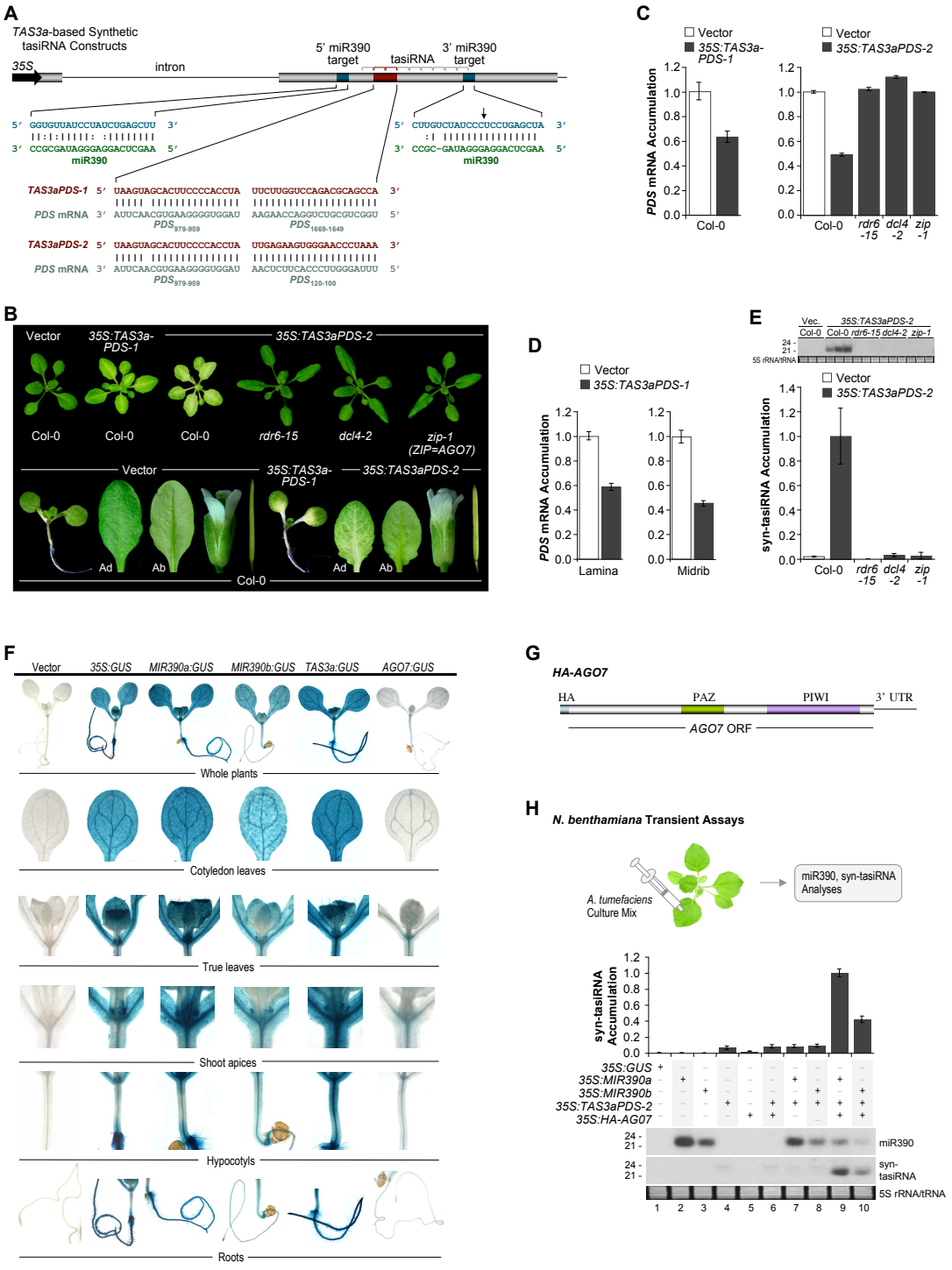

Figure 3.1. Functionality and genetic requirements of *TAS3a*-based syn-tasiRNA.

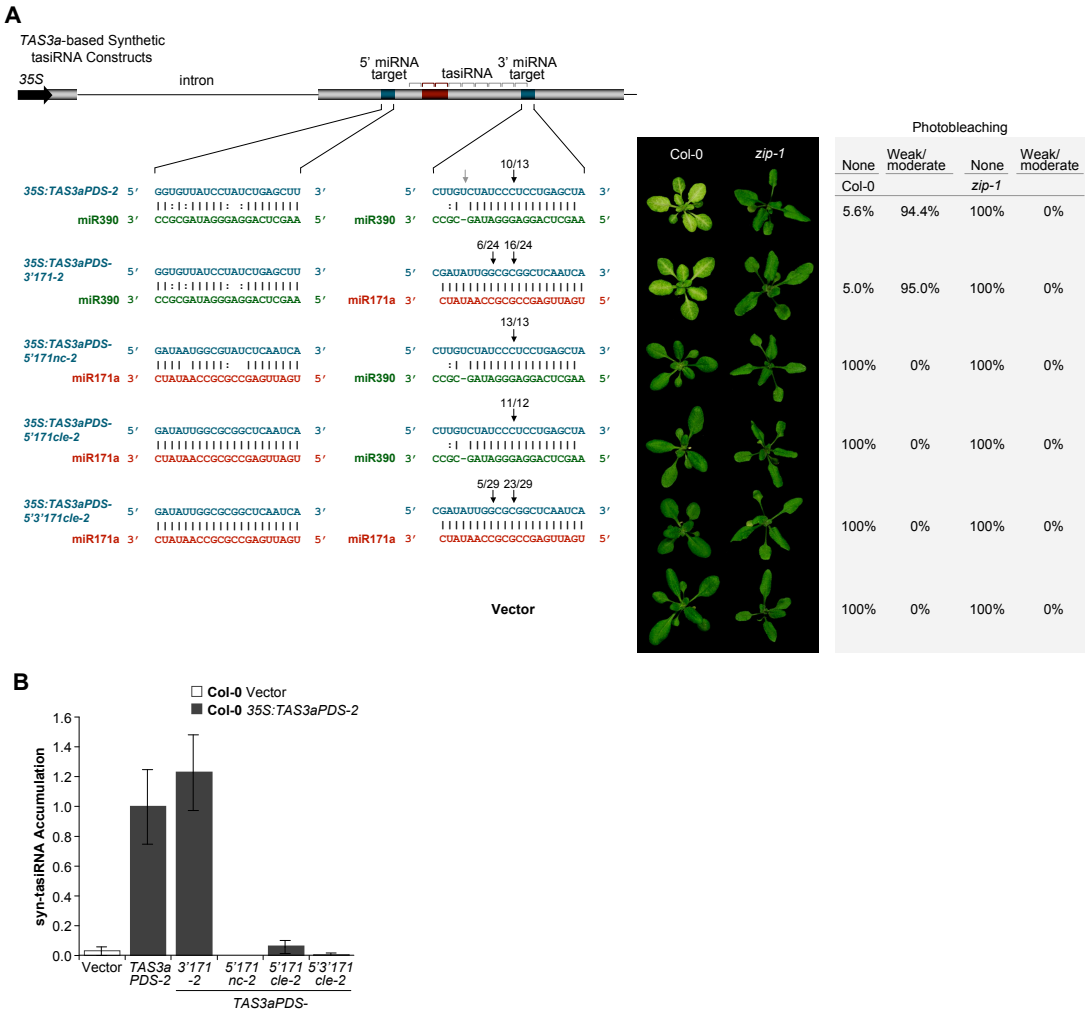

Figure 3.2. Requirement and specificity of miR390 for syn-tasiRNA formation. (A) The 3' and/or 5' miR390 target sites in *35S:TAS3aPDS-2* were substituted for miR171 target sites. The proportion of cloned 5'RACE products corresponding to cleavage at the canonical position at each target site in Col-0 plants is indicated above the black arrows. 5' RACE products from non-canonical positions at each target site are indicated by grey arrows, although proportions are not indicated. The percentages of plants that displayed photobleaching are shown next to representative images of rosettes (for each line, $n \geq 5$ primary transformants analyzed). (B) Mean relative level ± SE of syn-tasiRNA (Col-0 *35S:TAS3aPDS-2* = 1.0).

Figure 3.3. AGO7 and miR390 requirements for processing of *TAS3a*-derived transcripts. (A) 5' RACE assay of cleavage of endogenous *TAS3a* transcripts. (B) Schematic for transient expression assay in *N. benthamiana*. (C) RNA blot assays for small RNAs, with mean relative levels +/- SEs of syn-tasiRNA and blot images shown for one replicate (*35S:MIR171a* + *35S:MIR390a* + *35S:TAS3aPDS-2* + *35S:HA-AGO7* = 1.0). (D) 5' RACE assay of miRNA-guided cleavage. Mean relative levels +/- SEs of 3' cleavage product accumulation corresponding to cleavage at the 3' miRNA target sites, with gel images shown for one replicate (*35S:MIR171a* + *35S:MIR390a* + *35S:TAS3aPDS-2* + *35S:HA-AGO7* = 1.0). (E) Summary of miR390 and AGO7 requirements for cleavage and syn-tasiRNA formation in modified *TAS3a*-based syn-tasiRNA transcripts.

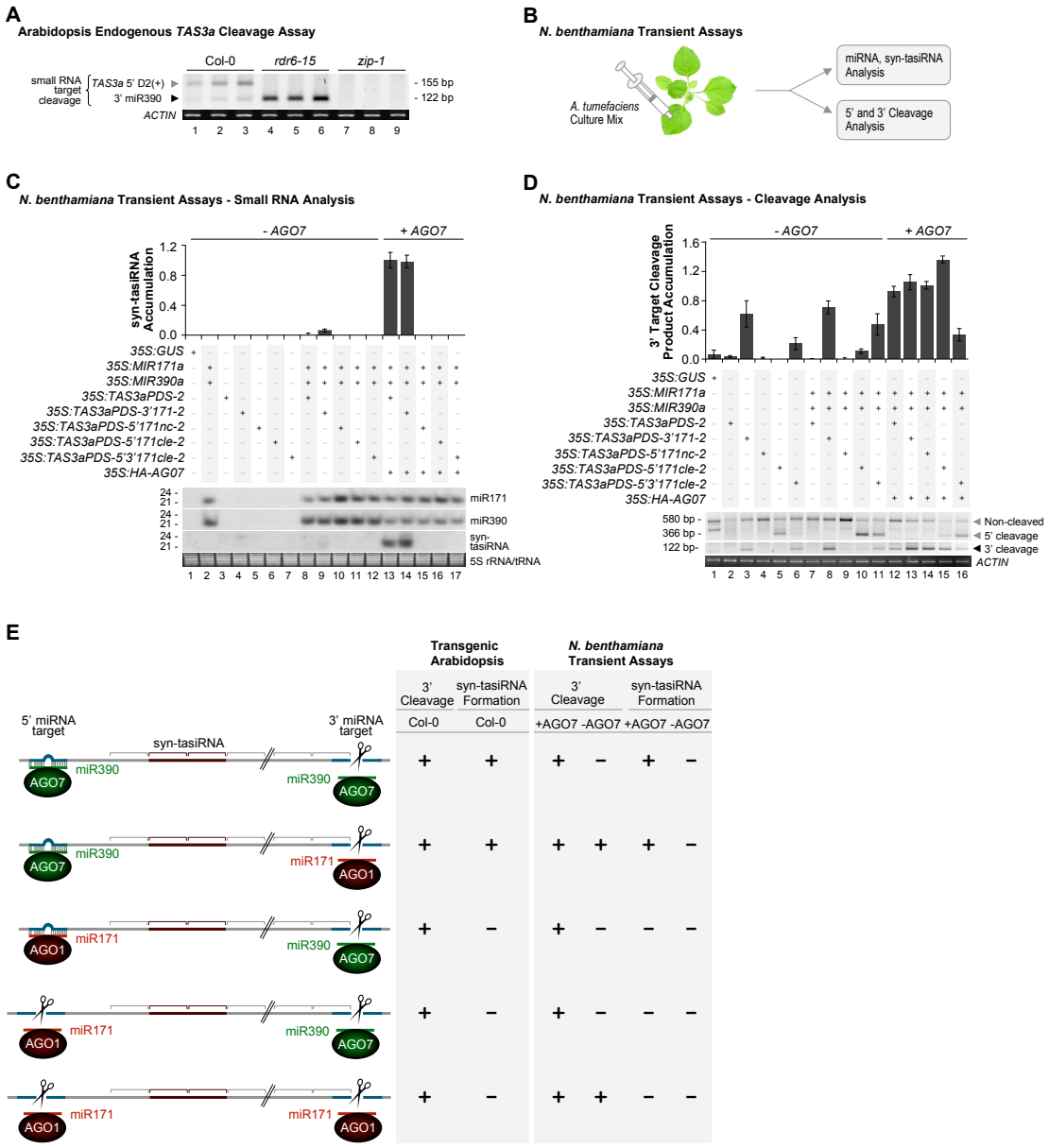

Figure 3.3. AGO7 and miR390 requirements for processing of *TAS3a*-derived transcripts.

Figure 3.4. Small RNA interactions with AGO1, AGO2 and AGO7. (A) Wild-type (Col-0) and *zip-1* vector- and *AGO7:HA-AGO7*-transformed plants. Mean +/- SE of leaf blade length/petiole length ratios for leaves 1 – 6 ($n \geq 17$ for each line) are shown in the line graph. Mean relative levels +/- SE of *TAS3a* tasiRNA (Col-0 vector-transformed = 1.0) are shown in the bar graph. (B) Analysis of Arabidopsis small RNA populations associated with HA-AGO7. Protein and RNA blot assays using input (in) and HA-AGO7 IP (HA) fractions are on the right of the flowchart. Enrichment or depletion of the indicated miRNA and tasiRNA families in the HA-AGO7 IP fraction relative to the input fraction is shown in the lower graph. (C) Protein and RNA blot assays using input (in) and IP (HA) fractions from *N. benthamiana* following co-expression of empty vector or *35S:HA-AGO7* and *35S:TAS3aPDS-2* or *35S:TAS1cPDS-2,* and various 35S-promoter driven *MIRNA* constructs. (D) Protein and RNA blot assays using input (in) and IP (HA) fractions from *N. benthamiana* following co-expression of empty vector, *35S:HA-AGO1, 35S:HA-AGO7*, or *35S:HA-AGO2* and various 35S-promoter driven *MIRNA* constructs. (E) Enrichment or depletion of the indicated miRNA and tasiRNA families in the Arabidopsis HA-AGO2 IP fraction relative to the input fraction. Underrepresentation ranged from -1.1 to -255 fold, but the display was limited at -6.0. Families for which no reads were obtained from one fraction, but for which at least 14 reads were obtained in the other fraction, are marked with an asterisk.

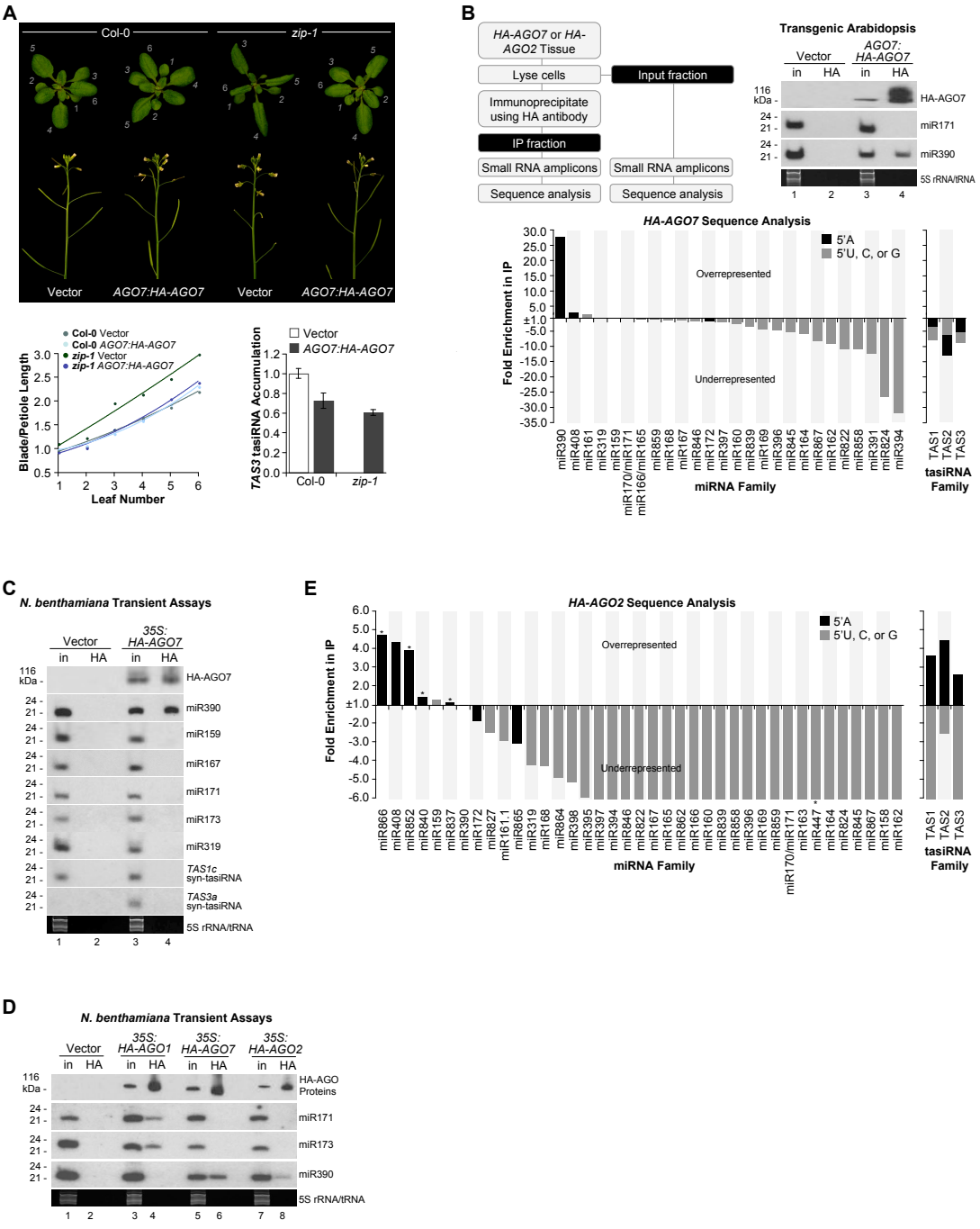

Figure 3.4. Small RNA interactions with AGO1, AGO2 and AGO7.

Figure 3.5. Specificity determinants for AGO1, AGO2 and AGO7. (A) Predicted foldbacks of *MIR171a* and *MIR390a* mutant and chimeric constructs. (B) Protein and RNA blot assays using input (in) and IP (HA) fractions from *N. benthamiana* following co-expression of empty vector, *35S:HA-AGO1*, *35S:HA-AGO7*, or *35S:HA-AGO2* and 35S-promoter driven parental or mutant *MIR171a* and *MIR390a* constructs. (C) RNA blot assays for miR390 and syn-tasiRNA from *N. benthamiana* assays. Mean relative levels +/- SE of syn-tasiRNA are shown with blot images for one replicate (*35S:MIR390a* + *35S:TAS3aPDS-2* + *35S:HA-AGO7* = 1.0). (D and E) Protein and RNA blot assays using input (in) and IP (HA) fractions of leaf tissue extracts from *N. benthamiana* following co-expression of empty vector, *35S:HA-AGO1*, or *35S:HA-AGO7* and 35S-promoter driven *MIR171a*, *MIR390a*, or *MIR171a*/*MIR390a* chimeric constructs.

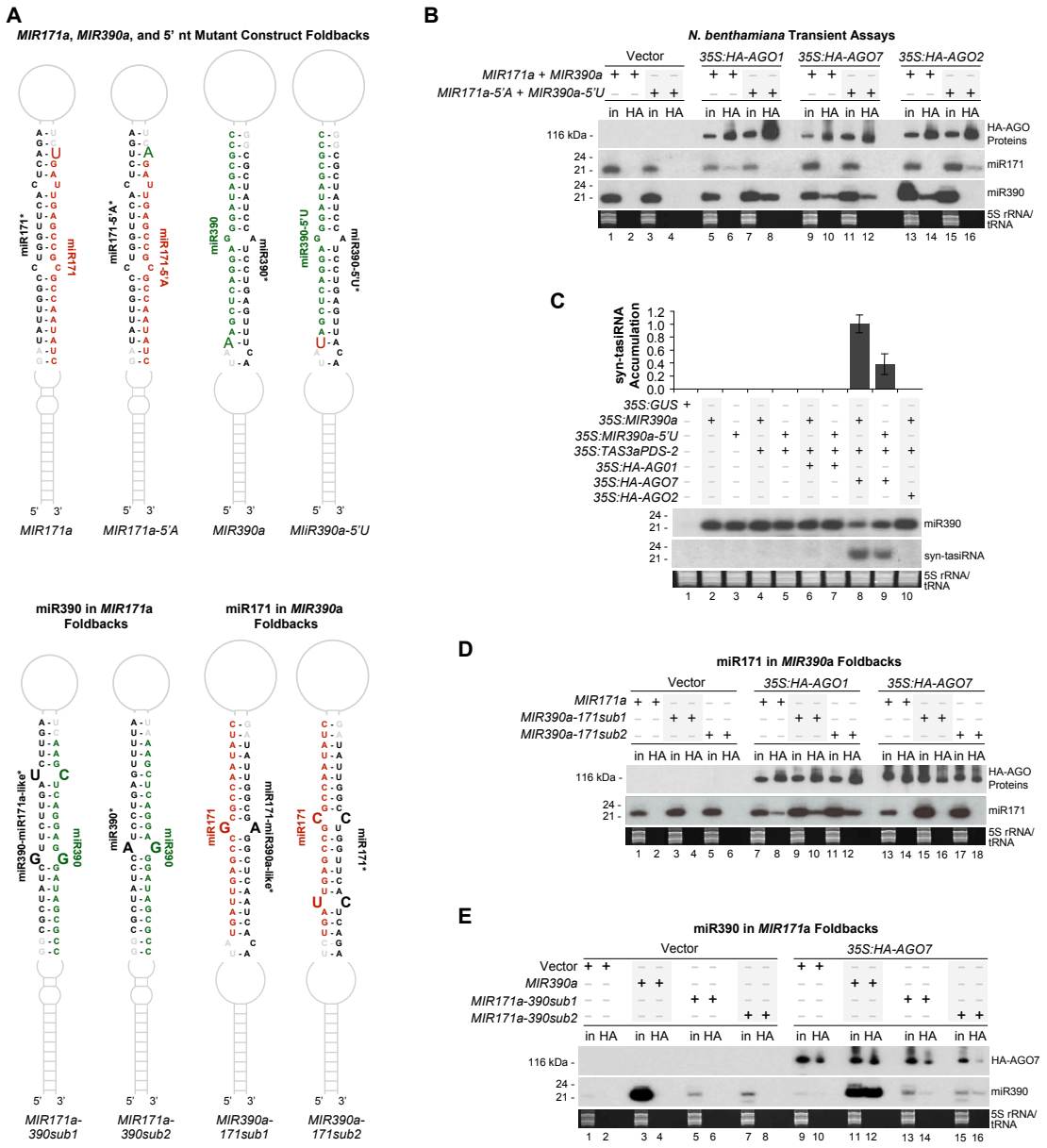

Figure 3.5. Specificity determinants for AGO1, AGO2 and AGO7.

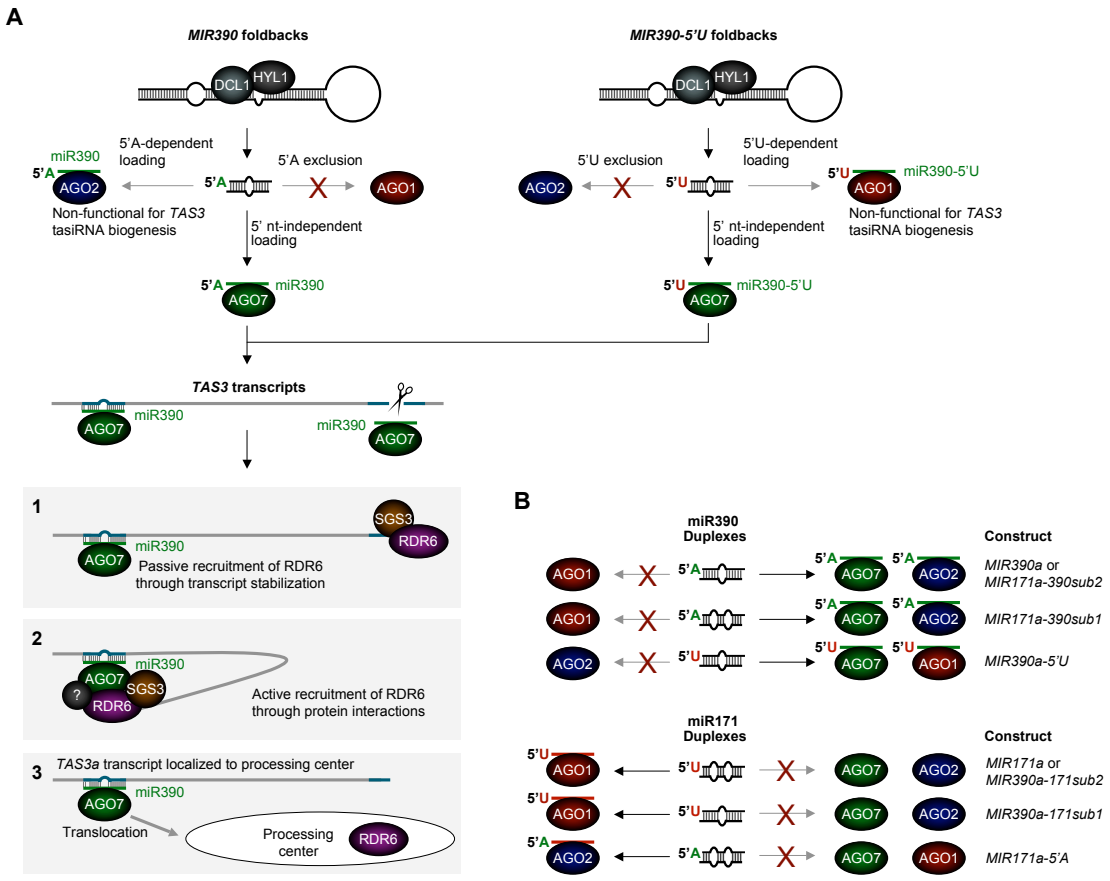

Figure 3.6. miR390-AGO specificity and three models for recruitment of RDR6 to *TAS3* transcripts. (A) 5' nucleotide specificity rules apply to AGO1 and AGO2, but not AGO7. Three models (1-3) to explain how the 5' miR390-AGO7 complex recruits RDR6 to *TAS3* transcripts are shown in the shaded boxes. (B) Summary of AGO specificity for miRNA derived from each of the *MIR171a* and *MIR390a* 5' substitution and chimeric constructs (Figure 3.5A).

SUPPLEMENTAL DATA
SUPPLEMENTAL RESULTS AND EXPERIMENTAL PROCEDURES

Synthetic tasiRNA Construct Design

All *TAS3a*-based syn-tasiRNA sequences were substituted at positions occupied by tasiR2141 and tasiR2142. Therefore, developmental defects associated with missexpression of active *TAS3* tasiRNAs was avoided. (Adenot et al., 2006; Allen et al., 2005; Fahlgren et al., 2006; Garcia et al., 2006; Hunter et al., 2006; Williams et al., 2005). The various syn-tasiRNA sequences were designed to target distinct regions of *PDS* transcripts and to avoid potential off-targeting effects. The syn-tasiRNA in the 5'D8(+) position was the same in both syn-tasiRNA constructs so that the specific contribution of syn-tasiRNA in the 5'D7(+) position could be assessed. Only siRNAs containing 5' ends from the thermodynamic (Gibbs free energy) weak ends of duplex intermediates were developed (Khvorova et al., 2003; Schwarz et al., 2003), although strand-asymmetry rules may not apply rigorously to tasiRNAs (Rajagopalan et al., 2006). The two *TAS3a*-based syn-tasiRNA constructs were distinguished with a *-1* (*35S:TAS3aPDS-1*) or *-2* (*35S:TAS3aPDS-2*) suffix. Mutated forms of the *35S:TAS3aPDS-2* construct were also given a *-2* suffix, however, mutant forms of the *35S:TAS3aPDS-1* construct were not given a suffix.

Transgene Primer Sequences

All *MIRNA* sequences were PCR-amplified from genomic DNA using Pfu Ultra polymerase (Stratagene) and forward primers that lie 250 nt upstream from the 5' end of the miRNA sequence and reverse primers that lie 250 nt downstream from the 3' end of

the miRNA sequence (primer sequences available on request). The *TAS1c* and *TAS3a* transcribed regions, and *MIR390a*, *MIR390b*, *TAS3a*, and *AGO7* and *AGO2* upstream regulatory sequences were amplified from genomic DNA using Pfu Ultra polymerase (Stratagene) and the following primers: TAS1c_F [caccAAACCTAAACCTAAACGGCTAAGC] and TAS1c_R [ATTTCACTTTACGATGTGGTG]; TAS3a_F [caccAGAGAGAGAAGAGCTCCCATGG] and TAS3a_R [CCTTACCCCCTTTAATTTTGTTGC]; MIR390a_Prom_F [caccCTGACCGGTAAATTGGCAATAGAC] and MIR390a_Prom_R [TTGGGTTGTGACTTAGAGAAAGATA]; MIR390b_Prom_F [caccGCATGCAGATTATTCTCTCAGATAT] and MIR390b_Prom_R [CTACTCAATCTGAAATTTACATCCAT]; TAS3a_Prom_F [caccCTCAGGTTTTTTTTGTTTGTCTTTGG] and TAS3a_Prom_R [GAGAGAGAGAGAAATAGAAAACAG]; AGO7_Prom_F [caccTGTCTCTTCTTCTGTACATGC] and AGO7_Prom_R [TTTTCTTCCATGGCTGCTG]; AGO2_Prom_F [caccGATTCCGGGAGAGAGTTCCC] and AGO2_Prom_R [TGGATCTGATCGGGAAACACTG] (note that “cacc” sequences at the beginning of forward (F) primers were included for cloning purposes). The *AGO7* ORF was amplified from cDNA in frame with an N-terminal triple-HA epitope tag using the following primers: 3XHA-AGO7_F [caccATGGCCTATCCTTATGATGTACCTGATTATGCCTACCCATACGACGTTCC

AGACTACGCTTACCCATACGACGTTCCAGACTACGCTGAAGAAAAAACTCAT CATCATC] and AGO7_3920_R [GGAAACTTTAGGAGTCCCTAC]. A portion of the *AGO7* genomic sequence, including 3' regulatory sequence, was amplified from genomic DNA and ligated to an internal EcoRI site in the AGO7 cDNA sequence to generate a full-length ORF clone with authentic 3' regulatory sequence (primers: 3XHA-AGO7_F [caccATGGCCTATCCTTATGATGTACCTGATTATGCCTACCCATACGACGTTCC AGACTACGCTTACCCATACGACGTTCCAGACTACGCTGAAGAAAAAACTCAT CATCATC] and AGO7_+416_R [GGTTGAAAGTTTGGCCTTGA]). The *AGO2* coding region was amplified from genomic DNA in frame with an N-terminal triple-HA epitope tag using the following primers: 3XHA-AGO2_F [caccATGTATCCTTATGATGTACCTGATTATGCCTACCCATACGACGTTCCAGA CTACGCTTACCCATACGACGTTCCAGACTACGCTGAGAGAGGTGGTTATCGA GGAGGTCG] and AGO2-3'UTR_R [AGCAAAATATGAAATAATTA]. The *AGO1* ORF was amplified from cDNA in frame with an N-terminal triple-HA epitope tag using the following primers: 3XHA-AGO1_F [caccATGGCCTATCCTTATGATGTACCTGATTATGCCTACCCATACGACGTTCC AGACTACGCTTACCCATACGACGTTCCAGACTACGCTGTGAGAAAGAGAAGA ACGGATGC] and AGO1_R [TCAGCAGTAGAACATGACAC].

TAS3a-based Syn-tasiRNA 3' Target Site Substitutions

3' miR171 and miR159 target sites were designed to resemble authentic *SCL* (At2g45160, At3g60630, and At4g00150) and *MYB* (At3g11440 and At5g06100) targets, respectively (Llave et al., 2002b; Palatnik et al., 2003).

Tissue and RNA Isolation, and Primer Sequences for Quantitative PCR

RNA samples were treated with DNaseI (Ambion) and reverse transcribed using Superscript III (Invitrogen) and oligo(dT) primer. Multiplexed, quantitative RT-PCR was done using *PDS*- and *ACT2*-specific primers. Amplification products from the experimentally determined linear range were analyzed. For comparison of *PDS* levels in lamina and midrib tissue in Col-0 vector- and *35S:TAS3aPDS-1*-transformed plants, the midribs from expanded leaves were dissected out of the leaf blades and RNA was isolated from the midrib and the non-midrib leaf tissue. The following *PDS* and *ACT2* primers were used for multiplexed quantitative RT-PCR: PDS_F [GAACAACGAGATGCTGACATG] and PDS_R [TTCCAGGGATCTGGTAAAAGGAG]; ACT2_F [GCCATCCAAGCTGTTCTCTC] and ACT2_R [GAACCACCGATCCAGACACT].

RNA Blot Assays

For small RNA blot assays, total RNA (10 ug) was resolved by denaturing polyacrylamide-gel electrophoresis in parallel with positively hybridizing RNA standards and transferred to positively-charged membranes. 5S rRNA and tRNA were stained using EtBr to confirm equal loading of RNA and uniform transfer to membranes.

Oligonucleotide probes were end-labeled using ^{32}P-ATP and Optikinase (USB) and hybridized to membranes. Hybridization signals were measured using an Instant Imager (Packard Bioscience).

5' RACE Assay Primer Sequences

The following gene-specific PCR primers were used for 5' RACE Assays: TAS3a_3'_target_5'_RACE [CATACATCAATAACAAACAAAAGATATATG]; TAS3a_5'_target_5'_RACE [TGGACCAAGAATAGGTGGGGAAGTGC].

SUPPLEMENTAL TABLES

Table S3.1. Free energy of miRNA/5' target interactions in syn-tasiRNA constructs.

Construct	miRNA	delta G (kcal/mol)
35S:TAS3aPDS-1[a]	miR390	-13.41
35S:TAS3aPDS-5'390mut	miR390	-1.94
35S:TAS3aPDS-5'390cle	miR390	-29.8
35S:TAS3aPDS-5'159nc	miR159	-13.91
35S:TAS3aPDS-5'167nc	miR167	-13.76
35S:TAS3aPDS-5'169nc	miR169	-15.26
35S:TAS3aPDS-5'171nc	miR171	-12.07
35S:TAS3aPDS-5'173nc	miR173	-15.77

[a]The delta G value for *35S:TAS3aPDS-1* is identical to that of endogenous *TAS3a*.

Table S3.2. Total reads and proportion of total miRNA+tasiRNA reads for each miRNA and tasiRNA family from HA-AGO7 input and IP fractions.

		Input Fraction		IP Fraction	
miRNA	Locus	Reads	Proportion of Total[a]	Reads	Proportion of Total[b]
miR156	a,b,c,d,e,f	2	0.000196	0	0.000000
miR156	g	0	0.000000	0	0.000000
miR156	h	0	0.000000	0	0.000000
miR157	a,b,c,d	0	0.000000	0	0.000000
miR158	a	18	0.001760	0	0.000000
miR158	b	1	0.000098	0	0.000000
miR159	a	5044	0.493252	7928	0.557289
miR159	b	754	0.073734	2188	0.153803
miR159	c	0	0.000000	1	0.000070
miR160	a,b,c	98	0.009583	47	0.003304
miR161.1	a	196	0.019167	819	0.057571
miR161.2	a	56	0.005476	23	0.001617
miR162	a,b	33	0.003227	5	0.000351
miR163	a	36	0.003520	19	0.001336
miR164	a,b	62	0.006063	14	0.000984
miR164	c	0	0.000000	0	0.000000
miR165	a,b	22	0.002151	28	0.001968
miR166	a,b,c,d,e,f,g	185	0.018091	179	0.012583
miR167	a,b	1092	0.106787	862	0.060593
miR167	c	0	0.000000	0	0.000000
miR167	d	0	0.000000	0	0.000000
miR168	a,b	621	0.060728	512	0.035990
miR169	a	37	0.003618	7	0.000492
miR169	b,c	2	0.000196	3	0.000211
miR169	d,e,f,g	0	0.000000	2	0.000141
miR169	h,i,j,k,l,m,n	1	0.000098	0	0.000000
miR170	a	2	0.000196	7	0.000492
miR171	a	25	0.002445	32	0.002249
miR171	b,c	1	0.000098	0	0.000000
miR172	a,b	111	0.010855	78	0.005483
miR172	c,d	5	0.000489	1	0.000070
miR172	e	0	0.000000	1	0.000070
miR173	a	2	0.000196	0	0.000000
miR319	a,b	258	0.025230	477	0.033530
miR319	c	17	0.001662	31	0.002179
miR390	a,b	12	0.001173	462	0.032476
miR391	a	9	0.000880	1	0.000070
miR393	a,b	0	0.000000	2	0.000141
miR394	a,b	23	0.002249	1	0.000070
miR395	a,d,e	1	0.000098	1	0.000070

miR395	b,c,f	1	0.000098	3	0.000211
miR396	a	5	0.000489	6	0.000422
miR396	b	90	0.008801	21	0.001476
miR397	a	0	0.000000	0	0.000000
miR397	b	18	0.001760	11	0.000773
miR398	a	0	0.000000	0	0.000000
miR398	b,c	1	0.000098	0	0.000000
miR399	a	0	0.000000	0	0.000000
miR399	b,c	1	0.000098	0	0.000000
miR399	d	0	0.000000	0	0.000000
miR399	e	0	0.000000	0	0.000000
miR399	f	2	0.000196	1	0.000070
miR400	a	0	0.000000	0	0.000000
miR402	a	0	0.000000	0	0.000000
miR403	a	4	0.000391	0	0.000000
miR408	a	24	0.002347	102	0.007170
miR447	a,b	11	0.001076	3	0.000211
miR447	c	0	0.000000	0	0.000000
miR472	a	0	0.000000	0	0.000000
miR771	a	0	0.000000	0	0.000000
miR773	a	2	0.000196	0	0.000000
miR774	a	0	0.000000	0	0.000000
miR775	a	0	0.000000	0	0.000000
miR776	a	1	0.000098	0	0.000000
miR777	a	3	0.000293	0	0.000000
miR778	a	0	0.000000	0	0.000000
miR779	a	0	0.000000	0	0.000000
miR780	a	1	0.000098	1	0.000070
miR781	a	2	0.000196	0	0.000000
miR822	a	8	0.000782	1	0.000070
miR823	a	2	0.000196	0	0.000000
miR824	a	193	0.018873	10	0.000703
miR825	a	3	0.000293	1	0.000070
miR826	a	0	0.000000	0	0.000000
miR827	a	3	0.000293	0	0.000000
miR828	a	0	0.000000	0	0.000000
miR829	a	1	0.000098	0	0.000000
miR830	a	0	0.000000	0	0.000000
miR831	a	0	0.000000	0	0.000000
miR832	a	0	0.000000	0	0.000000
miR833	a	0	0.000000	0	0.000000
miR834	a	0	0.000000	0	0.000000
miR835	a	0	0.000000	0	0.000000
miR836	a	0	0.000000	0	0.000000

miR837	a	0	0.000000	0	0.000000
miR838	a	0	0.000000	0	0.000000
miR839	a	36	0.003520	13	0.000914
miR840	a	0	0.000000	2	0.000141
miR841	a	0	0.000000	0	0.000000
miR842	a	0	0.000000	0	0.000000
miR843	a	0	0.000000	0	0.000000
miR844	a	0	0.000000	0	0.000000
miR845	a	90	0.008801	26	0.001828
miR845	b	26	0.002543	4	0.000281
miR846	a	11	0.001076	8	0.000562
miR847	a	0	0.000000	0	0.000000
miR848	a	0	0.000000	0	0.000000
miR849	a	0	0.000000	0	0.000000
miR850	a	0	0.000000	0	0.000000
miR851	a	17	0.001662	0	0.000000
miR852	a	0	0.000000	0	0.000000
miR853	a	0	0.000000	0	0.000000
miR856	a	0	0.000000	0	0.000000
miR857	a	0	0.000000	0	0.000000
miR858	a	8	0.000782	1	0.000070
miR859	a	5	0.000489	5	0.000351
miR860	a	5	0.000489	0	0.000000
miR861	a	0	0.000000	0	0.000000
miR862	a	2	0.000196	1	0.000070
miR863	a	0	0.000000	0	0.000000
miR864	a	1	0.000098	0	0.000000
miR865	a	0	0.000000	0	0.000000
miR866	a	0	0.000000	0	0.000000
miR867	a	36	0.003520	6	0.000422
miR868	a	0	0.000000	0	0.000000
miR869	a	0	0.000000	4	0.000281
miR870	a	0	0.000000	0	0.000000

		Input Fraction		IP Fraction	
tasiRNA	Locus	Reads	Proportion of Total[a]	Reads	Proportion of Total[b]
TAS1	a,b,c	200	0.019558	84	0.005905
TAS2	a	515	0.050362	145	0.010193
TAS3	a,b,c	172	0.016820	36	0.002531
TAS4	a	0	0.000000	0	0.000000

[a]Total miRNA+tasiRNA reads for the HA-AGO7 input fraction was 10,226.

[b]Total miRNA+tasiRNA reads for the HA-AGO7 IP fraction was 14,226.

Table S3.3. Total reads and proportion of total miRNA+tasiRNA reads for each miRNA and tasiRNA family from HA-AGO2 input and IP fractions.

		Input Fraction		IP Fraction	
miRNA	Locus	Reads	Proportion of Total[a]	Reads	Proportion of Total[b]
miR156	a,b,c,d,e,f	6	0.000163	0	0.000000
miR156	g	0	0.000000	0	0.000000
miR156	h	0	0.000000	0	0.000000
miR157	a,b,c,d	0	0.000000	0	0.000000
miR158	a	18	0.000490	1	0.000002
miR158	b	1	0.000027	0	0.000000
miR159	a	22238	0.604770	175143	0.389743
miR159	b	2415	0.065677	220489	0.490650
miR159	c	1	0.000027	132	0.000294
miR160	a,b,c	453	0.012319	99	0.000220
miR161.1	a	520	0.014142	2454	0.005461
miR161.2	a	76	0.002067	63	0.000140
miR162	a,b	42	0.001142	2	0.000004
miR163	a	464	0.012619	50	0.000111
miR164	a,b	213	0.005793	21	0.000047
miR164	c	1	0.000027	0	0.000000
miR165	a,b	49	0.001333	15	0.000033
miR166	a,b,c,d,e,f,g	406	0.011041	94	0.000209
miR167	a,b	1603	0.043594	530	0.001179
miR167	c	0	0.000000	0	0.000000
miR167	d	4	0.000109	13	0.000029
miR168	a,b	1822	0.049550	5254	0.011692
miR169	a	47	0.001278	8	0.000018
miR169	b,c	5	0.000136	0	0.000000
miR169	d,e,f,g	5	0.000136	1	0.000002
miR169	h,i,j,k,l,m,n	1	0.000027	0	0.000000
miR170	a	3	0.000082	0	0.000000
miR171	a	67	0.001822	9	0.000020
miR171	b,c	5	0.000136	0	0.000000
miR172	a,b	228	0.006201	1549	0.003447
miR172	c,d	11	0.000299	34	0.000076
miR172	e	0	0.000000	1	0.000002
miR173	a	3	0.000082	0	0.000000
miR319	a,b	1592	0.043295	4861	0.010817
miR319	c	89	0.002420	61	0.000136
miR390	a,b	45	0.001224	536	0.001193
miR391	a	6	0.000163	0	0.000000
miR393	a,b	1	0.000027	0	0.000000
miR394	a,b	91	0.002475	81	0.000180
miR395	a,d,e	15	0.000408	11	0.000024

miR395	b,c,f	0	0.000000	20	0.000045
miR396	a	26	0.000707	9	0.000020
miR396	b	127	0.003454	15	0.000033
miR397	a	2	0.000054	0	0.000000
miR397	b	233	0.006337	254	0.000565
miR398	a	1	0.000027	0	0.000000
miR398	b,c	4	0.000109	12	0.000027
miR399	a	0	0.000000	0	0.000000
miR399	b,c	4	0.000109	0	0.000000
miR399	d	0	0.000000	0	0.000000
miR399	e	0	0.000000	0	0.000000
miR399	f	1	0.000027	0	0.000000
miR400	a	0	0.000000	0	0.000000
miR402	a	0	0.000000	0	0.000000
miR403	a	4	0.000109	0	0.000000
miR408	a	198	0.005385	10686	0.023779
miR447	a,b	34	0.000925	0	0.000000
miR447	c	0	0.000000	0	0.000000
miR472	a	0	0.000000	0	0.000000
miR771	a	2	0.000054	0	0.000000
miR773	a	1	0.000027	0	0.000000
miR774	a	0	0.000000	0	0.000000
miR775	a	0	0.000000	1	0.000002
miR776	a	6	0.000163	0	0.000000
miR777	a	2	0.000054	0	0.000000
miR778	a	1	0.000027	0	0.000000
miR779	a	0	0.000000	0	0.000000
miR780	a	2	0.000054	0	0.000000
miR781	a	1	0.000027	2	0.000004
miR822	a	24	0.000653	13	0.000029
miR823	a	5	0.000136	0	0.000000
miR824	a	577	0.015692	47	0.000105
miR825	a	9	0.000245	2	0.000004
miR826	a	0	0.000000	1	0.000002
miR827	a	2	0.000054	10	0.000022
miR828	a	0	0.000000	0	0.000000
miR829	a	0	0.000000	0	0.000000
miR830	a	0	0.000000	0	0.000000
miR831	a	0	0.000000	0	0.000000
miR832	a	0	0.000000	0	0.000000
miR833	a	0	0.000000	0	0.000000
miR834	a	0	0.000000	0	0.000000
miR835	a	1	0.000027	0	0.000000
miR836	a	0	0.000000	0	0.000000

miR837	a	0	0.000000	14	0.000031
miR838	a	2	0.000054	2	0.000004
miR839	a	47	0.001278	9	0.000020
miR840	a	0	0.000000	18	0.000040
miR841	a	0	0.000000	0	0.000000
miR842	a	0	0.000000	0	0.000000
miR843	a	2	0.000054	3	0.000007
miR844	a	0	0.000000	5	0.000011
miR845	a	196	0.005330	10	0.000022
miR845	b	67	0.001822	10	0.000022
miR846	a	12	0.000326	8	0.000018
miR847	a	0	0.000000	0	0.000000
miR848	a	6	0.000163	0	0.000000
miR849	a	0	0.000000	0	0.000000
miR850	a	0	0.000000	0	0.000000
miR851	a	10	0.000272	0	0.000000
miR852	a	0	0.000000	48	0.000107
miR853	a	1	0.000027	1	0.000002
miR856	a	0	0.000000	0	0.000000
miR857	a	1	0.000027	0	0.000000
miR858	a	25	0.000680	4	0.000009
miR859	a	13	0.000354	2	0.000004
miR860	a	2	0.000054	0	0.000000
miR861	a	0	0.000000	0	0.000000
miR862	a	4	0.000109	1	0.000002
miR863	a	0	0.000000	0	0.000000
miR864	a	2	0.000054	5	0.000011
miR865	a	1	0.000027	4	0.000009
miR866	a	0	0.000000	58	0.000129
miR867	a	160	0.004351	11	0.000024
miR868	a	0	0.000000	0	0.000000
miR869	a	7	0.000190	0	0.000000
miR870	a	0	0.000000	0	0.000000

		Input Fraction		IP Fraction	
tasiRNA	Locus	Reads	Proportion of Total[a]	Reads	Proportion of Total[b]
TAS1	a,b,c	441	0.011993	11023	0.024529
TAS2	a	1520	0.041337	14164	0.031519
TAS3	a,b,c	439	0.011939	1392	0.003098
TAS4	a	0	0.000000	5	0.000011

[a]Total miRNA+tasiRNA reads for the HA-AGO2 input fraction was 36,772.

[b]Total miRNA+tasiRNA reads for the HA-AOG2 IP fraction was 449,381.

Figure S3.1. Requirement and specificity of miR390 at the 3' target site for *TAS3a*-based syn-tasiRNA formation. (A) The 3' miR390 target site in *35S:TAS3aPDS-1* was mutated or substituted for heterologous miRNA target sites. The proportion of cloned 5' RACE products corresponding to cleavage at the canonical position at each target site is indicated above the black arrows. Cleavage events at non-canonical positions at each of the target sites are indicated by grey arrows, although the proportions of 5' RACE products for these are not indicated. The percentages of Col-0 vector- and *35S:TAS3aPDS*-transformed plants that displayed photobleaching (white arrows) are shown next to representative images of rosettes (for each line, $n \geq 18$ primary transformants analyzed). (B) Sense alignment of miR171a with miR171b and miR171c and antisense alignment of miR171a, miR171b, and miR171c with *35S:TAS3aPDS-3'171*. Cleavage guided by miR171b and miR171c occurs 3 bases upstream (5') from cleavage guided by miR171a.

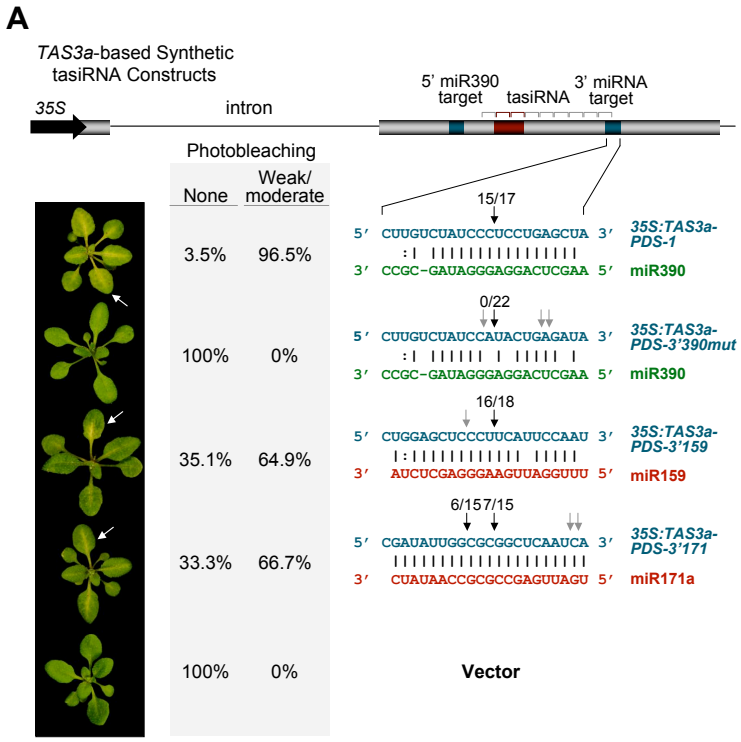

Figure S3.1. Requirement and specificity of miR390 at the 3' target site for *TAS3a*-based syn-tasiRNA formation.

Figure S3.2. Requirement and specificity of miR390 at the 5' target site for *TAS3a*-based syn-tasiRNA formation. (A) The 5' miR390 target of *35S:TAS3aPDS-1* was mutated to be non-functional (*35S:TAS3aPDS-5'390mut*) or substituted for predicted non-cleavable sites designed to be recognized by heterologous miRNA. The proportion of cloned 5' RACE products showing cleavage at the canonical position at each target site is indicated above the black arrows. 5' RACE products from non-canonical positions at each target site are indicated by grey arrows, although the proportions of 5' RACE products for these are not indicated. The percentages of plants that displayed photobleaching (white arrow) are shown next to representative images of rosettes (for each line $n \geq 30$ primary transformants analyzed). (B) RNA blot assay for small RNA generated upstream (5') and downstream (3') of the 5' miRNA target sites. Probes for 3' and 5' regions of 35S:*TAS3aPDS*-based constructs are indicated by horizontal dashed arrows in the schematic in (A).

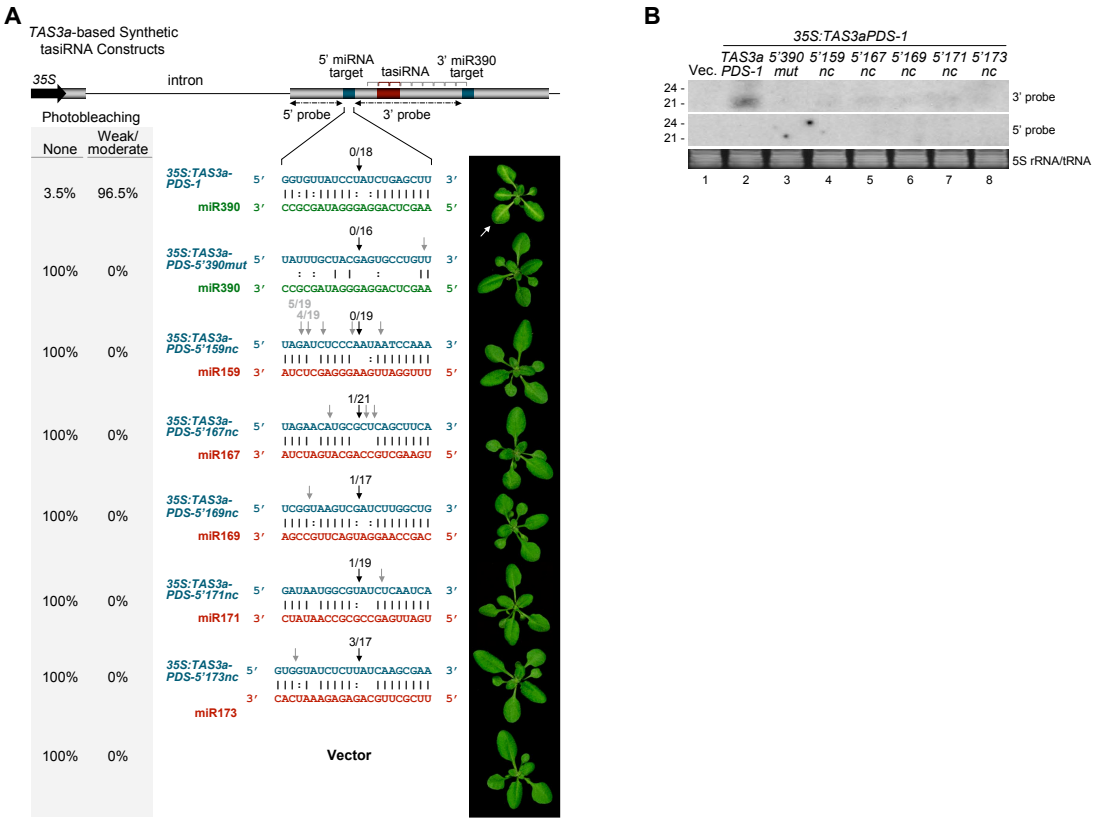

Figure S3.2. Requirement and specificity of miR390 at the 5' target site for *TAS3a*-based syn-tasiRNA formation.

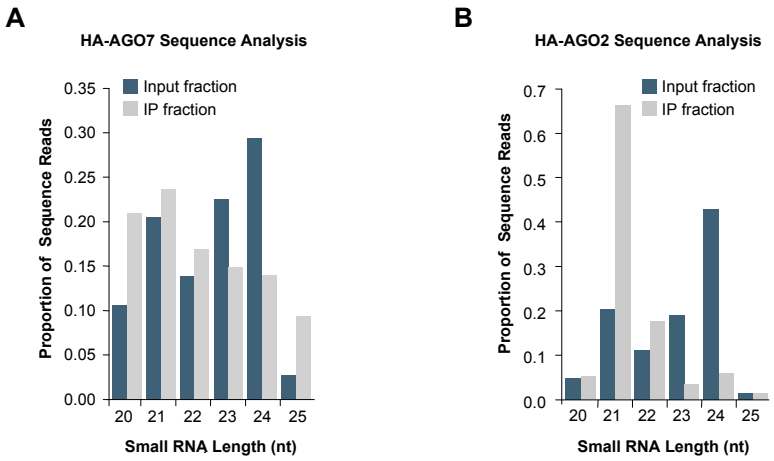

Figure S3.3. **Small RNA size distribution in HA-AGO7 and HA-AGO2 input and IP fractions from Arabidopsis.** (A) HA-AGO7 sequence analysis. Proportions of total 20-25 nt small RNA are shown for each of the indicated size classes. (B) HA-AGO2 sequence analysis**.**

CHAPTER 4

Specificity of miR173-Guided Initiation Cleavage for Trans-Active siRNA Formation in Plants

Taiowa A. Montgomery, Seong Jeon Yoo, Noah Fahlgren, Sunny D. Gilbert, Miya D. Howell, Amanda Alexander, Goretti Nguyen, Christopher M. Sullivan, Edwards Allen, and James C. Carrington

In preparation for submission.

ABSTRACT

miRNA-guided cleavage initiates entry of primary transcripts into the trans-acting siRNA (tasiRNA) biogenesis pathway involving RNA-DEPENDENT RNA POLYMERASE6 (RDR6), DICER-LIKE 4 (DCL4), and SUPPRESSOR OF GENE SILENCING3 (SGS3). *Arabidopsis thaliana TAS1* and *TAS2* families yield tasiRNA that form through miR173-guided initiation cleavage on the 5' side of the siRNA-generating regions. *TAS1* and *TAS2* tasiRNA target several transcripts encoding pentatricopeptide repeat (PPR) proteins and proteins of unknown function. Here, the *TAS1c* locus was modified to produce synthetic (syn) tasiRNA to target an endogenous transcript encoding PHYTOENE DESATURASE (PDS), and used to test the unique requirement for miR173 in routing *TAS1c* transcripts through the tasiRNA pathway. miR173 was unique from other miRNA in its ability to initiate *TAS1c*-based syn-tasiRNA formation. Surprisingly, targeting by miR173 was sufficient to route non-*TAS* transcripts into the tasiRNA pathway as well. AGO1 was previously shown to associate with miR173. We show that AGO1 is required for *TAS1* and *TAS2* tasiRNA formation, indicating that the miR173-AGO1 complex functions in a distinct mode from other miRNA-AGO1 complexes.

INTRODUCTION

MicroRNA (miRNA) and trans-acting short interfering RNA (tasiRNA) are formed through distinct biogenesis pathways, although both function posttranscriptionally to guide endonucleolytic cleavage or translational repression of target RNA transcripts (Chapman and Carrington, 2007; Filipowicz et al., 2008). For miRNA, self-complementary foldback structures within primary transcripts (usually RNA polymerase II products) are processed into ~21 nt miRNA/miRNA* duplexes. In plants, this likely occurs on nascent transcripts bound to the cap binding complex (CBC), and involves the combined activities of the zinc-finger protein SERRATE (SE), the RNaseIII-type enzyme DICER-LIKE1 (DCL1), and the double-stranded RNA binding protein HYPONASTIC LEAVES1 (HYL1) (Grigg et al., 2005; Han et al., 2004; Laubinger et al., 2008; Park et al., 2002; Reinhart and Bartel, 2002). For tasiRNA in plants, primary transcripts are first processed by miRNA-guided cleavage at initiation sites. One of the products is stabilized, possibly by SUPPRESSOR OF GENE SILENCING3 (SGS3), and converted to dsRNA by RNA-DEPENDENT RNA POLYMERASE6 (RDR6) (Allen et al., 2005; Peragine et al., 2004; Vazquez et al., 2004b; Yoshikawa et al., 2005). The resulting double-stranded RNA is processed sequentially by DICER-LIKE4 (DCL4) into 21 nt siRNA duplexes in register with the miRNA-guided cleavage site (Gasciolli et al., 2005; Xie et al., 2005b; Yoshikawa et al., 2005).

One strand of each miRNA or tasiRNA duplex is selectively sorted to one or more ARGONAUTE (AGO) proteins according to the 5' nucleotide or other sequence/structural elements of the small RNA (Mi et al., 2008; Montgomery et al.,

2008; Takeda et al., 2008). AGO proteins, which contain a 3' RNA binding domain (PAZ), a central domain that confers small RNA recognition or binding function, and an RNaseH-like domain (PIWI) (Tolia and Joshua-Tor, 2007), provide the effector component for silencing complexes. Null alleles for factors essential for miRNA formation, such as DCL1, are embryonic lethal. In contrast, mutations in tasiRNA specific factors, such as RDR6, SGS3, and DCL4, display only modest patterning and developmental timing defects (Gasciolli et al., 2005; Peragine et al., 2004; Xie et al., 2005b; Yoshikawa et al., 2005), which are due primarily to misregulation of *TAS3* tasiRNA targets (Adenot et al., 2006; Fahlgren et al., 2006; Garcia et al., 2006; Hunter et al., 2006).

Arabidopsis thaliana has eight characterized tasiRNA-generating (*TAS*) loci belonging to four families. *TAS1* and *TAS2* tasiRNA target multiple different mRNAs, including several encoding pentatricopeptide repeat (PPR) proteins (Allen et al., 2005; Axtell et al., 2006; Chen et al., 2007; Howell et al., 2007; Peragine et al., 2004; Vazquez et al., 2004b). *TAS4* tasiRNA target mRNA encoding several MYB transcription factors (Rajagopalan et al., 2006). *TAS3* tasiRNA target *AUXIN RESPONSE FACTORs* (*ARF3* and *ARF4*), which function in adaxial/abaxial patterning of lateral organs and developmental timing (Adenot et al., 2006; Allen et al., 2005; Alvarez et al., 2006; Fahlgren et al., 2006; Garcia et al., 2006; Hunter et al., 2006; Pekker et al., 2005). In addition to its role in development via the tasiRNA pathway, the RDR6/SGS3/DCL4 silencing pathway contributes to antiviral defense and posttranscriptional transgene

silencing (Beclin et al., 2002; Dalmay et al., 2000; Deleris et al., 2006; Mourrain et al., 2000; Muangsan et al., 2004).

Aside from initiation cleavage events, it is not clear how transcripts are routed into the RDR6/SGS3/DCL4 silencing pathway. It was recently shown that transcripts with two or more miRNA and/or tasiRNA target sites are more likely to spawn RDR6- and DCL4-dependent siRNA (Axtell et al., 2006; Howell et al., 2007) than are singly targeted transcripts, suggesting a role for multiple small RNA-directed cleavage or small RNA-associated factors to mark transcripts for passage through this pathway. The *TAS3a* primary transcript is an example of a dual-targeted RNA, in which miR390-AGO7 complexes provide distinct functions at two target sites. The miR390-AGO7 complex associates with a target site near the 5' end of the transcript in a non-cleavage, presumably stable, mode. The miR390-AGO7 complex also interacts with a site near the 3' end to affect cleavage. The primary requirement for miR390-AGO7 at the 3' target site is cleavage, and this can be affected by other miRNA-AGO complexes (such as miR171-AGO1) in modified constructs. Interaction at the 5' target site, however, appears to involve a non-replaceable, specialized function of miR390-AGO7 (Montgomery et al., 2008). These features were accommodated in a model stating that the stable miR390-AGO7 complex marks the transcript for routing (that is, recognition by RDR6) once the 3' end has been cleaved.

The *TAS3* family is highly conserved in land plants, whereas *TAS1*, *TAS2* and *TAS4* families are restricted to Arabidopsis or close relatives (Allen et al., 2005; Axtell et al., 2006; Axtell et al., 2007; Rajagopalan et al., 2006; Talmor-Neiman et al., 2006; Vazquez

et al., 2004b). Unlike *TAS3* transcripts, *TAS1*, *TAS2*, and *TAS4* transcripts each have only a single known miRNA target site. miR173 functions to initiate tasiRNA biogenesis from *TAS1* and *TAS2* loci, whereas miR828 serves to initiate *TAS4* tasiRNA formation. These three families also differ from *TAS3* in that the tasiRNA-generating regions in *TAS1*, *TAS2* and *TAS4* transcripts originate from the RNA fragment on the 3' side of the cleavage site (Allen et al., 2005; Rajagopalan et al., 2006; Yoshikawa et al., 2005). Thus, the mechanism of *TAS1*, *TAS2*, and *TAS4* tasiRNA formation may suggest a distinct route into the RDR6/SGS3/DCL4 silencing pathway. In this paper, the *TAS1c* locus was manipulated to explore the cis-requirements for tasiRNA formation. The results indicate that miR173 has a unique ability to trigger phased tasiRNA from *TAS1* and *TAS2* transcripts, and from synthetic transcripts containing an ectopic miR173 target site, in the absence of a second small RNA target site. miR173 functions through association with AGO1 during *TAS1* and *TAS2* tasiRNA formation, indicating that the AGO1-miR173 complex functions in a distinct mode from other AGO1-miRNA complexes.

RESULTS

TAS1c-Based Synthetic tasiRNA

A hallmark of tasiRNA biogenesis is formation of phased arrays of siRNA from an initiation point defined by miRNA-guided cleavage of a *TAS* primary transcript. The predictable pattern of tasiRNA formation from the cleavage site has been exploited previously to develop synthetic (syn) tasiRNA from modified *TAS* genes (Montgomery et al., 2008). *TAS3a*-based syn-tasiRNA that targeted the mRNA encoding PHYTOENE

DESATURASE (PDS) were effectively used to dissect *TAS3* tasiRNA biogenesis and effector requirements (Montgomery et al., 2008). We developed a similar system based on a modified *TAS1c* locus, in which sequences at the 3'D3(+) and 3'D4(+) positions at processing cycles 3 and 4 from the miR173-guided initiation site were substituted for syn-tasiRNA sequences with perfect or near perfect complementarity to two sites within PDS mRNA (Figures 4.1A and 4.1E). The 3'D3(+) and 3'D4(+) positions normally yield active tasiRNAs that target transcripts encoding proteins of unknown function (Allen et al., 2005; Peragine et al., 2004; Vazquez et al., 2004b). Each of three syn-tasiRNA genes (*35S:TAS1cPDS-1, -2,* and *-3*) contained the same syn-tasiRNA at the 3'D3(+) position, but a different syn-tasiRNA at the 3'D4(+) position. Each syn-tasiRNA was designed to possess a 5' uridine, which promotes association with AGO1(Mi et al., 2008; Montgomery et al., 2008; Takeda et al., 2008). Each construct was expressed using the 35S promoter and introduced into wild-type and mutant *Arabidopsis thaliana* plants. Mapping of both authentic *TAS1c* and *35S:TAS1cPDS-2* transcripts revealed the dominant poly(A) site at position 810 nt from the transcription start site (Figure S4.1A) (Allen et al., 2005), indicating that the *TAS1c*-based syn-tasiRNA constructs contained the authentic *TAS1c* 3' terminator sequence.

The majority of wild-type (Col-0) plants transformed with each *TAS1c*-based syn-tasiRNA construct displayed a photobleached phenotype, a characteristic of PDS silencing, although there was variation in phenotype severity among individual transformants (Figure 4.1B; Table 4.1). The photobleached phenotype was concurrent with accumulation of syn-tasiRNA and a significant reduction in *PDS* mRNA levels

(Bonferroni corrected $p < 0.05$, two-sample t-test) (Figures 4.1C and 4.1D). To test the genetic requirements of *TAS1c*-based syn-tasiRNAs, *dcl4-2*, *rdr6-15*, and *zip-1* mutants were transformed with each of the *TAS1c*-based syn-tasiRNA constructs. In *zip-1* mutants, which lack AGO7, the photobleached phenotype was indistinguishable from that in Col-0 plants, whereas photobleaching was undetectable in *rdr6-15* and *dcl4-2* mutants (Figure 4.1B; Table 4.1). *PDS* mRNA was reduced to similar levels in *35S:TAS1cPDS-2*-transformed Col-0 and *zip-1* plants, but unchanged in *rdr6-15* and *dcl4-2* mutants, relative to vector-transformed Col-0 plants (Figure 4.1C). Syn-tasiRNA were detected in Col-0 and *zip-1* plants, but not in *rdr6-15* and *dcl4-2* plants, transformed with each construct (Figure 4.1D; Table 4.1). Relative *PDS* mRNA and syn-tasiRNA levels were not significantly different between Col-0 and *zip-1 35S:TAS1cPDS-2*-transformed plants ($p = 0.23$ and 0.29, respectively, two-sample t-tests) (Figures 4.1C and 4.1D). These results indicate that *TAS1c*-based syn-tasiRNA have genetic requirements similar to those of authentic *TAS1* tasiRNA, and are distinguishable from *TAS3* tasiRNA by the lack of a requirement for AGO7 (Adenot et al., 2006; Allen et al., 2005; Fahlgren et al., 2006; Gasciolli et al., 2005; Hunter et al., 2006; Peragine et al., 2004; Vazquez et al., 2004b; Xie et al., 2005b; Yoshikawa et al., 2005).

A potential application of syn-tasiRNA is silencing of genes in a wide-range of plant species. However, miR173 is only known to exist in Arabidopsis (Jones-Rhoades et al., 2006). To determine if *TAS1c*-based syn-tasiRNA could be generated in a species lacking miR173, a dual-gene construct that delivers both *MIR173* and syn-tasiRNA (*35S:TAS1cPDS/MIR173*, with a unique set of PDS mRNA-targeting syn-tasiRNA) was

tested in *Nicotiana benthamiana* leaves using transient delivery assays (Figure 4.1E) (Llave et al., 2002b). The dual-gene construct yielded both miR173 and syn-tasiRNAs with efficiency similar to coexpression of the independent constructs *35S:TAS1cPDS-4* and *35S:MIR173* ($p = 0.43$ and 0.50, respectively, two-sample t-test) (Figures 4.1F and 4.1G; Table 4.1). Expression of *35S:TAS1cPDS-4* alone failed to yield syn-tasiRNA (Figure 4.1G; Table 4.1). In transgenic Arabidopsis Col-0 plants, both *35S:TAS1cPDS-4* and *35S:TAS1cPDS-4/MIR173* constructs resulted in similar patterns of photobleaching (Figure 4.1H; Table 4.1). No photobleaching or developmental defects were observed in Col-0 plants transformed with *35S:MIR173* alone (data not shown). Thus, a single-construct, dual-gene system can expand *TAS1c*-based syn-tasiRNA technology to non-Arabidopsis species.

Role of miR173 in *TAS1c*-Based syn-tasiRNA Formation

miR173 guides initiation cleavage of *TAS1* and *TAS2* transcripts. To determine if miR173 possesses unique properties that facilitate tasiRNA initiation, or if miR173 provides simply a generic guide function for transcript cleavage, syn-tasiRNA constructs were developed in which the miR173 target site in *35S:TAS1cPDS-2* was substituted for miR169 (*35S:TAS1cPDS-169*), miR171 (*35S:TAS1cPDS-171*), miR390 (*35S:TAS1cPDS-390*), or miR167 (*35S:TAS1cPDS-167*) target sites. The substitutions were designed to mimic authentic miRNA target sites, except *35S:TAS1cPDS-169* and *35S:TAS1cPDS-167*, which were designed to have perfect complementarity to miR169 and miR167, respectively (Figure 4.2A). Each target site, however, conformed to "rules" for miRNA-

guided cleavage. Each heterologous miRNA has been shown to accumulate to relatively high levels in Col-0 inflorescence, seedling and leaf tissues (Axtell et al., 2006; Fahlgren et al., 2007; Rajagopalan et al., 2006; Xie et al., 2005b). Transgenic Col-0 and *rdr6-15* plants containing each construct were analyzed.

In contrast to plants expressing the miR173-targeted *35S:TAS1cPDS-2* construct, no photobleaching was detected in Col-0 plants transformed with *35S:TAS1cPDS-169*, *35S:TAS1cPDS-171*, or *35S:TAS1cPDS-390* constructs (Figure 4.2A). Rarely, weak photobleaching was observed in Col-0 plants transformed with the *35S:TAS1cPDS-167* construct (data not shown). *PDS* mRNA levels were reduced in lines with the miR173-targeted construct, but were not significantly affected in the miRNA-target site substitution lines ($p > 0.46$, two-sample t-tests) (Figure 4.2B). Syn-tasiRNAs failed to accumulate to detectable levels in leaf tissue of Col-0 *35S:TAS1cPDS-169*-, *35S:TAS1cPDS-171*-, and *35S:TAS1cPDS-390*-transformed plants (Figure 4.2C), although in flower tissue, syn-tasiRNA from each of these constructs accumulated to low levels (data not shown).

To determine if the heterologous target sites were functional in transformed plants, cleavage at each site was tested using RNA ligase-mediated 5' RACE (Llave et al., 2002b). PCR products with 5' ends corresponding to positions of canonical miRNA-guided cleavage were detected in Col-0 plants transformed with each construct, although the levels of 5'RACE products detected were highest in *35S:TAS1cPDS-2*- and *35S:TAS1cPDS-171*-transformed plants (Figures 4.2A and 4.2D).

The *35S:TAS1cPDS-2* and *35S:TAS1cPDS-171* constructs were examined in more detail in *N. benthamiana* leaves in combination with *35S:MIR173* or *35S:MIR171a*, which produce active miR173 and miR171, respectively (Montgomery et al., 2008) (Figure 4.3A). Syn-tasiRNA were efficiently generated from *35S:TAS1cPDS-2* transcripts and were dependent on coexpression of *35S:MIR173* (Figure 4.3B; lanes 4-5). In contrast, *35S:TAS1cPDS-171* failed to generate syn-tasiRNAs when coexpressed with either *35S:MIR171a* alone or with a combination of *35S:MIR171a* and *35S:MIR173* (Figure 4.3B; lanes 7-9). To determine if the miR171 target site was functional in the transient assay, cleavage was tested using RNA blot and 5' RACE assays. Cleavage of the *35S:TAS1cPDS-2* transcript was dependent on coexpression of *35S:MIR173* (Figure 4.3C; lanes 7-10, and 4.3D; lanes 1-4). With the *35S:TAS1cPDS-171* construct, cleavage was detected in leaves that coexpressed *35S:MIR171a*, but also at lower levels in leaves that lacked *35S:MIR171a* (Figures 4.3C; lanes 11-14, and 4.3D; lanes 5-8). As shown previously (Llave et al., 2002b; Montgomery et al., 2008), *N. benthamiana* contains active miR171 that functions on ectopically expressed target transcripts. Therefore, failure to form miR171-initiated syn-tasiRNAs in Arabidopsis and *N. benthamiana* was not due to a lack of cleavage.

TAS1 and *TAS2* transcripts normally yield tasiRNA from the 3' RNA fragment generated by miR173-guided cleavage. To determine if miR171 initiated aberrant entry of the 5' fragment into the tasiRNA pathway, RNA blot assays were done using probes corresponding to the regions directly 5' or 3' of the miR173 and miR171 target site of *35S:TAS1cPDS-2* and *35S:TAS1cPDS-171*, respectively, in the *N. benthamiana* transient

system. Using the parental construct, siRNAs from the 3' side (corresponding to the tasiRNA region), but not from the 5' side, of the miR173 target were detected (Figure 4.3B; lane 5). In contrast, targeting by miR171 failed to trigger siRNA formation from either side of the target site (Figure 4.3B; lanes 7 and 9). Collectively, these data indicate that miR173 and/or associated factors possess unique properties that facilitate directional routing of cleaved *TAS1c* RNA precursor into the tasiRNA biogenesis pathway.

miR173 Triggers Phased siRNA Formation from Non-*TAS* Transcripts

TAS3 transcripts in Arabidopsis require two miR390 target sites – one that is cleaved by miR390-AGO7, and one that is not cleaved but that associates with miR390-AGO7 (Axtell et al., 2006; Howell et al., 2007; Montgomery et al., 2008). Only a single miR173 target site has been identified in each of the *TAS1* and *TAS2* transcripts (Allen et al., 2005; Yoshikawa et al., 2005). To determine if a single miR173 target site is sufficient to directionally route a transcript into the tasiRNA pathway, a series of synthetic target sites were fused to 425 bases of smGFP coding sequence. In addition to a construct with a functional miR173 target site (*35S:GFP-173*), constructs containing either a defective miR173 target site resulting from four additional target-miR173 mispairs (*35S:GFP-173mut*) or a functional miR171 target site (*35S:GFP-171*) were made (Figure 4.4A). The resulting constructs were expressed alone or in combination with either *35S:MIR173* or *35S:MIR171a* in *N. benthamiana* leaves. As a syn-tasiRNA control, *35S:TAS1cPDS-2* was coexpressed with *35S:MIR173*. Strikingly, the *35S:GFP-173* construct containing a functional miR173 site, as well as the *35S:TAS1cPDS-2* control, yielded siRNA

specifically when coexpressed with *35S:MIR173* (Figure 4.4B; lanes 3, 6, and 7). The *35S:GFP-173mut* construct failed to yield *GFP* siRNA when coexpressed with *35S:MIR173,* indicating that miR173-guided cleavage is likely necessary (Figure 4.4B; lane 8). The *35S:GFP-171* construct also failed to yield *GFP* siRNA, even when coexpressed with ectopic *35S:MIR171a* (Figure 4.4B; lanes 4 and 5). Both the *35S:GFP-173* and *35S:GFP-171* transcripts were efficiently cleaved at the predicted miR173- or miR171-guided cleavage sites, as determined by 5' RACE and RNA blot assays (Figures 4.4A and 4.4B). No miR173-guided cleavage was detected with *35S:GFP-173mut* transcript (Figure 4.4A).

To determine if the *GFP* siRNA from *35S:GFP-173* transcript (coexpressed with *35S:MIR173*) were phased and in register with the miR173-guided cleavage site, as are authentic *TAS1* and *TAS2* tasiRNA, small RNA from the *N. benthamiana* transient assay were sequenced (Figure 4.4C) using deep sequencing-by-synthesis (SBS) technology (Illumina 1G) (Montgomery et al., 2008). Small RNA reads with perfect matches to either the *35S:GFP-173* transcript, or the hygromycin resistance gene (HYG^R) transcript from the base plasmid, were identified and quantified. *35S:GFP-173*-derived reads were predominantly 21 nt, whereas *35S:*HYG^R-derived reads were nearly evenly distributed between the 21 and 24 nt size classes (Figure S4.2). To assess tasiRNA-like phasing, 21 nt small RNA reads from both strands were consolidated into one set of values by summing sense and antisense reads that were offset by 2 nt (Howell et al., 2007). This accounts for the known properties of DICER and DICER-LIKE enzymes, which leave a 2 nt, 3' overhang at each end of a small RNA duplex (Elbashir et al., 2001). Consolidated

reads from across the *GFP-173* and *HYG*^{R} transcripts were plotted (Figures 4.4D and 4.4E).

Approximately 98% of all 21 nt small RNA reads from *35S:GFP-173* originated to the 3' side of the miR173 target site. This region contained a series of distinct peaks, separated by 21 nt increments and clustered just downstream of the miR173 target site, extending for 5 processing cycles with at least 367 reads each (Figure 4.4D). A similarly spaced pattern of peaks was not detected from *35S:HYG*^{R} (Figure 4.4E). Approximately 60% of total (13,384) 21 nt reads from *35S:GFP-173* were in 21 nt register with the cleavage site, although 78% of these were from the second phase cycle relative to the target site (Figure 4.4D; Table S4.1). When this highly-abundant position was removed from the analysis, 25% of the remaining reads were in phase with the miR173-guided cleavage site; no other 21 nt phase exceeded 8% of the total reads in the depleted dataset. Small RNA reads from *35S:HYG*^{R} were evenly distributed across the 21 possible registers, with no more than 8% of the total reads coming from any single registry (Figure 4.4E; Table S4.2). These results indicate that miR173, functioning through a single target site, is sufficient to initiate phased siRNA formation in a directional manner.

Search for Additional cis-Elements for *TAS1c* syn-tasiRNA Biogenesis

Although the *35S:GFP-173* results indicate the sufficiency of a single miR173 target site, it is possible that authentic *TAS1* and *TAS2* tasiRNA formation is enhanced by additional cis-regulatory elements. To test for such sequences in the *TAS1c* locus, a series of internal and 5' and 3' end deletions were made of *35S:TAS1cPDS-2* (Figures 4.5A and S4.1A).

The internal deletions were designed to preserve the predominant tasiRNA-yielding region and the authentic poly(A) signal (Figure 4.5A). The predominant tasiRNA-yielding region of *TAS1c* was identified using Col-0 leaf and whole plant small RNA sequencing data obtained from ASRP (Backman et al., 2007). 21 nt sense and antisense reads from *TAS1c* were consolidated as described above and plotted across the *TAS1c* transcript. tasiRNA are effectively produced from 8 processing cycles downstream of the miR173-guided cleavage site, although, processing becomes offset by 1 nt at position 3'D4 (Figure 4.5A) (Howell et al., 2007). In one construct, the *TAS1c* sequence from positions 550-750 nt relative to the transcription start site, was replaced with an equally sized portion of smGFP coding sequence (*35S:TAS1cPDS-550-750gfp*). Three additional constructs were made with internal deletions that spanned positions 550-650 nt, 550-700 nt, and 550-750 nt, relative to the transcription start site (*35S:TAS1cPDS-550-650del, 35S:TAS1cPDS-550-700del,* and *35S:TAS1cPDS-550-750del*) (Figure 4.5A). Each construct was expressed alone or in combination with *35S:MIR173* in *N. benthamiana* leaves. When coexpressed with *35S:MIR173*, *35S:TAS1cPDS-550-750gfp* yielded syn-tasiRNA at levels indistinguishable from the parental *35S:TAS1cPDS-2* construct ($p = 0.19$, two-sample t-test) (Figure 4.5B). However, deleting positions 550-750 nt significantly reduced syn-tasiRNA formation (Bonferroni corrected $p < 0.05$, two-sample t-test). Deletions at positions 550-650 nt and 550-700 nt resulted in a modest reduction in syn-tasiRNA formation, relative to the parental construct (Figure 4.5B). In each case where a reduction in syn-tasiRNA was observed, a proportional reduction in transcript

accumulation was observed, suggesting that the length or structure of the transcript may affect its stability (Figure 4.5B).

Deleting the entire *TAS1c*-derived sequence upstream (5') of the miR173 target site did not significantly affect syn-tasiRNA levels ($p = 0.68$, two-sample t-test) (Figure S4.1B). Additional deletions were made at the 3' end of *35S:TAS1cPDS-2* ranging from positions 662-837 nt relative to the transcription start site (Figure S4.1A). Each of the *35S:TAS1cPDS-2* constructs with 3' deletions yielded syn-tasiRNA, although both syn-tasiRNA and transcript levels were reduced proportionally in constructs with deletions upstream of position 762 nt (Figures S4.1B and S4.1C). For this series of constructs, the region affecting transcript accumulation may be involved with 3' termination, as the dominant poly(A) site is located at position 810.

Consistent with previous studies (Yoshikawa et al., 2005), only weak similarity was identified between the three *TAS1* loci and the *TAS2* locus outside of the tasiRNA yielding region. However, an 8 nt motif (TTTGTAAT) was identified near the 3' ends of the tasiRNA generating regions of the all *TAS1* and *TAS2* loci. This motif occurs at least twice at each locus (data not shown). In *TAS1c*, the motif occurs first at position 714 nt, and secondly at position 744 nt, relative to the transcription start site. This motif could conceivably be involved in transcript accumulation, as the deletions upstream of position 762 nt cause a reduction in transcript levels (Figure S4.1C). A 61 nt segment of *TAS1c*, 702-762 nt downstream of the transcription start site and encompassing both of the TTTGTAAT motifs, was introduced at the 3' end of *35S:GFP-173*. The resulting construct (*35S:GFP-173tttg*) was coexpressed with or without *35S:MIR173* in *N.*

benthamiana leaves. The levels of miR173-dependent siRNA from the GFP sequence were indistinguishable from those measured using *35S:GFP-173* (Figure 4.4B), indicating that the TTTGTAAT motifs and other sequences tested do not contribute to tasiRNA formation, or that they do not function in the context tested.

miR173-AGO1 Complexes Function in *TAS1* and *TAS2* Initiation Cleavage

Each of the Arabidopsis *TAS1* and *TAS2* miR173 targets has a mispair at position 9, relative to the 5' end of the miRNA, although the nucleotide at this position differs between the target sites. In *TAS1b*, there is an additional mispair at position 10 (Figure S4.3A). miRNA-guided cleavage occurs between positions 10 and 11 and mispairs at either of these positions are rare (Allen et al., 2005; Ossowski et al., 2008). Aside from miR173 targets in *TAS1* and *TAS2*, mispairs at position 9 are also relatively uncommon (Allen et al., 2005; Ossowski et al., 2008). Conceivably, these mispairs could facilitate tasiRNA formation by stabilizing an AGO complex at the target site long enough for RDR6 recruitment to occur, without compromising cleavage. To test this possibility, the mispair at position 9 of the miR173 target site in *35S:TAS1cPDS-2* was repaired to generate a target site with perfect complementarity to miR173 aside from a single G:U pair at position 15, relative to the 5' end of miR173 (*35S:TAS1cPDS-173fix*) (Figure S4.3B). Additionally, a mispair was introduced at position 9, relative to miR171, of the miR171-targeted construct *35S:TAS1cPDS-171* (*35S:TAS1cPDS-171-2*) to mimic the basepair composition of authentic miR173-*TAS1* and -*TAS2* target interactions. When coexpressed with *35S:MIR173* in *N. benthamiana* leaves, *35S:TAS1cPDS-173fix* yielded

syn-tasiRNA at a level similar to *35S:TAS1cPDS-2* (Figure S4.3C; lanes 4-7). In contrast, *35S:TAS1cPDS-171-2* failed to yield syn-tasiRNA even when coexpressed with *35S:MIR171a*, as did *35S:TAS1cPDS-171* (Figure S4.3C; lanes 8-11). Thus, the ability of miR173 to trigger tasiRNA formation is likely more complicated than can be explained by basepair composition between miR173 and *TAS1* and *TAS2* targets.

The genetic requirements of miR173 are similar to those of other miRNA, including dependence on DCL1, HYL1, SE, HEN1, and HST (Figure 4.6B) (Xie et al., 2005a; Yoshikawa et al., 2005). miR173 could have additional biogenesis or effector requirements that distinguish it from other miRNA. miR390 is specifically required for *TAS3* tasiRNA formation due to a unique association with AGO7. Although AGO7 is not required for *TAS1* and *TAS2* tasiRNA formation, it is possible that miR173 has a distinct AGO interaction that facilitates tasiRNA formation. miR173 was shown to associate with AGO1 (Mi et al., 2008; Montgomery et al., 2008), however, it is unclear if miR173-AGO1 is the tasiRNA initiator complex. In *ago1-25*, a weak allele of *AGO1* (Morel et al., 2002), miR173 levels are reduced by ~43% (Figure 4.6B), suggesting that at least a portion of the miR173 population is stabilized through association with AGO1. In contrast, miR390, a miRNA that does not function in association with AGO1, is unaffected (Figure 4.6C). The level of tasiR255, a relatively abundant tasiRNA derived from each of the *TAS1* loci is reduced by ~52% in *ago1-25* (Figure 4.6D) and below detectable levels in *ago1-1*, a null allele of *AGO1* (Adenot et al., 2006). We also tested tasiR255 levels in mutant alleles for each of the other nine AGOs, except AGO6, which functions partially redundantly with AGO4 in transcriptional gene silencing (Zheng et al.,

2007). In each of the other AGO mutants tested, tasiR255 levels were either unaffected or elevated (Figure S4.4). This suggests that AGO1 is the only AGO involved in tasiRNA formation, although, we cannot rule out the possibility that some of the alleles used were weak or that multiple AGOs function redundantly during *TAS1* and *TAS2* tasiRNA formation.

Following processing, tasiRNA are sorted into distinct AGO-complexes (Figure 4.6A). tasiR255 has a 5'U and associates with AGO1 (Baumberger and Baulcombe, 2005; Mi et al., 2008). Thus, although the reduction in tasiR255 in *ago1* mutants could result, at least in part, from defects in tasiRNA formation, it could also be due entirely to destabilization of the mature tasiRNA. To distinguish between these possibilities, we tested *TAS2* 3'D4(+) levels in *ago1-25* and in the *ago1-36*, a likely null allele of AGO1(Baumberger and Baulcombe, 2005). *TAS2* 3'D4(+) contains a 5'A and was shown to associate with AGO2 and to be excluded from AGO1 (Mi et al., 2008). To yield a tasiRNA with a 5'U, *TAS2* 3'D4(+) would have to be misprocessed by at least 4 nt. Furthermore, *TAS2* 3'D4(+) is a relatively abundant tasiRNA, whereas, the 5'U-containing tasiRNA offset by 4 nt is extremely rare (ASRP database) (Backman et al., 2007). *TAS2* 3'D4(+) levels were reduced by ~40% in *ago1-25*, relative to Col-0 ($p < 0.05$, two-sample t-test) and completely absent in *ago1-36* (Figure 4.6E).

To test if the miR173-AGO1 complex is required for cleavage of *TAS1c*, 5' RACE was done using RNA extracts from three independent pools of either Col-0 or *ago1-36* plants. 5' RACE products corresponding to cleavage at the miR173 target site were efficiently detected in each of the Col-0 replicates (Figure 4.6F; lanes 1-3). 5' RACE

products were lost entirely in each of the *ago1-36* replicates (Figure 4.6F). These results indicate that AGO1 is required for initiation cleavage of *TAS1* and *TAS2*.

Deep Sequencing-Based Analysis of AGO1-dependent tasiRNA

To more exhaustively assess AGO1-dependence across tasiRNA loci, small RNA amplicons were prepared from Col-0 and *ago1-25* and sequenced using SBS technology (Figure 4.7A). To account for the relatively weak effect of the *ago1-25* allele, inherent variability in small RNA levels, and to facilitate statistical analyses, three independent biological replicates of both Col-0 and *ago1-25* were tested. In Col-0, mapped small RNA reads were nearly evenly distributed between the 21 and 24 nt size classes, whereas, in *ago1-25*, the 21 nt size class was depleted, causing the 24 nt size class to predominate (Figure S4.6). An average of ~4.0 and ~6.5 million total reads were obtained from each of the Col-0 and *ago1-25* replicates, respectively, comprising at least 10,000 tasiRNA reads each. Small RNA reads in individual libraries were normalized using the total reads/library. Total *TAS1* and *TAS2* tasiRNA were reduced by ~45% in *ago1-25*, relative to Col-0 (Bonferroni corrected $p < 0.05$, two sample t-test). *TAS1* and *TAS2* tasiRNA were differentially affected depending on the 5' nt of both the tasiRNA and its passenger strand (Figures 4.7B, 4.7C, and S4.6A). 5'U-containing tasiRNA reads were reduced by ~56% in *ago1-25*, relative to Col-0 (Bonferroni corrected $p < 0.05$, two sample t-test) (Figure 4.7B). 5'A-, C-, and G-containing tasiRNA were reduced by ~32% in *ago1-25*, relative to Col-0 (Bonferroni corrected $p < 0.05$, two sample t-test), consistent with a requirement for AGO1 in *TAS1* and *TAS2* tasiRNA formation. While the majority of

tasiRNA were reduced in *ago1-25*, tasiRNA containing a 5'A, C, or G and having a passenger strand with a 5'U tended to be upregulated or unaffected (Figure 4.7C). Removing *TAS1* and *TAS2* tasiRNA with 5'U-containing passenger strands from the analysis resulted in a 43% reduction in tasiRNA containing 5'A, C, and G in *ago1-25*, relative to Col-0 (Bonferroni corrected $p < 0.05$, two sample t-test) (Figure 4.7B).

Unlike *TAS1* and *TAS2* tasiRNA formation, *TAS3* tasiRNA formation does not require AGO1, although *TAS3* tasiRNA containing 5'U likely function through association with AGO1 (Mi et al., 2008; Montgomery et al., 2008). Thus, while *TAS3* tasiRNA containing 5'U should be destabilized by the reduced activity of AGO1 in *ago1-25*, *TAS3* tasiRNA containing 5'A, C, and G should be unaffected. Indeed, *TAS3* tasiRNA containing 5'U were reduced by ~58% in *ago1-25* relative to Col-0 (Bonferroni corrected $p < 0.05$, two-sample t-test), whereas the level of tasiRNA containing 5'A, C, and G was unchanged ($p = 0.72$, two-sample t-test) (Figures 4.7D). Some specific *TAS3* tasiRNA containing a 5'A, C, or G, such as tasiR1778 (containing a 5'C) were reduced in *ago1-25* (see Allen et al [2005] for tasiRNA nomenclature). These tasiRNA were typically in phase with cleavage guided by a tasiRNA derived from the complementary strand of *TAS3* (*TAS3a* 5'D2[-]) that was previously shown to associate with AGO1 (Allen et al., 2005; Mi et al., 2008). This is consistent with the requirement for AGO7 at the 5' target site but the ability of AGO1 to substitute at the 3' target site if delivered via an alternate miRNA (or conceivably a tasiRNA) guide (Montgomery et al., 2008).

Total 5'U-containing miRNA were reduced by ~67% in *ago1-25*, relative to Col-0 (Figure 4.7E), although the majority of miRNA reads (~83-90%) were miR159

(Bonferroni corrected $p < 0.05$, two sample t-test) (data not shown). When miR159 was removed from the analysis, the remaining 5'U-containing miRNA were reduced by ~62% in *ago1-25*, relative to Col-0 (Bonferroni corrected $p < 0.05$, two sample t-test). In contrast, miRNA containing 5'C were unaffected ($p = 0.24$, two-sample t-test). Although the majority of individual 5'A-containing miRNA were unaffected in *ago1-25*, the level of miR172a/miR172b, a highly sequenced 5'A-containing miRNA, was reduced by ~55% ($p = 0.006$, two-sample t-test), resulting in an overall reduction in 5'A-containing miRNA (Figure 4.7E). For each of the three known 5'G-contaning miRNA (miR172e, miR416a, and miR861a), too few reads were obtained to assess AGO1-dependence. Based on these results and those of the previous section, we conclude that AGO1 is required for stabilization specifically of 5'U-containing tasiRNA and miRNA, and for the biogenesis of *TAS1* and *TAS2* tasiRNA. That *TAS1* and *TAS2* tasiRNA containing 5'A, C, and G and with passenger strands containing 5'U, are unaffected or upregulated in *ago1-25*, despite an overall reduction in tasiRNA formation, indicates increased stability of these tasiRNA in the absence of AGO1.

DISCUSSION

We developed a *TAS1c*-based syn-tasiRNA system and used it to test the specific requirement for miR173 in *TAS1* and *TAS2* tasiRNA formation. miR173 guides cleavage at *TAS1* and *TAS2* transcripts, defining a discrete 5' end of the pre-tasiRNA transcript and an initiation point for phased siRNA formation by RDR6, SGS3, and DCL4. Heterologous miRNA target site substitutions in the *TAS1c*-based syn-tasiRNA construct

were functional for cleavage, but failed to initiate syn-tasiRNA formation, suggesting that miR173 has additional, unique properties or associated cofactors required for routing transcripts into the RDR6/SGS3/DCL4 silencing pathway. When introduced into GFP coding sequence, the authentic miR173 target site was functional to direct phased siRNA formation downstream of the miR173 target site, but only in the presence of miR173. A similar GFP-based construct with a miR171 target site failed to yield siRNA when provided ectopic miR171. Thus, a single miR173 target site, but not other miRNA target sites, is sufficient to route a transcript into the tasiRNA pathway.

How might miR173 function to route *TAS1* and *TAS2* transcripts into the RDR6/SGS3/DCL4 silencing pathway? There are at least two events – transcript cleavage and recruitment of RDR6 - necessary for efficient transcript routing through this pathway. Transcript cleavage may be necessary to separate the siRNA-generating fragment, which is usually the 3' fragment, from the 5' cap (Gazzani et al., 2004; Herr et al., 2006) (Axtell et al., 2006). This may physically dissociate the fragment from cap-associated factors, such as the cap-binding complex in the nucleus. Most miRNA targets that undergo miRNA-directed cleavage, however, do not spawn siRNA as they are degraded by other mechanisms, such as through the XRN4/EIN5-dependent pathway (Gazzani et al., 2004; Gregory et al., 2008; Olmedo et al., 2006; Souret et al., 2004) (German et al., 2008). Recruitment of RDR6 to the processed transcript prior to degradation, therefore, is a critical prerequisite for siRNA biogenesis. We suggest that miR173 possesses unique properties that facilitate both cleavage and recruitment of RDR6.

For cleavage of *TAS1* and *TAS2* transcripts, miR173 functions through AGO1. This conclusion is based on three sets of data. First, miR173, which contains a 5'U, has been shown to co-immunoprecipitate with AGO1 (Mi et al., 2008; Montgomery et al., 2008). AGO1 also co-immunoprecipitates with most other miRNA and tasiRNA that contain a 5'U (Mi et al., 2008; Montgomery et al., 2008). This is in contrast to AGO2, which associates with miRNA and tasiRNA containing a 5'A (Mi et al., 2008; Montgomery et al., 2008; Takeda et al., 2008). Secondly, reduction of AGO1 function in *ago1-25* mutant plants results in a reduction of miR173 and tasiRNA containing 5'U (AGO1-associated), 5'A (AGO2-associated), 5'C (AGO5-associated) and 5'G (AGO association unknown) from *TAS1* and *TAS2* loci. Additionally, 5'A-containing *TAS2* tasiRNA are completely lost in the AGO1 null allele *ago1-36*. If AGO1 functioned only with mature tasiRNA, the loss of AGO1 in *ago1-25* and other *ago1* mutants would not explain the reduction in 5'A-, C- and G-containing tasiRNA and miR173. Finally, AGO1 is required for cleavage of *TAS1c*. Thus, AGO1-miR173 complexes function at the initiation cleavage step, before processing and sorting of tasiRNA, and AGO1-tasiRNA(5'U) complexes function in target repression.

Recruitment of RDR6, and subsequent DCL4-mediated siRNA duplex formation, distinguish AGO1-miR173-processed *TAS1* and *TAS2* transcripts from the vast majority of other AGO1-miRNA-directed cleavage products. That introduction of a single miR173 target site, but not other target sites, into a foreign sequence (GFP) is sufficient to trigger directional, phased siRNA formation indicates that miR173 or AGO1-miR173 complexes possess unique information for recruitment. Conceivably, miR173 or miR173-AGO1

complex associates with a unique cofactor that recruits RDR6. An attractive candidate for such a cofactor is SGS3, which was previously shown to stabilize the cleavage fragments of *TAS1* and *TAS2* transcripts (Yoshikawa et al., 2005), although the mechanism of SGS3 recruitment to cleaved products and its precise role in tasiRNA formation are unclear. One possibility is that SGS3 associates with AGO1 during loading of miR173, and is subsequently directed to *TAS1* and *TAS2* transcripts by the miR173-AGO1 complex. SGS3, in turn, may recruit RDR6 to the transcript. Another possibility is that miR173 contains a unique chemical modification that stabilizes the miR173-AGO1 complex at the target site following cleavage and in effect recruits RDR6, although this idea has no experimental support. A thorough analysis of miR173 indicated that its only modification is a single 2' methyl group on the 3' nt, a common feature on plant miRNA (Yu et al., 2005). Yet another possibility is miR173-AGO1 interacts directly with RDR6 for recruitment. Exactly how miR173-AGO1 transmits a signal to recruit RDR6 is a key problem to address in future studies.

Computational searches and deletion mapping failed to reveal evidence for a second miRNA target site in *TAS1c* transcripts. Deleting the entire *TAS1c* sequence upstream of the miR173 target site did not significantly affect *TAS1c*-based syn-tasiRNA formation, indicating that any prospective cis-acting elements would have to be downstream of the miR173 target site. Substituting 200 nt of *TAS1c* sequence outside of the predominant tasiRNA-yielding region of a *TAS1c*-based syn-tasiRNA construct, for smGFP coding sequence, while maintaining the transcript length and poladenylation signal did not effect syn-tasiRNA formation. Internal and 3' deletions just downstream of the predominant

tasiRNA-yielding region of the *TAS1c*-based syn-tasiRNA construct resulted in a modest reduction in syn-tasiRNA formation, however, this was accounted for by effects on transcript accumulation. An 8 nt motif was identified downstream of the predominant tasiRNA yielding regions in each of the *TAS1* and *TAS2* loci. This motif occurs twice in *TAS1c* between the deletion that yielded normal levels of syn-tasiRNA and the deletion that yielded reduced levels of syn-tasiRNA. The *TAS1c* sequence containing the two motifs and spanning the region between the high and low syn-tasiRNA yielding deletions was introduced into smGFP coding sequence downstream from a miR173 target site. This additional *TAS1c* sequence did not enhance siRNA formation, relative to an otherwise identical miR173-targeted GFP construct. Thus, it is likely that miR173 provides all the information necessary for routing *TAS1* and *TAS2* transcripts into the tasiRNA pathway.

TAS1c-based syn-tasiRNAs were affectively used to silence *PDS*. The phenotype severity resulting from each syn-tasiRNA construct ranged from moderate, patchy photobleaching to strong ubiquitous photobleaching of all green tissues. Phenotype severity also varied somewhat between constructs, possibly due to differences in the accessibility of each syn-tasiRNA target on the *PDS* mRNA. miRNA-AGO accessibility to a target site is determined by the RNA secondary structure and is known to be important for RNA silencing in animals (Ameres et al., 2007). Variability in silencing efficiency has also been reported for artificial miRNA (amiRNA) and hairpin RNAi constructs (Kerschen et al., 2004; Schwab et al., 2006). As a plant-based tool for gene silencing, syn-tasiRNAs offer several advantages over other RNAi methods. First, because tasiRNA formation occurs in sequential 21 nt increments in phase with the

miRNA-guided cleavage site, syn-tasiRNA formation is highly predictable. In contrast, small RNA formation from hairpin RNAi constructs is unpredictable and prone to off-target effects. Secondly, although amiRNA constructs are also very predictable, they have the limitation of producing only a single small RNA, whereas, multiple syn-tasiRNAs can be generated from a single *TAS1c*-based construct, as demonstrated here. In fact, *TAS1c* gives rise to at least 7 relatively abundant tasiRNAs (Howell et al., 2007), suggesting that as many syn-tasiRNAs could be generated from a single *TAS1c*-based construct. The ability to generate multiple specific small RNA allows for silencing of multiple genes or gene families from a single construct. Additionally, varying the number of syn-tasiRNAs that target a specific gene could allow for fine-tuning the level of suppression of a particular gene. *TAS1c*-based syn-tasiRNAs have some disadvantages as well, most notably their dependence on miR173, a miRNA known only to exist in Arabidopsis (Jones-Rhoades et al., 2006). This limitation was at least partially overcome by generating a single component dual-gene construct that expresses both *TAS1c* transcript and miR173 precursor, in effect, expanding the functionality of *TAS1c*-based syn-tasiRNAs to non-Arabidopsis species.

EXPERIMENTAL PROCEDURES

Synthetic tasiRNA Design

Syn-tasiRNA sequences were designed to target distinct regions of *PDS* mRNA and to avoid potential off-targeting effects. Each syn-tasiRNA sequence contained a 5'U, which is required for efficient loading into AGO1 (Mi et al., 2008; Montgomery et al., 2008;

Takeda et al., 2008). *TAS1c*-based syn-tasiRNA sequences were substituted for tasiR255 and tasiR850 at positions 3' D3(+) and 3'D4(+) of *TAS1c*, respectively. The syn-tasiRNA in the 3'D3(+) position was the same for each of the *35S:TAS1cPDS-1*, *35S:TAS1cPDS-2*, and *35S:TAS1cPDS-3* constructs, but the syn-tasiRNA in the 3'D4(+) position was different (Figure 4.1). The *35S:TAS1cPDS-4* construct contained two unique syn-tasiRNA RNA sequences, both with 3' ends designed to result in three target site mispairs to suppress transitive silencing effects (Moissiard et al., 2007).

Transgene Constructs

The *TAS1c* transcribed region was amplified from genomic DNA using the following primers: TAS1c_F [caccAAACCTAAACCTAAACGGCTAAGC] and TAS1c_R [ATTTCACTTTACGATGTGGTG]. Syn-tasiRNA sequences, miRNA target site mutations, and internal and 5' and 3' deletions were introduced into *35S:TAS1cPDS-2* by site-directed PCR mutagenesis (Ho et al., 1989). *GFP* sequence was amplified from *pRTL2 smGFP* plasmid DNA (Johansen 2001). miRNA target sites and *TAS1c* sequence were introduced into the *GFP* sequence via PCR. *MIR171a* and *MIR173* were amplified from genomic DNA using the following primers: MIR171a_F [caccTGCTCCATACCTTCCATTTCC] and MIR171a_R [GGCAAGGAAGCTGATTAAGGG]; MIR173_F [caccATAATTAGCAAGTAATAAGG] and MIR173_R [ATCTGTTATACAACCAAATCC]. The "cacc" sequence at the 5' end of each forward primer was for cloning purposes. PCR products were cloned into pENTR/D-TOPO

(Invitrogen), followed by recombination into pMDC32, a plant transformation vector containing a 35S promoter and nos terminator (Curtis and Grossniklaus, 2003). To generate the dual-gene construct *35S:TAS1cPDS/173*, a nos terminator and 35S promoter were introduced upstream of *MIR173* by site-directed PCR mutagenesis. The resulting PCR product was cloned into pENTR/D-TOPO. The *TAS1cPDS-4* sequence was then ligated upstream of the *nos-term-35S:MIR173* cassette and recombined into pMDC32, such that the 35S promoter of the pMDC32 vector drove expression of *TAS1cPDS-4* and the nos terminator of pMDC32 provided the termination signal for *35S:MIR173*. Pfu Ultra polymerase (Stratagene) was used for all PCRs.

Plant Materials and Growth Conditions

rdr6-15, dcl4-2, zip-1, *dcl1-7*, *hyl1-2*, *se-2*, *hen1-1*, *hst-15*, *ago1-25*, and *ago1-36* alleles were described previously (Allen et al., 2005; Allen et al., 2004; Baumberger and Baulcombe, 2005; Chen et al., 2002; Golden et al., 2002; Grigg et al., 2005; Hunter et al., 2003; Morel et al., 2002; Vazquez et al., 2004a; Xie et al., 2005b). *Arabidopsis thaliana* plants were transformed by floral dip using *Agrobacterium tumefaciens* GV3101 (Clough and Bent, 1998). Transformed plants were grown on Murashige and Skoog (MS) medium plates containing hygromycin (50 ug/ml). After 7 days, plants were transferred to a greenhouse with a 16 hr light/8 hr dark supplemental light cycle. In some instances, such as when severely photobleached, plants were grown for extended periods on MS media.

RNA Blot Assays and Quantitative RT-PCR

RNA was isolated using Trizol reagent (Invitrogen). Three chloroform extractions were done and RNA was precipitated in 0.5X isopropanol for 20 minutes. Duplicate or triplicate samples from pools of independent primary transformants or from infiltrated leaves of *N. benthamiana* plants were analyzed. For high-molecular weight (HMW) RNA blot assays, 5 ug total RNA was resolved by denaturing 1.5% agarose-gel electrophoresis. For small RNA blot assays, 10 ug total RNA was resolved by denaturing 17% polyacrylamide-gel electrophoresis. In most cases, RNA standards were run in parallel. RNA was transferred to positively-charged nitrocellulose membranes. DNA probes were randomly labeled using ^{32}P-dATP and klenow fragment. DNA and LNA oligonucleotide probes were end-labeled using ^{32}P-ATP and Optikinase (USB). Probes were hybridized to RNA on membranes in Sigma Perfect-Hyb Buffer (Sigma) at 68˚ (HMW blots) or 38˚ (small RNA blots). An Instant Imager (Packard Bioscience) was used to measure blot hybridization signals.

Quantitative RT-PCR was done as described (Montgomery et al., 2008) using the following *PDS* and *ACT2* primers: PDS_F [GAACAACGAGATGCTGACATG] and PDS_R [TTCCAGGGATCTGGTAAAAGGAG]; ACT2_F [GCCATCCAAGCTGTTCTCTC] and ACT2_R [GAACCACCGATCCAGACACT].

Transient Gene Expression

Transient gene expression in *N. benthamiana* leaves was done as described (Llave et al., 2000), using *Agrobacterium tumefaciens* GV3101. When multiple constructs were coexpressed, equal amounts of each *Agrobacterium* strain were used within each

experiment. The final concentration of *Agrobacterium* prior to injection was adjusted to an OD_{600} of 1.0 using *Agrobacterium* cultures containing empty vector. RNA was isolated 48 hr postinfiltration.

Cleavage Assays

miRNA-guided cleavage was assayed using a modified RNA ligase-mediated 5' RACE procedure, as described (Kasschau et al., 2003; Llave et al., 2002a), with the following gene-specific PCR primers: TAS1c_5'_RACE [AGCAACTGTTCTTTAGACGACTTGAAAATCTCAT]; TAS1cPDS-2_5'_RACE [CTAGTTCTGGCTGCGTCTGGACC]; GFP_5'_RACE [GGGCAGATTGTGTGGACAGGTAATGG].

Small RNA Sequencing

Small RNA amplicons for sequencing were prepared as described (Kasschau et al., 2007), with the exceptions that the adapters were customized to work with the Illumina 1G platform and the use of Phusion High-Fidelity Polymerase (Finnzymes) for RT-PCR. Sequencing-by-synthesis (SBS) was done with an Illumina 1G Genome Analyzer. 21 nt small RNA reads from *N. benthamiana* transformed with *35S:MIR173* and *35S:GFP-173* that matched the test sequences (*GFP* or *HYG*^{r}) were analyzed for phasing by merging sense and antisense (offset by 2 nt in the 5' direction) reads. Phase-representation radar plots were generated as done by Axtell et al. (2006). tasiRNA and miRNA reads from

Col-0 and *ago1-25* inflorescence tissue (flowers stages 1-12) were normalized against total unparsed reads in each library.

Statistical Analysis

S-PLUS (Insightful) and Excel (Microsoft) were used for all statistical tests and calculations. Bonferroni adjustments were made to *p*-value significance level cutoffs when doing multiple comparisons.

ACKNOWLEDEMENTS

We thank Amy Shatswell, Jesse Hansen, Sarah Dvorak, Josh Cuperus, and Heather Sweet for technical assistance, Scott Givan for computational assistance, and Mark Dasenko and Kristin Kasschau for DNA sequencing assistance. This work was supported by grants from the Monsanto Corporation and from NSF (MCB-0618433), NIH (AI43288) and USDA (2005-35319-15280).

Table 4.1. Effects of *TAS1c*-based synthetic tasiRNAs on wild-type and mutant plants.

		Syn-tasiRNAs[a]		Relative Photobleaching[b]		
Genotype	n	PDSd3[c]	PDSd4[d]	None	Moderate	Strong
Col-0						
Vector	156	-	-	100.0	0	0
35S:TAS1cPDS-1	121	+	+	9.1	27.3	63.6
35S:TAS1cPDS-2	56	+	+	5.4	46.4	48.2
35S:TAS1cPDS-3	28	+	+	3.6	37.0	60.7
35S:TAS1cPDS-4	20	NA	NA	5.0	20.0	75.0
35S:TAS1cPDS-4/MIR173	32	NA	NA	0	46.9	53.1
zip-1						
35S:TAS1cPDS-1	12	+	+	16.7	25.0	58.3
35S:TAS1cPDS-2	17	+	+	0	41.2	58.8
35S:TAS1cPDS-3	14	+	+	0	42.9	57.1
rdr6-15						
35S:TAS1cPDS-1	291	-	-	100.0	0	0
35S:TAS1cPDS-2	18	-	-	100.0	0	0
35S:TAS1cPDS-3	4	-	-	100.0	0	0
35S:TAS1cPDS-4	18	NA	NA	100.0	0	0
35S:TAS1cPDS-4/MIR173	16	NA	NA	100.0	0	0
dcl4-2						
35S:TAS1cPDS-1	5	-	-	100.0	0	0
35S:TAS1cPDS-2	15	-	-	100.0	0	0
35S:TAS1cPDS-3	8	-	-	100.0	0	0

[a] Syn-tasiRNAs are scored as either present (+) or absent (-) as determined by RNA blot assays.

[b] Photobleaching is shown as a percentage of plants in each category.

[c] The PDSd4 (position 3'D4(+)) syn-tasiRNA differs between each of the syn-tasiRNA constructs.

[d] The PDSd3 (position 3'D3(+)) syn-tasiRNA is the same in *35S:TAS1cPDS-1*, *35S:TAS1cPDS-2*, and *35S:TAS1cPDS-3*, and differs in *35S:TAS1cPDS-4*.

NA, not analyzed.

Figure 4.1. Validation of *TAS1c*-based synthetic (syn) tasiRNAs. (A) Organization of *TAS1c*-based syn-tasiRNA constructs. The miR173-guided cleavage site is indicated by the arrow. tasiRNA positions 3'D1(+) through 3'D10(+) are indicated by brackets. (B) Representative images of wild-type (Col-0) and mutant plants transformed with *TAS1c*-based syn-tasiRNA constructs. (C) Mean relative level +/- SEM of *PDS* mRNA after normalization to *ACT2* mRNA, as determined by quantitative RT-PCR (Col-0 vector = 1.0). (D) Mean levels +/- SEM of syn-tasiRNA as determined by RNA-blot assays (Col-0 *35S:TAS1cPDS-2* = 1.0). Inset shows small RNA blot and EtBr-stained 5S rRNA and tRNA. (E) Organization of the single-component, dual-gene *TAS1c*-based syn-tasiRNA construct *35S:TAS1cPDS/MIR173*. (F and G) Mean levels +/- SEM of miR173 and syn-tasiRNA in a transient-expression assay in *N. benthamiana*, as determined by RNA-blot assays (*35S:TAS1cPDS-4* + *35S:MIR173* = 1.0). Small RNA blots for one of three biological replicates are shown. EtBr-stained 5S rRNA and tRNA are shown as loading controls. (H) Representative images of Col-0 and *rdr6-15* vector-, *35S:TAS1cPDS-4*-, and *35S:TAS1cPDS/MIR173*-transformed plants.

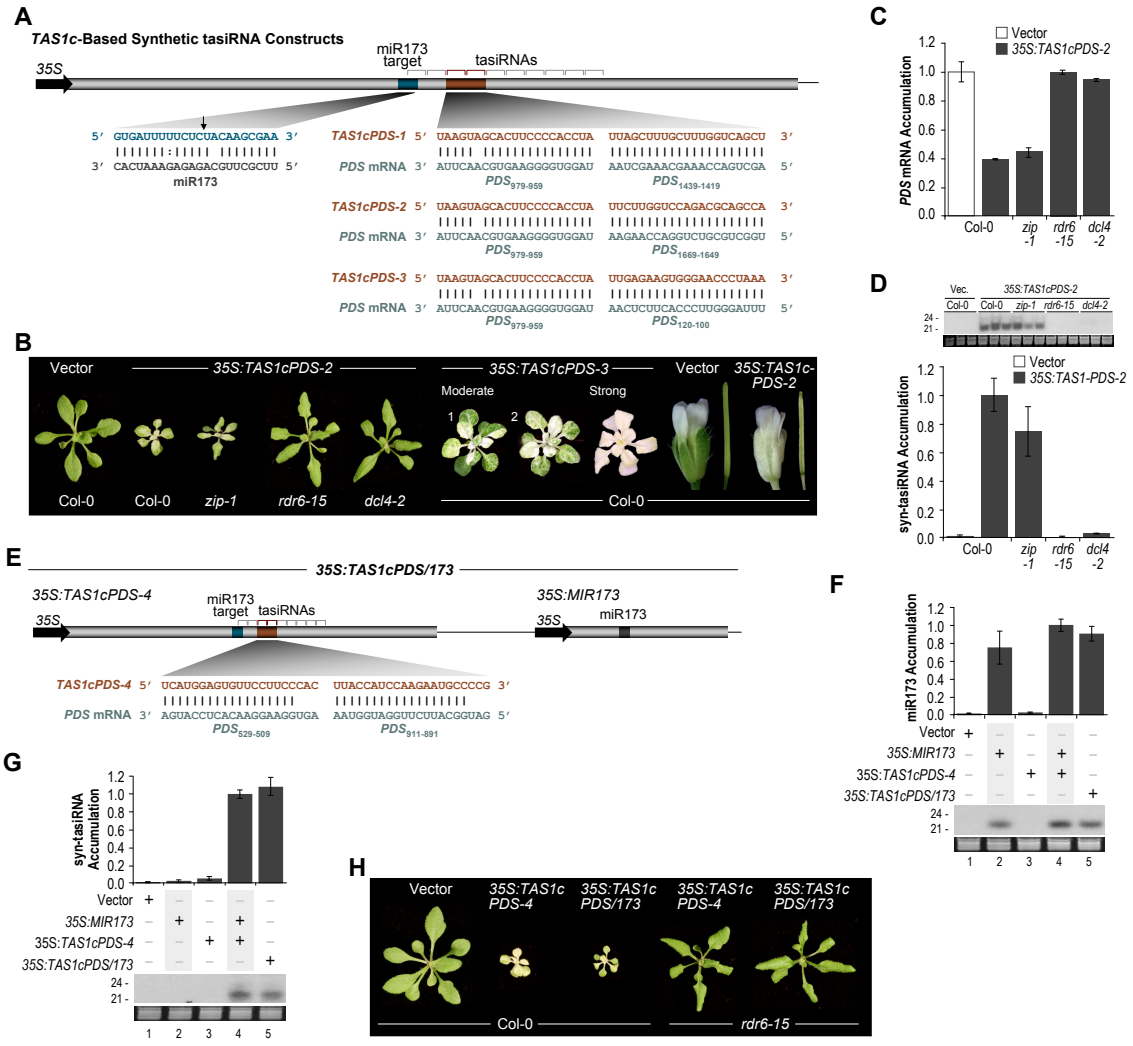

Figure 4.1. Validation of *TAS1c*-based synthetic (syn) tasiRNAs.

Figure 4.2. miR173 specificity in *TAS1c*-based syn-tasiRNA formation. (A) The miR173 target site in *35S:TAS1cPDS-2* was substituted for sites recognized by miR169 (*35S:TAS1cPDS-169*), miR171 (*35S:TAS1cPDS-171*), miR390 (*35S:TAS1cPDS-390*), or miR167 (*35S:TAS1cPDS-167*). The percentages of transgenic plants that displayed modest or strong photobleaching are shown next to representative images (for each line n > 30 primary transformants). The proportion of cloned 5' RACE products corresponding to cleavage at a particular site is shown above the arrows. Black arrows indicate the canonical miRNA-guided cleavage position. Dashed horizontal arrows indicate the 5' and 3' probe sequences used for RNA blot assays in Figures 4.3B and 4.3C. (B) Mean relative level +/- SEM of *PDS* mRNA after normalization to *ACT2* mRNA, as determined by quantitative RT-PCR (Col-0 vector = 1.0). (C) Mean relative level +/- SEM of syn-tasiRNAs, as determined by RNA-blot assays (Col-0 *35S:TAS1cPDS-2* = 1.0). (D) EtBR-stained 5' RACE products corresponding to cleavage of *TAS1c*-based syn-tasiRNA transcripts in Arabidopsis. 5' RACE products corresponding to cleavage at the canonical miRNA-guided cleavage site migrate at 135 bp. *ACTIN* RT-PCR products are shown as controls.

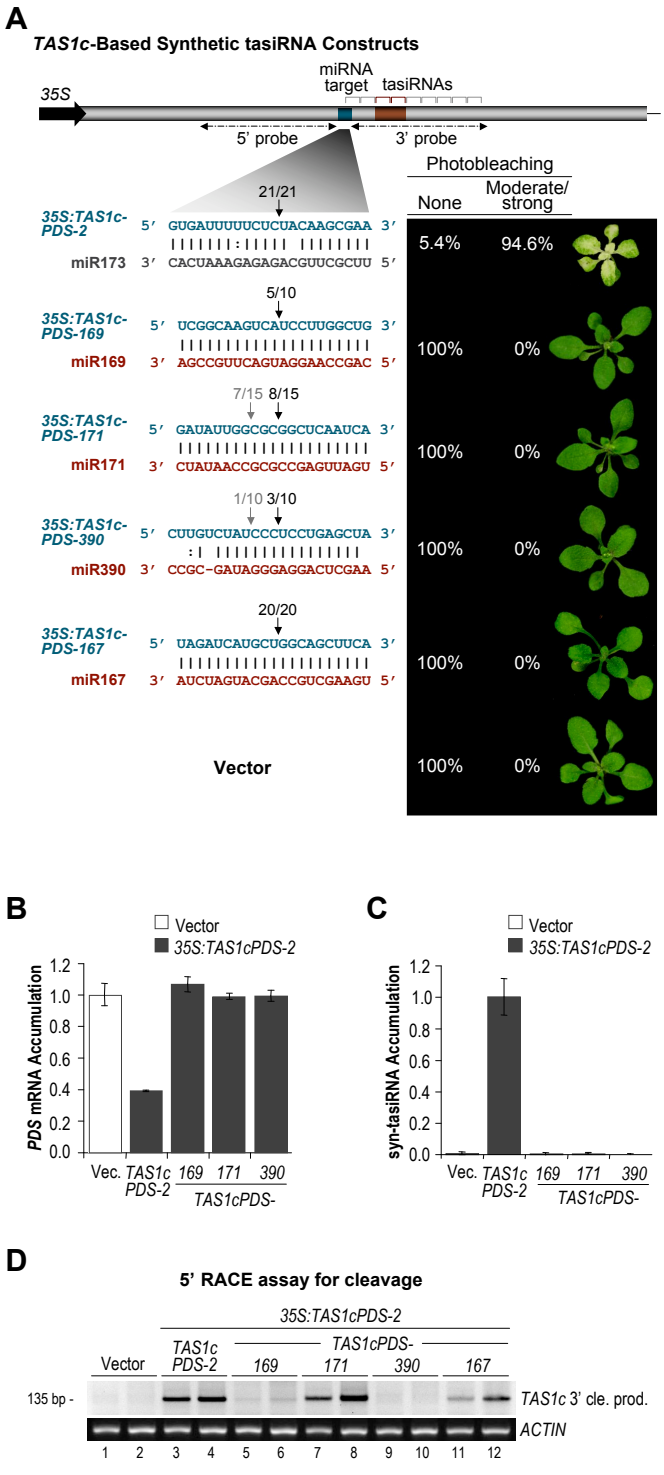

Figure 4.2. miR173 specificity in *TAS1c*-based syn-tasiRNA formation.

Figure 4.3. Specificity of miR173 for *TAS1c*-based syn-tasiRNA formation in *N. benthamiana* leaves. (A) Flowchart for RNA isolation and analyses following a transient expression assay in *N. benthamiana*. (B) *TAS1c*-based syn-tasiRNA constructs containing miR173 or miR171 target sites were expressed or coexpressed in *N. benthamiana* leaves as indicated above blot panels. One of two biological replicates is shown. Probe sequences for 5' and 3' regions of *TAS1c*-based syn-tasiRNA constructs are indicated by horizontal arrows in the schematic in Figure 4.2A. EtBr-stained 5S rRNA and tRNAs are shown as a loading control. (C) RNA blot assays for *TAS1c*-based syn-tasiRNA full-length transcripts and cleavage products (cle. prod.). The ratio of 3' cleavage product to full length transcript is shown above the blot images. EtBr stained 18S/25S rRNA is shown as a loading control. (D) EtBR-stained gel of 5' RACE products corresponding to cleavage of *TAS1c*-based syn-tasiRNA transcripts in *N. benthamiana* leaves. 5' RACE products corresponding to cleavage at the canonical miRNA-guided cleavage site migrate at 373 bp. *ACTIN* RT-PCR products are shown as controls.

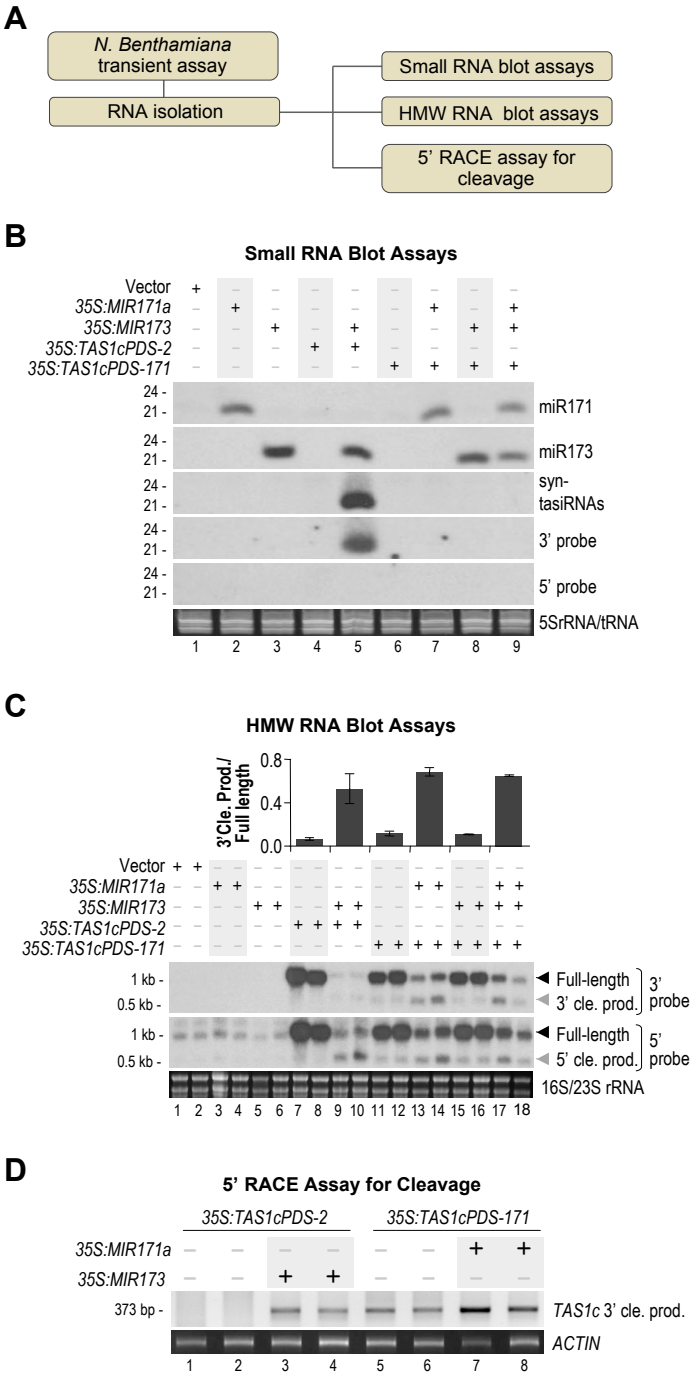

Figure 4.3. Specificity of miR173 for *TAS1c*-based syn-tasiRNA formation in *N. benthamiana* leaves.

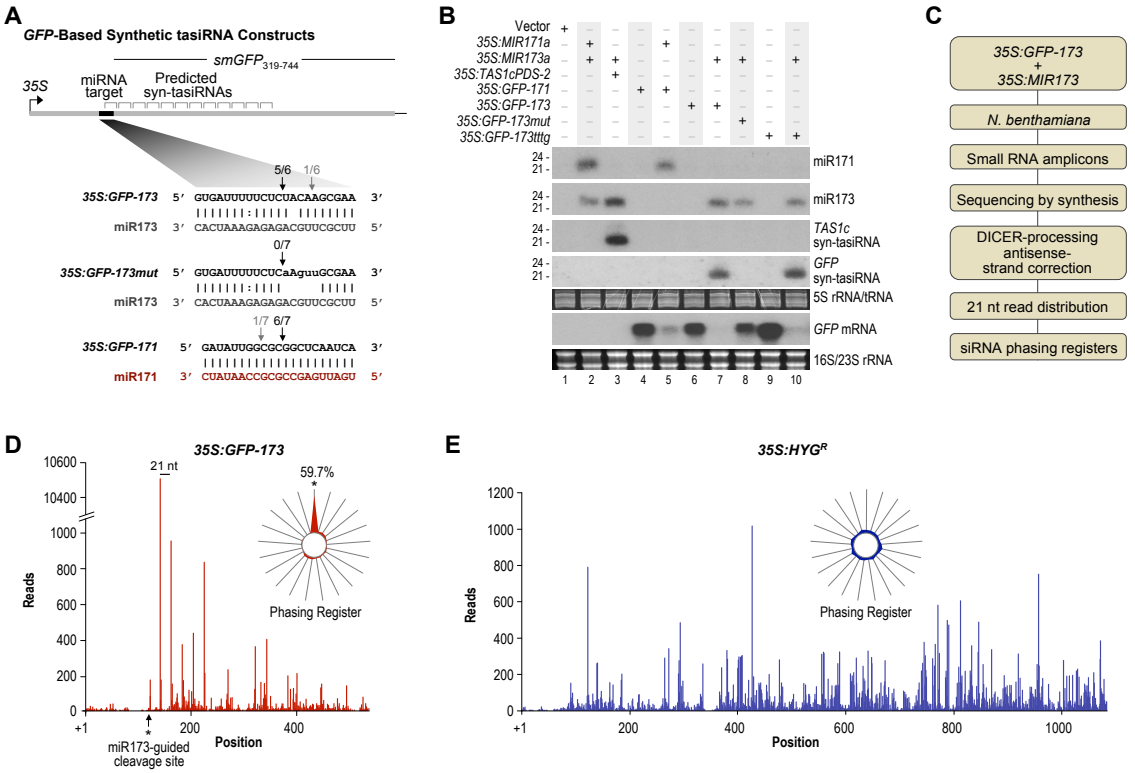

Figure 4.4. miR173 triggers phased siRNA formation from *GFP* transcripts. (A) Organization of the *GFP*-based syn-tasiRNA constructs. The proportion of cloned 5' RACE products corresponding to cleavage at a particular site is shown above the arrows. Black arrows indicate the canonical miRNA-guided cleavage position. (B) RNA blot assays. *TAS1c*- and *GFP*-based syn-tasiRNA constructs containing miR173 or miR171 target sites were expressed or coexpressed as indicated above the blot panels. One of two biological replicates is shown. EtBr-stained 5S rRNA/tRNA and 18S/25S rRNA is shown as a loading control. (C) Flowchart for analysis of small RNA from *N. benthamiana* expressing *35S:GFP-173* and *35S:MIR173*. (D and E) 21 nt small RNA read distributions across *35S:GFP-173* and *35S:HYG*^{R} transcripts. Radar plots (inset) display percentages of reads corresponding to each of the 21 possible phase registers.

Figure 4.5. The effect of internal deletions on *TAS1c*-based syn-tasiRNA formation. (A) tasiRNA distribution across the endogenous *TAS1c* locus in Col-0. 5,888 *TAS1c* tasiRNA reads from Col-0 leaf and whole plant Illumina 1G sequencing data sets were obtained from the ASRP database (Backman et al., 2007). The radar plot (inset) displays the percentages of reads corresponding to each of the 21 possible phase registers. Internal deletions were introduced at the positions indicated by the shaded boxes. (B) RNA blot assays. Parental *35S:TAS1cPDS-2* and modified constructs containing internal deletions were expressed individually or in combination with *35S:MIR173* as indicated above the blot panels. Mean relative level +/- SEM of syn-tasiRNA relative to miR173 (*35S:TAS1cPDS-2* + *35S:MIR173* = 1.0). One of three biological replicates is shown. EtBr-stained 5S rRNA/tRNA and 18S/23S rRNA are shown as loading controls.

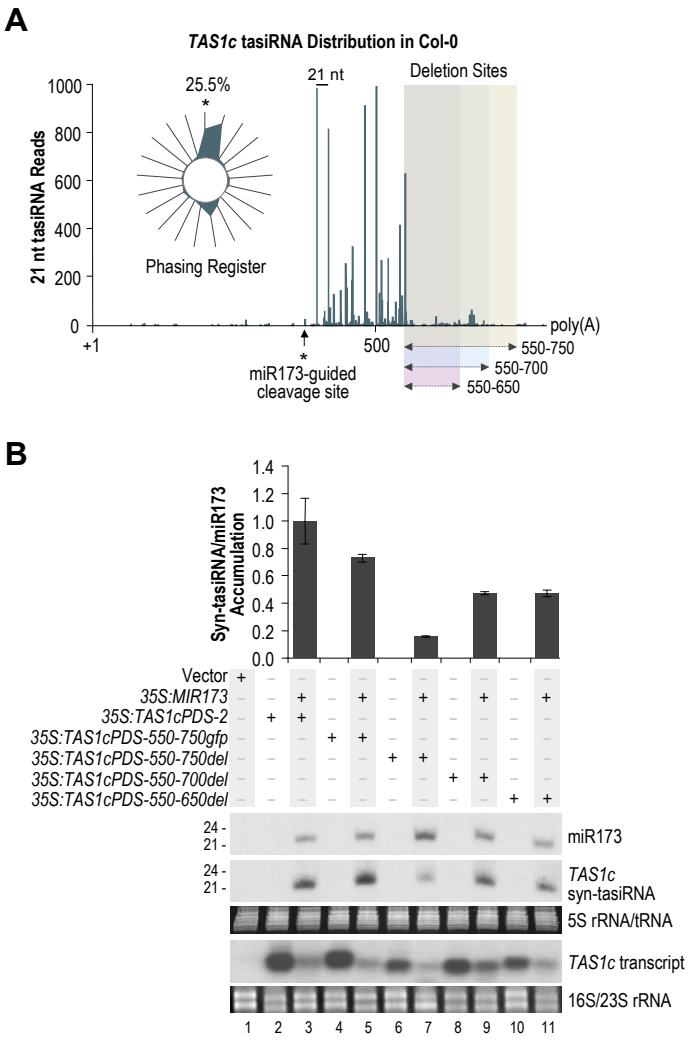

Figure 4.5. The effect of internal deletions on *TAS1c*-based syn-tasiRNA formation.

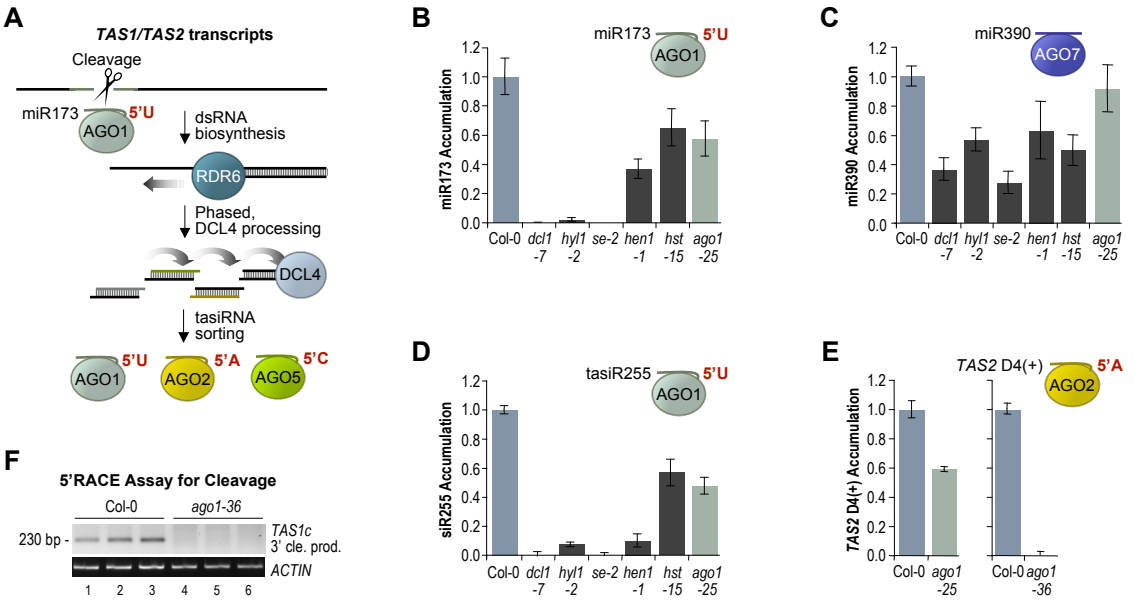

Figure 4.6. Role of AGO1 in *TAS1* and *TAS2* tasiRNA formation. (A) Model for *TAS1/TAS2* tasiRNA formation and sorting of tasiRNA into AGO proteins. (B-E) Mean relative levels +/- SEM of miR173, miR390, and two distinct tasiRNAs as determined by RNA blot assays (Col-0 = 1.0). (F) EtBR-stained 5' RACE products corresponding to cleavage of *TAS1c* transcripts in Arabidopsis. 5' RACE products corresponding to cleavage at the canonical miR173-guided cleavage site migrate at 230 bp. *ACTIN* RT-PCR products are shown as controls.

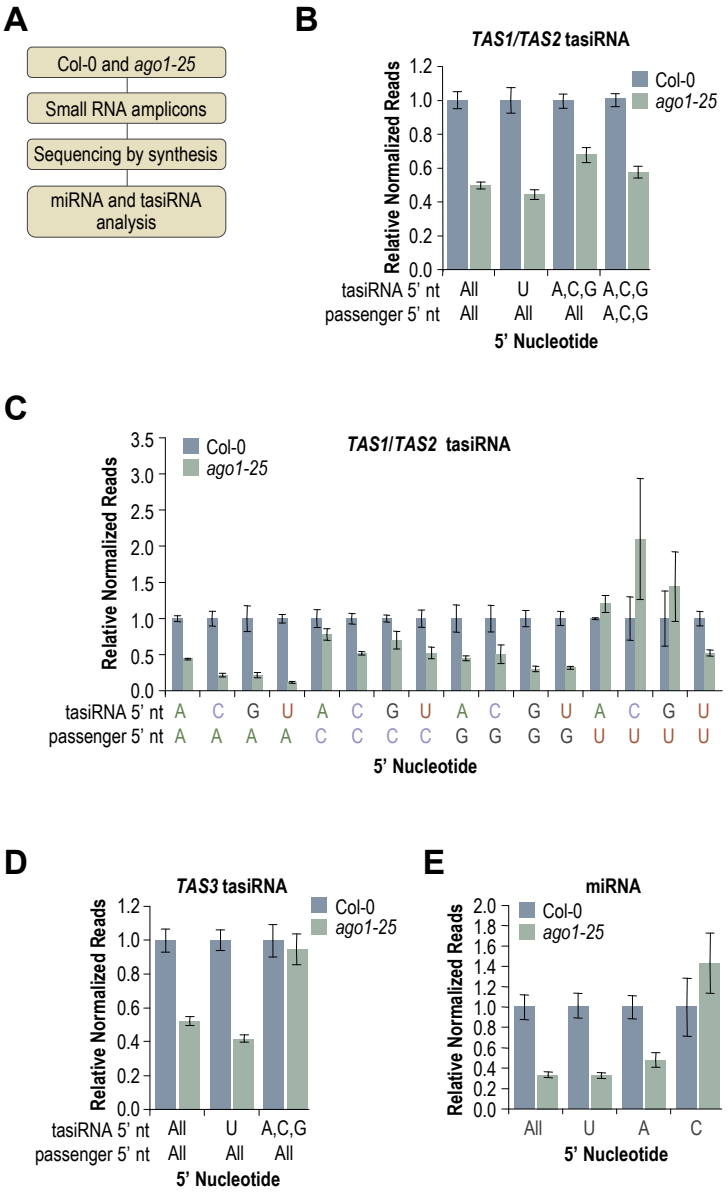

Figure 4.7. Deep sequencing-based analysis of AGO1-dependent small RNA. (A) Flowchart for miRNA and tasiRNA analysis. (B) Mean relative level +/- SEM of *TAS1* and *TAS2* tasiRNA (Col-0 = 1.0). (C) Mean relative level +/- SEM of *TAS1* and *TAS2* tasiRNA for each possible tasiRNA/passenger strand 5' nt combination (Col-0 = 1.0). (D) Mean relative level +/- SEM of *TAS3* tasiRNA (Col-0 = 1.0). (E) Mean relative level +/- SEM of miRNA (Col-0 = 1.0).

SUPPLEMENTAL DATA

SUPPLEMENTAL EXPERIMENTAL PROCEDURES

3' RACE

3' RACE for mapping the 3' ends of *35S:TAS1cPDS-2* and endogenous *TAS1c* transcripts were done as described (Xie et al., 2005a) with the following gene specific PCR primers: TAS1c_3'_RACE [CTAAGTTCAACATATCGACGAACTAGA] and TAS1cPDS-2_3'_RACE [CTTGGTCCAGACGCAGCCAGAAC].

ARGONAUTE Mutant Alleles

The *ago1-25*, *ago2-1*, *ago3-1*, *ago4-1*, *ago5-2*, *zip-1*, *ago8-1* alleles were previously described (Hunter et al., 2003; Lobbes et al., 2006; Morel et al., 2002; Takeda et al., 2008; Zilberman et al., 2003). The *ago9* (SALK_126176, insertion in intron 11) and *ago10* (SALK_019738, insertion in intron 15) alleles were obtained from The Arabidopsis Biological Resource Center (Alonso et al., 2003). Homozygous mutant plants were generated and confirmed by PCR-based genotype analysis.

Table S4.1. Small RNA phasing registry for reads mapped to *35S:GFP-173*.

Registry[a]	Counts	Mean counts/cycle	Proportion
-1	23	3.8	0.0010
-2	18	3.0	0.0008
-3	11	1.8	0.0005
-4	8	1.3	0.0004
-5	15	2.5	0.0007
-6	18	3.0	0.0008
-7	6	1.0	0.0003
-8	4	0.7	0.0002
-9	12	2.0	0.0005
-10	15	2.5	0.0007
-11	8	1.3	0.0004
-12	37	6.2	0.0017
-13	16	2.7	0.0007
14	16	2.7	0.0007
-15	20	3.3	0.0009
-16	42	7.0	0.0019
-17	56	9.3	0.0025
-18	16	2.7	0.0007
-19	16	2.7	0.0007
-20	8	1.3	0.0004
-21	37	6.2	0.0017
1	13384	704.4	0.5972
2	698	36.7	0.0311
3	958	50.4	0.0427
4	752	39.6	0.0336
5	350	18.4	0.0156
6	163	8.6	0.0073
7	251	13.2	0.0112
8	451	23.7	0.0201
9	215	11.3	0.0096
10	376	19.8	0.0168
11	446	23.5	0.0199
12	780	41.1	0.0348
13	821	43.2	0.0366
14	767	40.4	0.0342
15	252	13.3	0.0112
16	168	8.8	0.0075
17	285	15.0	0.0127
18	296	15.6	0.0132
19	176	9.3	0.0079
20	137	7.2	0.0061
21	282	14.8	0.0126
Total	**22410**		**1.0000**

[a] The phasing registry for the miR173-guided cleavage site upstream (5') of the miR173 target site = -1. The phasing registry for the miR173-guided cleavage site downstream (3') of the miR173 target site = +1.

Table S4.2. Small RNA phasing registry for reads mapped to *35S:HYG*^{R}.

Registry[a]	Counts	Mean counts/cycle	Proportion
1	2869	55.2	0.0487
2	2652	51.0	0.0450
3	2587	49.8	0.0439
4	2242	43.1	0.0381
5	1463	28.1	0.0248
6	2446	47.0	0.0415
7	3720	71.5	0.0632
8	2320	44.6	0.0394
9	1894	36.4	0.0322
10	3403	65.4	0.0578
11	2176	41.8	0.0369
12	2995	57.6	0.0509
13	3628	69.8	0.0616
14	2821	54.3	0.0479
15	4454	85.7	0.0756
16	2245	43.2	0.0381
17	3028	58.2	0.0514
18	3760	72.3	0.0638
19	2408	46.3	0.0409
20	2237	43.0	0.0380
21	3547	68.2	0.0602
Total	**58895**		**1.0000**

[a] The phasing registry for the transcription start site = 1.

Figure S4.1. *TAS1c*-based syn-tasiRNA construct 5' and 3' deletions. (A) Mapping of authentic *TAS1c* and *35S:TAS1cPDS-2* primary transcript 3' ends, and positions of 3' truncations in the deletion series. The positions of 3' ends were determined by 3' RACE and nucleotide sequence analysis, with a minimum of 25 clones analyzed. The ratio of poly(A)-proximal sites at each position is indicated on the y-axis. (B and C) Syn-tasiRNA formation and primary transcript accumulation from *TAS1c*-based syn-tasiRNA constructs in the *N. benthamiana* transient expression assay. Constructs were expressed in the presence or absence of *35S:MIR173* as indicated above the blot panels. (B) Mean relative level +/- SEM of syn-tasiRNAs (*35S:TAS1cPDS-2* + *35S:MIR173* = 1.0). RNA blot data for one of three biological replicates is shown. EtBr-stained 5S rRNA and tRNAs are shown as a loading control. (C) Mean relative level +/- SEM of primary *TAS1c*-based syn-tasiRNA transcripts (*35S:TAS1cPDS-2* = 1.0) for the same samples as shown in panel B. RNA blot data for one of three biological replicates is shown. EtBr stained 18S/23S rRNAs are shown as a loading control.

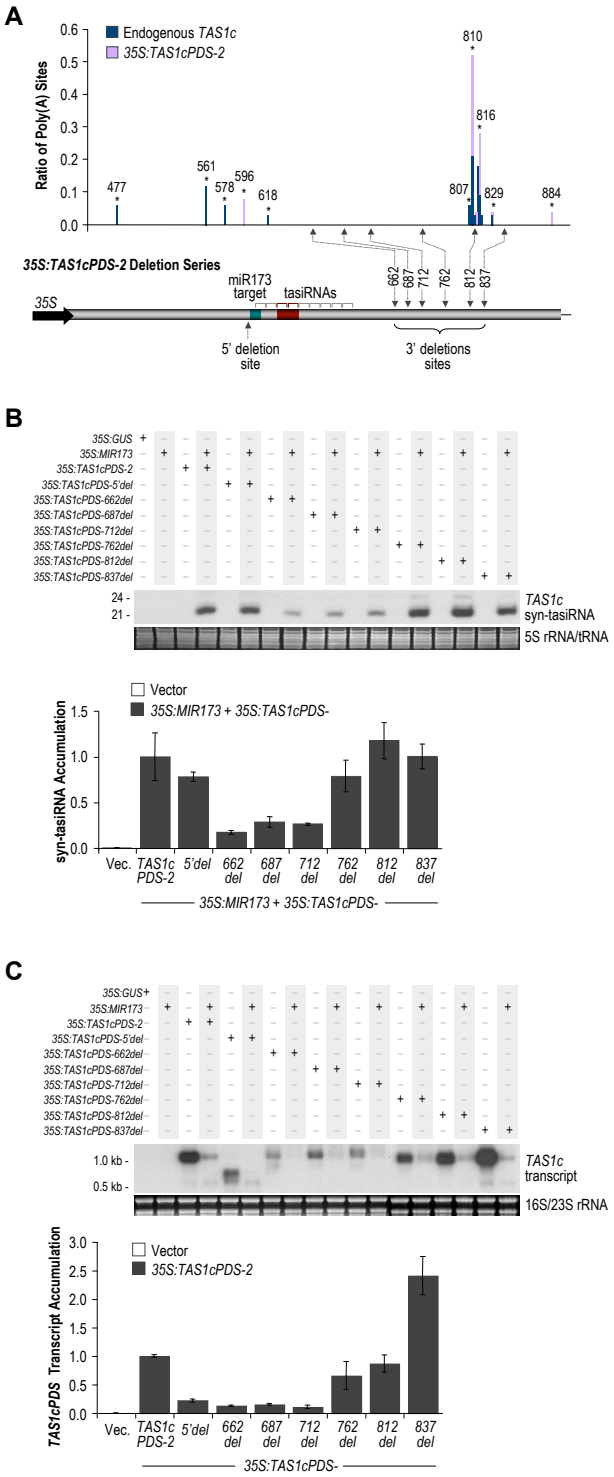

Figure S4.1. *TAS1c*-based syn-tasiRNA construct 5' and 3' deletions.

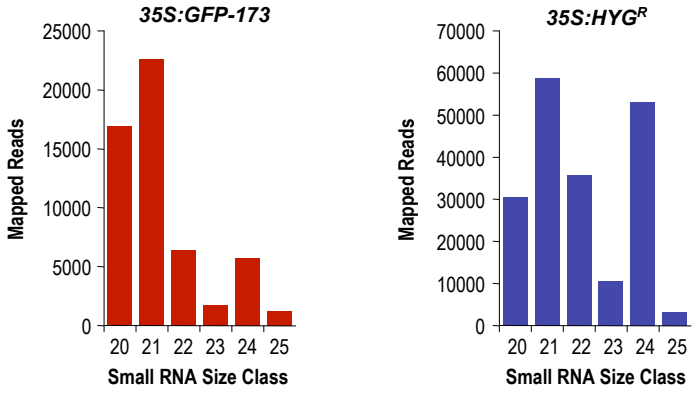

Figure S4.2. Size distribution for small RNA reads matching perfectly to either *35S:GFP-173* or *35S:HYG^R*. The proportion of total 20-25 nt small RNA reads is shown for each size class.

Figure S4.3. Effect of mispairing at the miR173 target site in *35S:TAS1cPDS-2* on syn-tasiRNA formation. (A) Alignment of the miR173 target sites from *TAS1* and *TAS2* transcripts. The miR173-guided cleavage site is indicated by the arrow. (B) Organization of *35S:TAS1cPDS-2* and mutant constructs. (C) Mean relative level +/- SEM of syn-tasiRNAs (*35S:TAS1cPDS-2* + *35S:MIR173* = 1.0). *TAS1c*-based syn-tasiRNA constructs containing authentic or mutated miR173 or miR171 target sites were expressed or coexpressed in *N. benthamiana* leaves as indicated above the blot panels. RNA blot assays show one of three biological replicates. EtBr-stained 5S rRNAs and tRNAs are shown as a loading control.

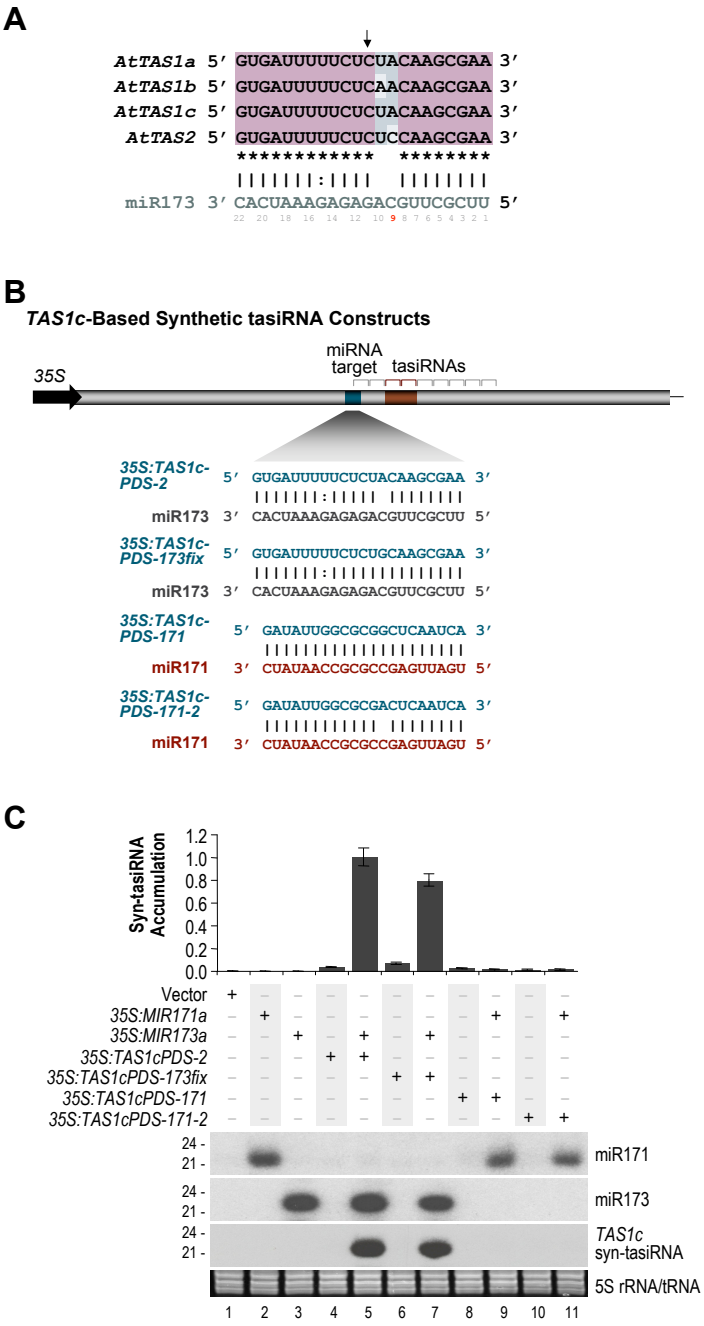

Figure S4.3. Effect of mispairing at the miR173 target site in *35S:TAS1cPDS-2* on syn-tasiRNA formation.

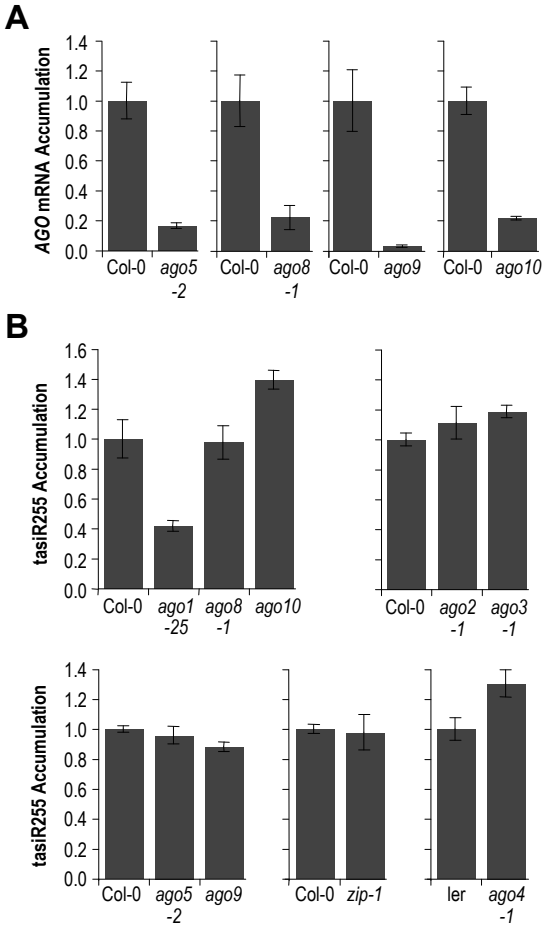

Figure S4.4. *TAS1* tasiR255 levels in AGO mutants. (A) RNA blot assays for AGO mRNA. Mean relative level +/- SEM for each AGO mRNA as indicated (Col-0 = 1.0). (B) RNA blot assays for tasiR255. Mean relative level +/- SEM of tasiR255 (Col-0 or ler = 1.0).

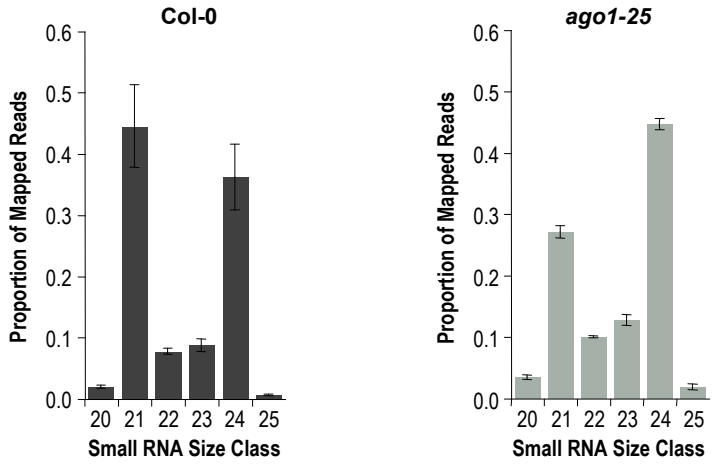

Figure S4.5. Size distribution for small RNA reads from Col-0 and *ago1-25*. The mean proportion +/- SD of total 20-25 nt small RNA reads is shown for each size class.

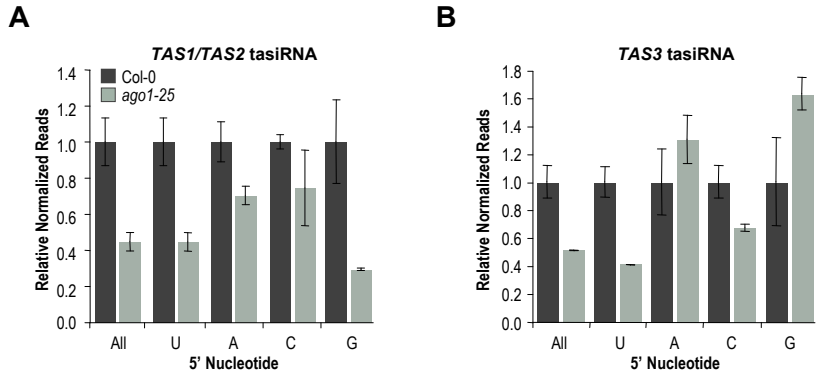

Figure S4.6. Deep sequencing-based analysis of AGO1-dependent tasiRNA. (A) Mean relative level +/- SD of *TAS1* and *TAS2* tasiRNA according to the 5' nt (Col-0 = 1.0). (B) Mean relative level +/- SD of *TAS3* tasiRNA according to the 5' nt (Col-0 = 1.0).

CHAPTER 5

General Conclusion

Taiowa A. Montgomery

The work describe here has provided important advances in our understanding of the basic mechanisms of small RNA formation and RNA silencing. Furthermore, we have uncovered an important role for tasiRNA in plant development. We show that the juvenile-to-adult phase transition in plants is suppressed by *TAS3* tasiRNAs, in an AGO7-dependent manner, through negative regulation of *ARF3* mRNA. Furthermore, all of the developmental defects observed in general tasiRNA defective plants, such as those deficient in *RDR6*, *SGS3*, and *DCL4*, as well as the *TAS3* specific factor AGO7, can be phenocopied by derepressing *ARF3*. Thus, the primary role of tasiRNA in plant development is to fine-tune the expression of *ARF3* and likely the closely related and redundant gene *ARF4*. The biological role of *TAS1* and *TAS2* tasiRNA remains to be determined. It is possible that under the luxurious growth conditions in the lab, *TAS1* and *TAS2* tasiRNA are dispensable for proper development, but under natural growing conditions or when exposed to stress *TAS1* and *TAS2* tasiRNA have an important role.

We developed an affective synthetic (syn) tasiRNA reporter system to test the requirements for *TAS1/TAS2* and *TAS3* tasiRNA formation. Using a *TAS3a*-based syn-tasiRNA system, we identified mechanistic features by which two miR390 target sites function specifically with AGO7 to route *TAS3* transcripts through the RDR6/SGS3/DCL4 pathway. Cleavage at the 3' target site of *TAS3a*-derived transcripts forms the 3' end at which RDR6 initiates transcription, synthesizing a dsRNA substrate for subsequent processing by DCL4. Cleavage at the miR390 target site requires AGO7, irrespective of targeting at the 5' site, suggesting that AGO7 functions as a miR390-guided slicer. The requirement for AGO7 slicer function is bypassed when the 3' miR390

target site is substituted for heterologous miRNA target sites, indicating that AGO7 is dispensable at this site if another AGO is delivered via an alternate miRNA guide. The obvious prediction from this result, that AGO7 is uniquely associated with miR390, was confirmed in multiple co-IP assays. Therefore, the functionality of AGO7 at the 3' target site is dictated entirely by its miR390-guided slicer activity.

Although we could not identify a role for the miRNA 5' nucleotide as an AGO7 specificity determinant, the 5' nucleotide was clearly defined as an inclusion/exclusion specificity determinant for both AGO1 and AGO2. AGO1 prefers a 5'U and excludes a 5'A, whereas AGO2 possesses the reciprocal preference for 5'A and exclusion of 5'U. Thus, the selective pressure for a 5'U in the majority of plant miRNAs, which as a class function broadly through AGO1, is now understood. Given the widespread presence of 5'U in animal miRNA, as well as 5'U or other 5' nucleotide preferences in other small RNA classes, similar AGO selectivity determinants very likely explain at least some observed 5' nucleotide biases more widely.

Using a *TAS1c*-based syn-tasiRNA system we tested the specific requirement for miR173 in *TAS1* and *TAS2* tasiRNA formation. miR173 guides cleavage at *TAS1* and *TAS2* transcripts, defining a discrete 5' end of the pre-tasiRNA transcript and an initiation point for phased siRNA formation by RDR6, SGS3, and DCL4. Heterologous miRNA target site substitutions in the *TAS1c*-based syn-tasiRNA construct were functional for cleavage, but failed to initiate syn-tasiRNA formation, suggesting that miR173 has additional, unique properties or associated cofactors required for routing transcripts into the RDR6/SGS3/DCL4 silencing pathway. When introduced into GFP coding sequence,

the authentic miR173 target site was functional to direct phased siRNA formation downstream of the miR173 target site, but only in the presence of miR173. A similar GFP-based construct with a miR171 target site failed to yield siRNA when provided ectopic miR171. Thus, a single miR173 target site, but not other miRNA target sites, is sufficient to route a transcript into the tasiRNA pathway. Additionally, we determined that miR173 functions through association with AGO1 during *TAS1* and *TAS2* tasiRNA formation, indicating that the AGO1-miR173 complex functions in a distinct mode from other AGO1-miRNA complexes.

It is becoming increasingly evident that knowledge of the basic mechanisms underlying the various small RNA pathways is fundamental to our understanding of genome stability, pathogen defense, stress response, and virtually every aspect of plant and animal developmental. RNA silencing also has broad implications in therapeutics and crop improvements, and has been adapted widely by biologists as gene silencing tool to study the function of specific genes and gene families. The work described here focused on the basic mechanisms of small RNA formation and function in Arabidopsis, however, given the similarity in RNA silencing pathways between different organisms, these findings will likely have implications outside of plants as well.

BIBLIOGRAPHY

Adenot, X., Elmayan, T., Lauressergues, D., Boutet, S., Bouche, N., Gasciolli, V., and Vaucheret, H. (2006). DRB4-dependent TAS3 trans-acting siRNAs control leaf morphology through AGO7. Curr Biol *16*, 927-932.

Aguilera, A. (2005). Cotranscriptional mRNP assembly: from the DNA to the nuclear pore. Curr Opin Cell Biol *17*, 242-250.

Allen, E., Xie, Z., Gustafson, A. M., and Carrington, J. C. (2005). microRNA-directed phasing during trans-acting siRNA biogenesis in plants. Cell *121*, 207-221.

Allen, E., Xie, Z., Gustafson, A. M., Sung, G. H., Spatafora, J. W., and Carrington, J. C. (2004). Evolution of microRNA genes by inverted duplication of target gene sequences in *Arabidopsis thaliana*. Nat Genet *36*, 1282-1290.

Alonso, J. M., Stepanova, A. N., Leisse, T. J., Kim, C. J., Chen, H., Shinn, P., Stevenson, D. K., Zimmerman, J., Barajas, P., Cheuk, R.*, et al.* (2003). Genome-wide insertional mutagenesis of *Arabidopsis thaliana*. Science *301*, 653-657.

Alvarez, J., and Smyth, D. R. (1999). *CRABS CLAW* and *SPATULA*, two *Arabidopsis* genes that control carpel development in parallel with *AGAMOUS*. Development *126*, 2377-2386.

Alvarez, J. P., Pekker, I., Goldshmidt, A., Blum, E., Amsellem, Z., and Eshed, Y. (2006). Endogenous and synthetic microRNAs stimulate simultaneous, efficient, and localized regulation of multiple targets in diverse species. Plant Cell *18*, 1134-1151.

Ameres, S. L., Martinez, J., and Schroeder, R. (2007). Molecular basis for target RNA recognition and cleavage by human RISC. Cell *130*, 101-112.

Axtell, M. J., Jan, C., Rajagopalan, R., and Bartel, D. P. (2006). A Two-Hit Trigger for siRNA Biogenesis in Plants. Cell *127*, 565-577.

Axtell, M. J., Snyder, J. A., and Bartel, D. P. (2007). Common functions for diverse small RNAs of land plants. Plant Cell *19*, 1750-1769.

Backman, T. W., Sullivan, C. M., Cumbie, J. S., Miller, Z. A., Chapman, E. J., Fahlgren, N., Givan, S. A., Carrington, J. C., and Kasschau, K. D. (2007). Update of ASRP: the *Arabidopsis* Small RNA Project database. Nucleic Acids Res. *36*, D982-D985.

Baumberger, N., and Baulcombe, D. C. (2005). *Arabidopsis* ARGONAUTE1 is an RNA slicer that selectively recruits microRNAs and short interfering RNAs. Proc Natl Acad Sci USA *102*, 11928-11933.

Beclin, C., Boutet, S., Waterhouse, P., and Vaucheret, H. (2002). A branched pathway for transgene-induced RNA silencing in plants. Curr Biol *12*, 684-688.

Bezerra, I. C., Michaels, S. D., Schomburg, F. M., and Amasino, R. M. (2004). Lesions in the mRNA cap-binding gene ABA HYPERSENSITIVE 1 suppress FRIGIDA-mediated delayed flowering in Arabidopsis. Plant J *40*, 112-119.

Byrne, M. E., Barley, R., Curtis, M., Arroyo, J. M., Dunham, M., Hudson, A., and Martienssen, R. A. (2000). Asymmetric leaves1 mediates leaf patterning and stem cell function in *Arabidopsis*. Nature *408*, 967-971.

Chapman, E. J., and Carrington, J. C. (2007). Specialization and evolution of endogenous small RNA pathways. Nat Rev Genet *8*, 884-896.

Chapman, E. J., Prokhnevsky, A. I., Gopinath, K., Dolja, V. V., and Carrington, J. C. (2004). Viral RNA silencing suppressors inhibit the microRNA pathway at an intermediate step. Genes Dev *18*, 1179-1186.

Chen, H. M., Li, Y. H., and Wu, S. H. (2007). Bioinformatic prediction and experimental validation of a microRNA-directed tandem trans-acting siRNA cascade in Arabidopsis. Proc Natl Acad Sci USA *104*, 3318-3323.

Chen, X., Liu, J., Cheng, Y., and Jia, D. (2002). HEN1 functions pleiotropically in Arabidopsis development and acts in C function in the flower. Development *129*, 1085-1094.

Clarke, J. H., Tack, D., Findlay, K., Van Montagu, M., and Van Lijsebettens, M. (1999). The SERRATE locus controls the formation of the early juvenile leaves and phase length in Arabidopsis. Plant J *20*, 493-501.

Clough, S. J., and Bent, A. F. (1998). Floral dip: a simplified method for *Agrobacterium*-mediated transformation of *Arabidopsis thaliana*. Plant J *16*, 735-743.

Curtis, M. D., and Grossniklaus, U. (2003). A gateway cloning vector set for high-throughput functional analysis of genes in planta. Plant Physiol *133*, 462-469.

Dalmay, T., Hamilton, A., Rudd, S., Angell, S., and Baulcombe, D. C. (2000). An RNA-dependent RNA polymerase gene in Arabidopsis is required for posttranscriptional gene silencing mediated by a transgene but not by a virus. Cell *101*, 543-553.

Deleris, A., Gallego-Bartolome, J., Bao, J., Kasschau, K. D., Carrington, J. C., and Voinnet, O. (2006). Hierarchical action and inhibition of plant Dicer-like proteins in antiviral defense. Science *313*, 68-71.

Dunoyer, P., Himber, C., and Voinnet, O. (2005). DICER-LIKE 4 is required for RNA interference and produces the 21-nucleotide small interfering RNA component of the plant cell-to-cell silencing signal. Nat Genet *37*, 1356-1360.

El-Shami, M., Pontier, D., Lahmy, S., Braun, L., Picart, C., Vega, D., Hakimi, M. A., Jacobsen, S. E., Cooke, R., and Lagrange, T. (2007). Reiterated WG/GW motifs form functionally and evolutionarily conserved ARGONAUTE-binding platforms in RNAi-related components. Genes Dev *21*, 2539-2544.

Elbashir, S. M., Lendeckel, W., and Tuschl, T. (2001). RNA interference is mediated by 21- and 22-nucleotide RNAs. Genes Dev *15*, 188-200.

Fagard, M., Boutet, S., Morel, J. B., Bellini, C., and Vaucheret, H. (2000). AGO1, QDE-2, and RDE-1 are related proteins required for post-transcriptional gene silencing in plants, quelling in fungi, and RNA interference in animals. Proc Natl Acad Sci USA *97*, 11650-11654.

Fahlgren, N., Howell, M. D., Kasschau, K. D., Chapman, E. J., Sullivan, C. M., Cumbie, J. S., Givan, S. A., Law, T. F., Grant, S. R., Dangl, J. L., and Carrington, J. C. (2007). High-Throughput Sequencing of Arabidopsis microRNAs: Evidence for Frequent Birth and Death of MIRNA Genes. PLoS ONE *2*, e219.

Fahlgren, N., Montgomery, T. A., Howell, M. D., Allen, E., Dvorak, S. K., Alexander, A. L., and Carrington, J. C. (2006). Regulation of AUXIN RESPONSE FACTOR3 by TAS3 ta-siRNA affects developmental timing and patterning in Arabidopsis. Curr Biol *16*, 939-944.

Fang, Y., and Spector, D. L. (2007). Identification of nuclear dicing bodies containing proteins for microRNA biogenesis in living Arabidopsis plants. Curr Biol *17*, 818-823.

Filipowicz, W., Bhattacharyya, S. N., and Sonenberg, N. (2008). Mechanisms of post-transcriptional regulation by microRNAs: are the answers in sight? Nat Rev Genet *9*, 102-114.

Forstemann, K., Horwich, M. D., Wee, L., Tomari, Y., and Zamore, P. D. (2007). Drosophila microRNAs are sorted into functionally distinct argonaute complexes after production by dicer-1. Cell *130*, 287-297.

Fujioka, Y., Utsumi, M., Ohba, Y., and Watanabe, Y. (2007). Location of a possible miRNA processing site in SmD3/SmB nuclear bodies in Arabidopsis. Plant Cell Physiol *48*, 1243-1253.

Garcia, D., Collier, S. A., Byrne, M. E., and Martienssen, R. A. (2006). Specification of leaf polarity in Arabidopsis via the trans-acting siRNA pathway. Curr Biol *16*, 933-938.

Gasciolli, V., Mallory, A. C., Bartel, D. P., and Vaucheret, H. (2005). Partially redundant functions of *Arabidopsis* DICER-like enzymes and a role for DCL4 in producing trans-acting siRNAs. Curr Biol *15*, 1494-1500.

Gazzani, S., Lawrenson, T., Woodward, C., Headon, D., and Sablowski, R. (2004). A link between mRNA turnover and RNA interference in Arabidopsis. Science *306*, 1046-1048.

German, M. A., Pillay, M., Jeong, D. H., Hetawal, A., Luo, S., Janardhanan, P., Kannan, V., Rymarquis, L. A., Nobuta, K., German, R.*, et al.* (2008). Global identification of microRNA-target RNA pairs by parallel analysis of RNA ends. Nat Biotechnol. *26*, 941-946.

Golden, T. A., Schauer, S. E., Lang, J. D., Pien, S., Mushegian, A. R., Grossniklaus, U., Meinke, D. W., and Ray, A. (2002). Short integuments1/suspensor1/carpel factory, a Dicer homolog, Is a maternal effect gene required for embryo development in Arabidopsis. Plant Physiol *130*, 808-822.

Gregory, B. D., O'Malley, R. C., Lister, R., Urich, M. A., Tonti-Filippini, J., Chen, H., Millar, A. H., and Ecker, J. R. (2008). A link between RNA metabolism and silencing affecting Arabidopsis development. Dev Cell *14*, 854-866.

Grigg, S. P., Canales, C., Hay, A., and Tsiantis, M. (2005). SERRATE coordinates shoot meristem function and leaf axial patterning in Arabidopsis. Nature *437*, 1022-1026.

Hagen, G., and Guilfoyle, T. (2002). Auxin-responsive gene expression: genes, promoters and regulatory factors. Plant Mol Biol *49*, 373-385.

Han, M. H., Goud, S., Song, L., and Fedoroff, N. (2004). The Arabidopsis double-stranded RNA-binding protein HYL1 plays a role in microRNA-mediated gene regulation. Proc Natl Acad Sci USA *101*, 1093-1098.

Heisler, M. G., Atkinson, A., Bylstra, Y. H., Walsh, R., and Smyth, D. R. (2001). *SPATULA*, a gene that controls development of carpel margin tissues in *Arabidopsis*, encodes a bHLH protein. Development *128*, 1089-1098.

Herr, A. J., Molnar, A., Jones, A., and Baulcombe, D. C. (2006). Defective RNA processing enhances RNA silencing and influences flowering of Arabidopsis. Proc Natl Acad Sci USA *103*, 14994-15001.

Ho, S. N., Hunt, H. D., Horton, R. M., Pullen, J. K., and Pease, L. R. (1989). Site-directed mutagenesis by overlap extension using the polymerase chain reaction. Gene *77*, 51-59.

Howell, M. D., Fahlgren, N., Chapman, E. J., Cumbie, J. S., Sullivan, C. M., Givan, S. A., Kasschau, K. D., and Carrington, J. C. (2007). Genome-wide analysis of the RNA-DEPENDENT RNA POLYMERASE6/DICER-LIKE4 pathway in Arabidopsis reveals dependency on miRNA- and tasiRNA-directed targeting. Plant Cell *19*, 926-942.

Hugouvieux, V., Kwak, J. M., and Schroeder, J. I. (2001). An mRNA cap binding protein, ABH1, modulates early abscisic acid signal transduction in Arabidopsis. Cell *106*, 477-487.

Hunter, C., Sun, H., and Poethig, R. S. (2003). The *Arabidopsis* heterochronic gene *ZIPPY* is an ARGONAUTE family member. Curr Biol *13*, 1734-1739.

Hunter, C., Willmann, M. R., Wu, G., Yoshikawa, M., de la Luz Gutierrez-Nava, M., and Poethig, S. R. (2006). Trans-acting siRNA-mediated repression of ETTIN and ARF4 regulates heteroblasty in Arabidopsis. Development *133*, 2973-2981.

Izaurralde, E., Lewis, J., McGuigan, C., Jankowska, M., Darzynkiewicz, E., and Mattaj, I. W. (1994). A nuclear cap binding protein complex involved in pre-mRNA splicing. Cell *78*, 657-668.

Johansen, L. K., and Carrington, J. C. (2001). Silencing on the spot: induction and suppression of RNA silencing in the *Agrobacterium*-mediated transient expression system. Plant Physiol *126*, 930-938.

Jones-Rhoades, M. W., and Bartel, D. P. (2004). Computational identification of plant microRNAs and their targets, including a stress-induced miRNA. Mol Cell *14*, 787-799.

Jones-Rhoades, M. W., Bartel, D. P., and Bartel, B. (2006). MicroRNAs and their regulatory roles in plants. Annu Rev Plant Biol *57*, 19-53.

Kasschau, K. D., Fahlgren, N., Chapman, E. J., Sullivan, C. M., Cumbie, J. S., Givan, S. A., and Carrington, J. C. (2007). Genome-Wide Profiling and Analysis of Arabidopsis siRNAs. PLoS Biol *5*, e57.

Kasschau, K. D., Xie, Z., Allen, E., Llave, C., Chapman, E. J., Krizan, K. A., and Carrington, J. C. (2003). P1/HC-Pro, a viral suppressor of RNA silencing, interferes with *Arabidopsis* development and miRNA function. Dev Cell *4*, 205-217.

Kerschen, A., Napoli, C. A., Jorgensen, R. A., and Muller, A. E. (2004). Effectiveness of RNA interference in transgenic plants. FEBS Lett *566*, 223-228.

Khvorova, A., Reynolds, A., and Jayasena, S. D. (2003). Functional siRNAs and miRNAs exhibit strand bias. Cell *115*, 209-216.

Kuhn, J. M., Breton, G., and Schroeder, J. I. (2007). mRNA metabolism of flowering-time regulators in wild-type Arabidopsis revealed by a nuclear cap binding protein mutant, abh1. Plant J *50*, 1049-1062.

Kumagai, M. H., Donson, J., Della-Cioppa, G., Harvey, D., Hanley, K., and Grill, L. K. (1995). Cytoplasmic inhibition of carotenoid biosynthesis with virus-derived RNA. Proc Natl Acad Sci USA *92*, 1679-1683.

Laubinger, S., Sachsenberg, T., Zeller, G., Busch, W., Lohmann, J. U., Ratsch, G., and Weigel, D. (2008). Dual roles of the nuclear cap-binding complex and SERRATE in pre-mRNA splicing and microRNA processing in Arabidopsis thaliana. Proc Natl Acad Sci USA *105*, 8795-8800.

Lewis, J. D., and Izaurralde, E. (1997a). The role of the cap structure in RNA processing and nuclear export. Eur J Biochem *247*, 461-469.

Li, C. F., Pontes, O., El-Shami, M., Henderson, I. R., Bernatavichute, Y. V., Chan, S. W., Lagrange, T., Pikaard, C. S., and Jacobsen, S. E. (2006). An ARGONAUTE4-containing nuclear processing center colocalized with Cajal bodies in Arabidopsis thaliana. Cell *126*, 93-106.

Li, H., Xu, L., Wang, H., Yuan, Z., Cao, X., Yang, Z., Zhang, D., Xu, Y., and Huang, H. (2005). The putative RNA-dependent RNA polymerase RDR6 acts synergistically with ASYMMETRIC LEAVES1 and 2 to repress BREVIPEDICELLUS and microRNA165/166 in *Arabidopsis* leaf development. Plant Cell *17*, 2157-2171.

Liu, J., Valencia-Sanchez, M. A., Hannon, G. J., and Parker, R. (2005). MicroRNA-dependent localization of targeted mRNAs to mammalian P-bodies. Nat Cell Biol *7*, 719-723.

Liu, Z., Franks, R. G., and Klink, V. P. (2000). Regulation of gynoecium marginal tissue formation by LEUNIG and AINTEGUMENTA. Plant Cell *12*, 1879-1892.

Llave, C., Kasschau, K. D., and Carrington, J. C. (2000). Virus-encoded suppressor of posttranscriptional gene silencing targets a maintenance step in the silencing pathway. Proc Natl Acad Sci USA *97*, 13401-13406.

Llave, C., Kasschau, K. D., Rector, M. A., and Carrington, J. C. (2002a). Endogenous and silencing-associated small RNAs in plants. Plant Cell *14*, 1605-1619.

Llave, C., Xie, Z., Kasschau, K. D., and Carrington, J. C. (2002b). Cleavage of Scarecrow-like mRNA targets directed by a class of *Arabidopsis* miRNA. Science *297*, 2053-2056.

Lobbes, D., Rallapalli, G., Schmidt, D. D., Martin, C., and Clarke, J. (2006). SERRATE: a new player on the plant microRNA scene. EMBO Rep *7*, 1052-1058.

Lu, C., Kulkarni, K., Souret, F. F., Muthuvalliappan, R., Tej, S. S., Poethig, R. S., Henderson, I. R., Jacobsen, S. E., Wang, W., Green, P. J., and Meyers, B. C. (2006). MicroRNAs and other small RNAs enriched in the Arabidopsis RNA-dependent RNA polymerase-2 mutant. Genome Res *16*, 1276-1288.

Ma, J. B., Yuan, Y. R., Meister, G., Pei, Y., Tuschl, T., and Patel, D. J. (2005). Structural basis for 5'-end-specific recognition of guide RNA by the A. fulgidus Piwi protein. Nature *434*, 666-670.

Maquat, L. E. (2004). Nonsense-mediated mRNA decay: splicing, translation and mRNP dynamics. Nat Rev Mol Cell Biol *5*, 89-99.

Mi, S., Cai, T., Hu, Y., Chen, Y., Hodges, E., Ni, F., Wu, L., Li, S., Zhou, H., Long, C.*, et al.* (2008). Sorting of small RNAs into Arabidopsis argonaute complexes is directed by the 5' terminal nucleotide. Cell *133*, 116-127.

Moissiard, G., Parizotto, E. A., Himber, C., and Voinnet, O. (2007). Transitivity in Arabidopsis can be primed, requires the redundant action of the antiviral Dicer-like 4 and Dicer-like 2, and is compromised by viral-encoded suppressor proteins. RNA *13*, 1268-1278.

Montgomery, T. A., Howell, M. D., Cuperus, J. T., Li, D., Hansen, J. E., Alexander, A. L., Chapman, E. J., Fahlgren, N., Allen, E., and Carrington, J. C. (2008). Specificity of ARGONAUTE7-miR390 interaction and dual functionality in TAS3 trans-acting siRNA formation. Cell *133*, 128-141.

Morel, J. B., Godon, C., Mourrain, P., Beclin, C., Boutet, S., Feuerbach, F., Proux, F., and Vaucheret, H. (2002). Fertile hypomorphic ARGONAUTE (ago1) mutants impaired in post-transcriptional gene silencing and virus resistance. Plant Cell *14*, 629-639.

Mourrain, P., Beclin, C., Elmayan, T., Feuerbach, F., Godon, C., Morel, J. B., Jouette, D., Lacombe, A. M., Nikic, S., Picault, N.*, et al.* (2000). Arabidopsis SGS2 and SGS3 genes are required for posttranscriptional gene silencing and natural virus resistance. Cell *101*, 533-542.

Muangsan, N., Beclin, C., Vaucheret, H., and Robertson, D. (2004). Geminivirus VIGS of endogenous genes requires SGS2/SDE1 and SGS3 and defines a new branch in the genetic pathway for silencing in plants. Plant J *38*, 1004-1014.

Olmedo, G., Guo, H., Gregory, B. D., Nourizadeh, S. D., Aguilar-Henonin, L., Li, H., An, F., Guzman, P., and Ecker, J. R. (2006). ETHYLENE-INSENSITIVE5 encodes a 5'-->3' exoribonuclease required for regulation of the EIN3-targeting F-box proteins EBF1/2. Proc Natl Acad Sci USA *103*, 13286-13293.

Ori, N., Eshed, Y., Chuck, G., Bowman, J., and Hake, S. (2000). Mechanisms that control *knox* gene expression in the *Arabidopsis* shoot. Development *127*, 5523-5532.

Ossowski, S., Schwab, R., and Weigel, D. (2008). Gene silencing in plants using artificial microRNAs and other small RNAs. Plant J *53*, 674-690.

Palatnik, J. F., Allen, E., Wu, X., Schommer, C., Schwab, R., Carrington, J. C., and Weigel, D. (2003). Control of leaf morphogenesis by microRNAs. Nature *425*, 257-263.

Papp, I., Mur, L. A., Dalmadi, A., Dulai, S., and Koncz, C. (2004). A mutation in the Cap Binding Protein 20 gene confers drought tolerance to Arabidopsis. Plant Mol Biol *55*, 679-686.

Park, W., Li, J., Song, R., Messing, J., and Chen, X. (2002). CARPEL FACTORY, a Dicer homolog, and HEN1, a novel protein, act in microRNA metabolism in Arabidopsis thaliana. Curr Biol *12*, 1484-1495.

Parker, J. S., Roe, S. M., and Barford, D. (2005). Structural insights into mRNA recognition from a PIWI domain-siRNA guide complex. Nature *434*, 663-666.

Parry, D. H., Xu, J., and Ruvkun, G. (2007). A whole-genome RNAi Screen for C. elegans miRNA pathway genes. Curr Biol *17*, 2013-2022.

Pekker, I., Alvarez, J. P., and Eshed, Y. (2005). Auxin Response Factors Mediate Arabidopsis Organ Asymmetry via Modulation of KANADI Activity. Plant Cell *17*, 2899-2910.

Peragine, A., Yoshikawa, M., Wu, G., Albrecht, H. L., and Poethig, R. S. (2004). SGS3 and SGS2/SDE1/RDR6 are required for juvenile development and the production of trans-acting siRNAs in *Arabidopsis*. Genes Dev *18*, 2368-2379.

Prigge, M. J., and Wagner, D. R. (2001). The Arabidopsis serrate gene encodes a zinc-finger protein required for normal shoot development. Plant Cell *13*, 1263-1279.

Qi, Y., Denli, A. M., and Hannon, G. J. (2005). Biochemical specialization within Arabidopsis RNA silencing pathways. Mol Cell *19*, 421-428.

Qi, Y., He, X., Wang, X. J., Kohany, O., Jurka, J., and Hannon, G. J. (2006). Distinct catalytic and non-catalytic roles of ARGONAUTE4 in RNA-directed DNA methylation. Nature *443*, 1008-1012.

Rajagopalan, R., Vaucheret, H., Trejo, J., and Bartel, D. P. (2006). A diverse and evolutionarily fluid set of microRNAs in Arabidopsis thaliana. Genes Dev *20*, 3407-3425.

Redei, G., and Hirono, Y. (1964). Linkage studies. Arabidopsis Inf Serv *1*, 9-10.
Reinhart, B. J., and Bartel, D. P. (2002). Small RNAs correspond to centromere heterochromatic repeats. Science *297*, 1831.

Rivas, F. V., Tolia, N. H., Song, J. J., Aragon, J. P., Liu, J., Hannon, G. J., and Joshua-Tor, L. (2005). Purified Argonaute2 and an siRNA form recombinant human RISC. Nat Struct Mol Biol *12*, 340-349.

Roe, J. L., Nemhauser, J. L., and Zambryski, P. C. (1997). TOUSLED participates in apical tissue formation during gynoecium development in *Arabidopsis*. Plant Cell *9*, 335-353.

Ronemus, M., Vaughn, M. W., and Martienssen, R. A. (2006). MicroRNA-targeted and small interfering RNA-mediated mRNA degradation is regulated by argonaute, dicer, and RNA-dependent RNA polymerase in Arabidopsis. Plant Cell *18*, 1559-1574.

Ruby, J. G., Jan, C., Player, C., Axtell, M. J., Lee, W., Nusbaum, C., Ge, H., and Bartel, D. P. (2006). Large-Scale Sequencing Reveals 21U-RNAs and Additional MicroRNAs and Endogenous siRNAs in C. elegans. Cell *127*, 1193-1207.

Schwab, R., Ossowski, S., Riester, M., Warthmann, N., and Weigel, D. (2006). Highly specific gene silencing by artificial microRNAs in Arabidopsis. Plant Cell *18*, 1121-1133.

Schwab, R., Palatnik, J. F., Riester, M., Schommer, C., Schmid, M., and Weigel, D. (2005). Specific effects of microRNAs on the plant transcriptome. Dev Cell *8*, 517-527.

Schwarz, D. S., Hutvagner, G., Du, T., Xu, Z., Aronin, N., and Zamore, P. D. (2003). Asymmetry in the assembly of the RNAi enzyme complex. Cell *115*, 199-208.

Semiarti, E., Ueno, Y., Tsukaya, H., Iwakawa, H., Machida, C., and Machida, Y. (2001). The *ASYMMETRIC LEAVES2* gene of *Arabidopsis thaliana* regulates formation of a symmetric lamina, establishment of venation and repression of meristem-related homeobox genes in leaves. Development *128*, 1771-1783.

Souret, F. F., Kastenmayer, J. P., and Green, P. J. (2004). AtXRN4 degrades mRNA in Arabidopsis and its substrates include selected miRNA targets. Mol Cell *15*, 173-183.

Steiner, F. A., Hoogstrate, S. W., Okihara, K. L., Thijssen, K. L., Ketting, R. F., Plasterk, R. H., and Sijen, T. (2007). Structural features of small RNA precursors determine Argonaute loading in Caenorhabditis elegans. Nat Struct Mol Biol *14*, 927-933.

Sunkar, R., and Zhu, J. K. (2004). Novel and stress-regulated microRNAs and other small RNAs from *Arabidopsis*. Plant Cell *16*, 2001-2019.

Takeda, A., Iwasaki, S., Watanabe, T., Utsumi, M., and Watanabe, Y. (2008). The mechanism selecting the guide strand from small RNA duplexes is different among argonaute proteins. Plant Cell Physiol *49*, 493-500.

Talmor-Neiman, M., Stav, R., Klipcan, L., Buxdorf, K., Baulcombe, D. C., and Arazi, T. (2006). Identification of trans-acting siRNAs in moss and an RNA-dependent RNA polymerase required for their biogenesis. Plant J *48*, 511-521.

Tiwari, S. B., Hagen, G., and Guilfoyle, T. (2003). The roles of auxin response factor domains in auxin-responsive transcription. Plant Cell *15*, 533-543.

Tolia, N. H., and Joshua-Tor, L. (2007). Slicer and the Argonautes. Nat Chem Biol *3*, 36-43.

Tomari, Y., Du, T., and Zamore, P. D. (2007). Sorting of Drosophila small silencing RNAs. Cell *130*, 299-308.

Tyagi, R., Lai, R., and Duggleby, R. G. (2004). A new approach to 'megaprimer' polymerase chain reaction mutagenesis without an intermediate gel purification step. BMC Biotechnol *4*, 2.

Vaucheret, H., Vazquez, F., Crete, P., and Bartel, D. P. (2004). The action of ARGONAUTE1 in the miRNA pathway and its regulation by the miRNA pathway are crucial for plant development. Genes Dev *18*, 1187-1197.

Vazquez, F., Gasciolli, V., Crete, P., and Vaucheret, H. (2004a). The nuclear dsRNA binding protein HYL1 is required for microRNA accumulation and plant development, but not posttranscriptional transgene silencing. Curr Biol *14*, 346-351.

Vazquez, F., Vaucheret, H., Rajagopalan, R., Lepers, C., Gasciolli, V., Mallory, A. C., Hilbert, J. L., Bartel, D. P., and Crete, P. (2004b). Endogenous trans-acting siRNAs regulate the accumulation of *Arabidopsis* mRNAs. Mol Cell *16*, 69-79.

Williams, L., Carles, C. C., Osmont, K. S., and Fletcher, J. C. (2005). A database analysis method identifies an endogenous trans-acting short-interfering RNA that targets the *Arabidopsis ARF2*, *ARF3*, and *ARF4* genes. Proc Natl Acad Sci USA *102*, 9703-9708.

Willmann, M. R., and Poethig, R. S. (2005). Time to grow up: the temporal role of smallRNAs in plants. Curr Opin Plant Biol *8*, 548-552.

Xie, Z., Allen, E., Fahlgren, N., Calamar, A., Givan, S. A., and Carrington, J. C. (2005a). Expression of Arabidopsis MIRNA genes. Plant Physiol *138*, 2145-2154.

Xie, Z., Allen, E., Wilken, A., and Carrington, J. C. (2005b). DICER-LIKE 4 functions in trans-acting small interfering RNA biogenesis and vegetative phase change in *Arabidopsis thaliana*. Proc Natl Acad Sci USA *102*, 12984-12989.

Xie, Z., Johansen, L. K., Gustafson, A. M., Kasschau, K. D., Lellis, A. D., Zilberman, D., Jacobsen, S. E., and Carrington, J. C. (2004). Genetic and functional diversification of small RNA pathways in plants. PLoS Biol *2*, E104.

Xu, L., Xu, Y., Dong, A., Sun, Y., Pi, L., Xu, Y., and Huang, H. (2003). Novel *as1* and *as2* defects in leaf adaxial-abaxial polarity reveal the requirement for ASYMMETRIC LEAVES1 and 2 and ERECTA functions in specifying leaf adaxial identity. Development *130*, 4097-4107.

Yang, L., Liu, Z., Lu, F., Dong, A., and Huang, H. (2006). SERRATE is a novel nuclear regulator in primary microRNA processing in Arabidopsis. Plant J *47*, 841-850.

Yoshikawa, M., Peragine, A., Park, M. Y., and Poethig, R. S. (2005). A pathway for the biogenesis of trans-acting siRNAs in *Arabidopsis*. Genes Dev *19*, 2164-2175.

Yu, B., Yang, Z., Li, J., Minakhina, S., Yang, M., Padgett, R. W., Steward, R., and Chen, X. (2005). Methylation as a crucial step in plant microRNA biogenesis. Science *307*, 932-935.

Zhang, X., Yuan, Y. R., Pei, Y., Lin, S. S., Tuschl, T., Patel, D. J., and Chua, N. H. (2006). Cucumber mosaic virus-encoded 2b suppressor inhibits Arabidopsis Argonaute1 cleavage activity to counter plant defense. Genes Dev *20*, 3255-3268.

Zheng, X., Zhu, J., Kapoor, A., and Zhu, J. K. (2007). Role of Arabidopsis AGO6 in siRNA accumulation, DNA methylation and transcriptional gene silencing. Embo J *26*, 1691-1701.

Zilberman, D., Cao, X., and Jacobsen, S. E. (2003). ARGONAUTE4 control of locus-specific siRNA accumulation and DNA and histone methylation. Science *299*, 716-719.

Zilberman, D., Cao, X., Johansen, L. K., Xie, Z., Carrington, J. C., and Jacobsen, S. E. (2004). Role of *Arabidopsis* ARGONAUTE4 in RNA-directed DNA methylation triggered by inverted repeats. Curr Biol *14*, 1214-1220.